Oil & Natural Gas Technology

DOE Award No.: DE-FE0001243

Clean and Secure Energy from Domestic Oil Shale and Oil Sands Resources

Quarterly Progress Report
(April - June 2012)

Submitted by:
University of Utah
Institute for Clean and Secure Energy
155 South 1452 East, Room 380
Salt Lake City, Utah 84112

Prepared for:
United States Department of Energy
National Energy Technology Laboratory

August 7, 2012

Office of Fossil Energy

Clean and Secure Energy from Domestic Oil Shale and Oil Sands Resources

DOE Award No.: DE-FE0001243

Quarterly Progress Report

April 2012 to June 2012

Submitted by:
Institute for Clean and Secure Energy
155 S. 1452 E. Room 380
Salt Lake City, UT 84112

Principal Investigator: Philip J. Smith
Project Period: October 1, 2010 to September 30, 2013

Prepared for:
U.S. Department of Energy
National Energy Technology Laboratory

EXECUTIVE SUMMARY

The Clean and Secure Energy from Domestic Oil Shale and Oil Sands Resources program is part of the research agenda of the Institute for Clean and Secure Energy (ICSE) at the University of Utah. In this quarter, ICSE presented the 2012 University of Utah Unconventional Fuels Conference and met with representatives of Statoil about creation of a short course for Statoil employees.

In Task 3.0, the Subtask 3.2 research team conducted a suite of simulations to look at sensitivity of output variables such as temperature, NO_x concentrations, and heat flux to various scenario and model parameters. A comparison of experimental data and simulation results across the width of the furnace at various axial distances from the burner reveals that an expanded parameter space is needed before a data consistency analysis (validation/uncertainty quantification) can be applied.

The analyses of three different sections of the Skyline 16 core (GR-1, GR-2, and GR-3) continued in this quarter with plans to synthesize the data collected in a report/publication. The Subtask 4.3 researchers finished their collection of tar and char samples from the demineralized kerogen samples using the kerogen retort, completed the atmospheric pyrolysis tests using the TGA, repaired the pressurized TGA, and started the high pressure TGA pyrolysis experiments. The Subtask 4.7 team made final adjustments to their triaxial testing equipment and proposed a revised testing matrix. These adjustments included the addition of mechanical pressure gauges and pressure relief valves based on pre-testing safety evaluations. Subtask 4.9 researchers used a variety of analytical techniques to obtain structural data on the demineralized kerogen samples. The structural model has been developed and results are being gathered together for publication. Researchers in Subtask 4.8 drafted the Asphalt Wash 1 core and calibrated, graphed and summarized elemental abundance (X-Ray Fluorescence) data.

Task 4.0 projects focused on simulation of various in situ processes include Subtasks 4.1, 4.2, and 4.3. The Subtask 4.1 team continued implementation of a kinetic model to study product yield as a function of temperature and shale properties. They also expanded their knowledge base for coupling experiments with simulations by including additional scientific research papers. In Subtask 4.2, researchers used three different approaches to study thermally induced geomechanical changes: the material point method in the Uintah Computational Framework, the thermal/geomechanical options in STARS (a commercial thermal simulator), and the Advanced Reactive Transport Simulator with coupled thermal and geomechanical models. The Subtask 4.3 team derived detailed kinetic models for the conversion of kerogen based on the concepts of distribution of activation energies and thermal gravimetric analysis data. The kinetic models were then incorporated into a finite-element model in the COMSOL multiphysics framework.

Progress in economics and policy projects was made with the completion of 9 of 10 sections of the Market Assessment. In Subtask 5.3, researchers surveyed the legal standards articulated by the Environmental Protection Agency in addressing the role and value of modeling in assessing environmental risks or harms.

American Shale Oil (AMSO) and Task 7.0 researchers continued their collaboration with frequent meetings and a presentation highlighting all three subtasks by Dr. Alan Burnham of AMSO at the 2012 University of Utah Unconventional Fuels Conference. The Subtask 7.1 team developed methods for representing the matrix of experimental data that has been generated by AMSO. These methods include using hyperbolic relationships between stress and deformation to fit various constitutive behaviors and using neural networking protocols to interrelate constitutive behavior to the governing independent variables. In Subtask 7.2, researchers implemented the tools developed in Subtask 4.2 to study the ongoing AMSO pilot. Lastly,

Subtask 7.3 researchers have adjusted the computational representation of the geometry for the AMSO process. They continue to work closely with AMSO, as well as their third party contractors, who are providing the up-to-date field gyro surveys of wells drilled for accurate geometric representation of the heater test. They have also gathered and processed data related to the operation of the heater well that will be used in subsequent simulations.

PROGRESS, RESULTS, AND DISCUSSION

Task 1.0 - Project Management and Planning

During this quarter, there were no schedule/cost variances or other situations requiring updating/amending of the PMP.

Task 2.0 -Technology Transfer and Outreach

Task 2.0 focuses on outreach and education efforts and the implementation of External Advisory Board (EAB) recommendations. During this quarter, ICSE organized and held the 2012 University of Utah Unconventional Fuels Conference; a conference agenda is included as Appendix A. Conference presentations can be downloaded from http://www.icse.utah.edu/assets/archive/2012/ucf_agenda.htm. ICSE researchers who spoke at the conference included President David W. Pershing, Professor Philip Smith and John Ruple, Esquire. In addition, Dr. Alan Burnham of American Shale Oil (AMSO) presented work from all the projects under Subtask 7.0. Other speakers came from government and industry with a plenary talk given by former Senator Robert Bennett. Approximately 120 people attended the conference, including several journalists. There were several articles published about the conference in the local newspaper (Salt Lake Tribune) and a story by an AP writer in attendance was picked up by news outlets around the country. An example of the stories that ran is included as Appendix B. There is clearly much local and national interest about the development of these resources and a desire to understand what the issues are.

Three employees of Statoil visited ICSE during this quarter to find out about research related to in situ development of oil shale resources. Statoil has requested a short course to be delivered by ICSE personnel in Norway in September or October of this year on the topic of "In situ kerogen liquefaction – basis for efficient production forecasting." Additionally, Statoil has indicated an interest in funding a graduate student in a research topic of interest to the company.

It was decided this quarter that the next EAB meeting would likely not be held until the first quarter of 2013. Work also began this quarter on the next ICSE Energy Forum, in particular with identifying potential panelists for the event. Work continued this quarter on the Marriott Library's ICSE Collection, specifically on identifying documents missing from the initial document migration from ICSE's DSpace repository to the Marriott's ICSE Collection and developing a submission framework for future ICSE reports and documents. Conforming the contents of the ICSE Collection with the contents of ICSE's DSpace repository and finalization of the submission framework is expected next quarter.

Task 3.0 - Clean Oil Shale and Oil Sands Utilization with CO_2 Management

Subtask 3.1 (Phase I) – Macroscale CO_2 Analysis (PI: Kerry Kelly, David Pershing)

The completion of the Phase 1 milestone will be reported on next quarter.

<u>Subtask 3.1 (Phase II) – Lifecycle Greenhouse Gas Analysis of Conventional Oil and Gas Development in the Uinta Basin (PI: Kerry Kelly, David Pershing)</u>

This subtask is was on hold during this quarter. Subtask researchers are reconvening in early August to restart the project.


<u>Subtask 3.2 - Flameless Oxy-gas Process Heaters for Efficient CO_2 Capture (PI: Jennifer Spinti)</u>

The Subtask 3.2 team has completed a suite of seven simulations of the IFRF's oxy-gas experiments (Coraggio and Laiola, 2009). The purpose of these simulations is to test the sensitivity of output variables of interest (species concentrations, gas temperature, heat flux at the walls) to various model parameters and inlet/boundary conditions (e.g. scenario parameters) in order to identify the range of parameters to include in the validation/uncertainty quantification (V/UQ) study that will be completed next quarter. The simulations were performed with the ARCHES large eddy simulation (LES) code developed at the University of Utah. Recent changes to the boundary conditions have allowed the complex burner geometry at the exit plane of the burner to be approximated by a combination of well-resolved exit surface areas and velocity vectors. Figure 1 shows the inlet plane of the burner with four types of inlets. RFG is fed through the four primary RFG inlets; the only O_2 in this stream is that from air in-leakage. RFG with O_2 added is fed through the secondary and tertiary annular inlets. The Coraggio and Laiola paper (2009) does not provide details about the split between the two streams, so it had to be estimated. The natural gas inlets consist of a series of eight jets colocated in the secondary RFG + O_2 annular ring. Although the furnace is 2m x 2m x 6m, the computational domain is 2m x 2m x 4m to allow for increased resolution of the burner without requiring additional computational resources. The mesh resolution is 228 x 468 x 228, so the cell size in the furnace cross section is 0.877 cm and in the axial direction is 0.855 cm. All cases were run on 1344 for approximately 72 hours.
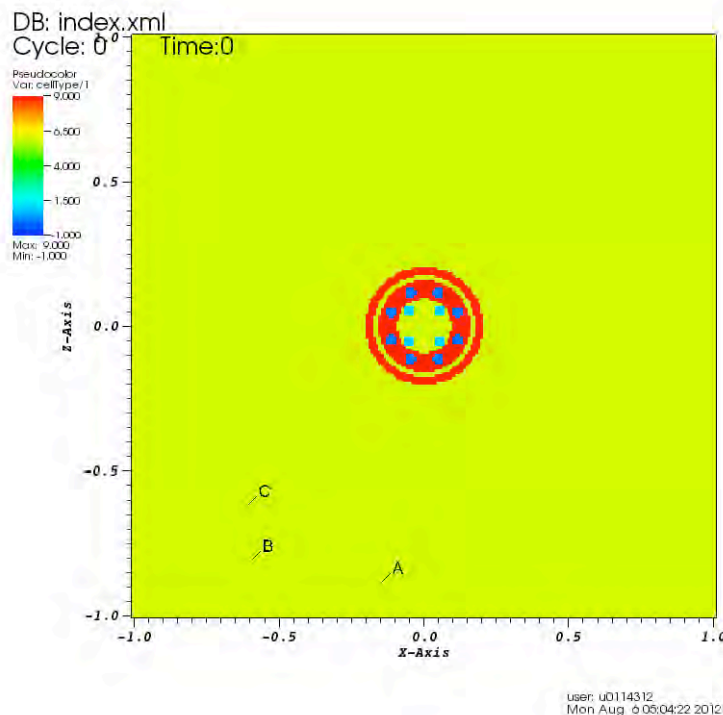
Figure 1: Burner inlet plane of IFRF furnace simulation showing primary RFG inlet (light blue), secondary and tertiary RFG + O_2 inlets (red), and natural gas inlets (blue).

Coraggio and Laiola paper (2009) report that, according to the IFRF classification system for flames, the flame is close to type-3. Type-3 flames are characterized by "intense but longer flames on the quarl with two internal recirculation zones." Figure 2 shows the vorticity field in a slice through the mid-plane of the furnace for the base case simulation compared to an IFRF drawing of the type-3 flame. Note that the actual furnace is situated horizontally. The vorticity field exhibits both the external and internal recirculation zones typical of type-3 flames.
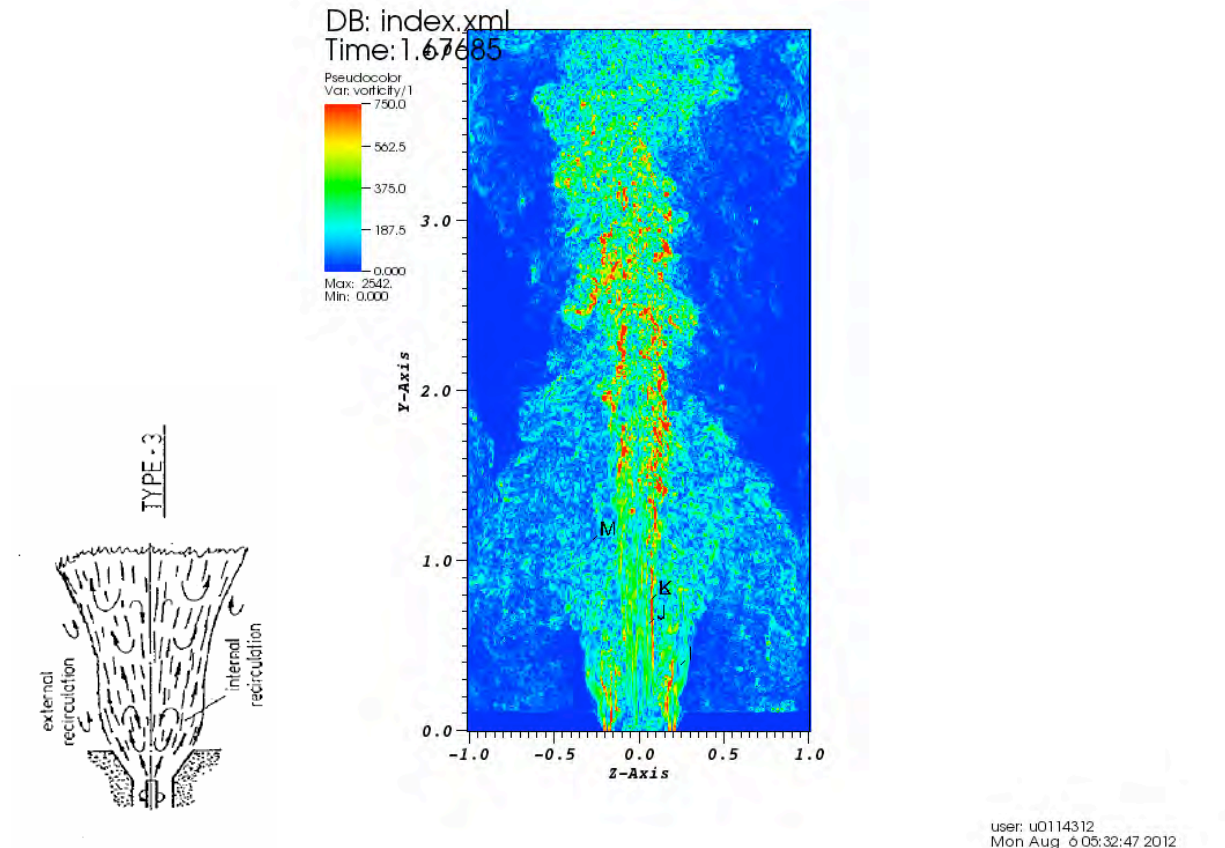

Figure 2: Type-3 flames in IFRF classification system compared with vorticity field from base case simulation of IFRF furnace.

The base case simulation assumes a wall temperature of 1350 K, a swirl number in the tertiary oxidant flow of the burner of 0.5, and air leakage into the recycled flue gas (RFG) stream (1296.4 kg/hr) of 199 kg/hr or 12.7% of the overall RFG stream, and flow rates of O_2 and natural gas as reported by Coraggio and Laiola (2009). Based on uncertainties noted by the authors and/or the lack of availability of detailed burner information, the following parameters were varied for the sensitivity study:

- Air in-leakage into RFG is increased to 268 kg/hr
- Increase O_2 addition to the RFG stream by 10%
- Wall temperature increased from 1350K to 1450K
- Split of RFG + O_2 stream between the secondary and tertiary inlets is scaled by the available exit surface area
- Increase natural gas flowrate by 5%
- Decrease the swirl number to 0.1

Experimental measurements were taken from the wall to the furnace centerline at six axial distance along the furnace. Five of those axial locations are within the domain size of the simulation and are used for data analysis. Experimental data includes heat flux at the walls, gas temperature, and CO_2, CO, O_2, and NO_x concentrations. This same set of data has been extracted from the suite of simulations and time-averaged. Figures 3-5 show comparisons of the CO_2, temperature and NO_x simulation and experimental data at three axial locations for the base case, the increase in wall temperature, and the change in the secondary/tertiary split.
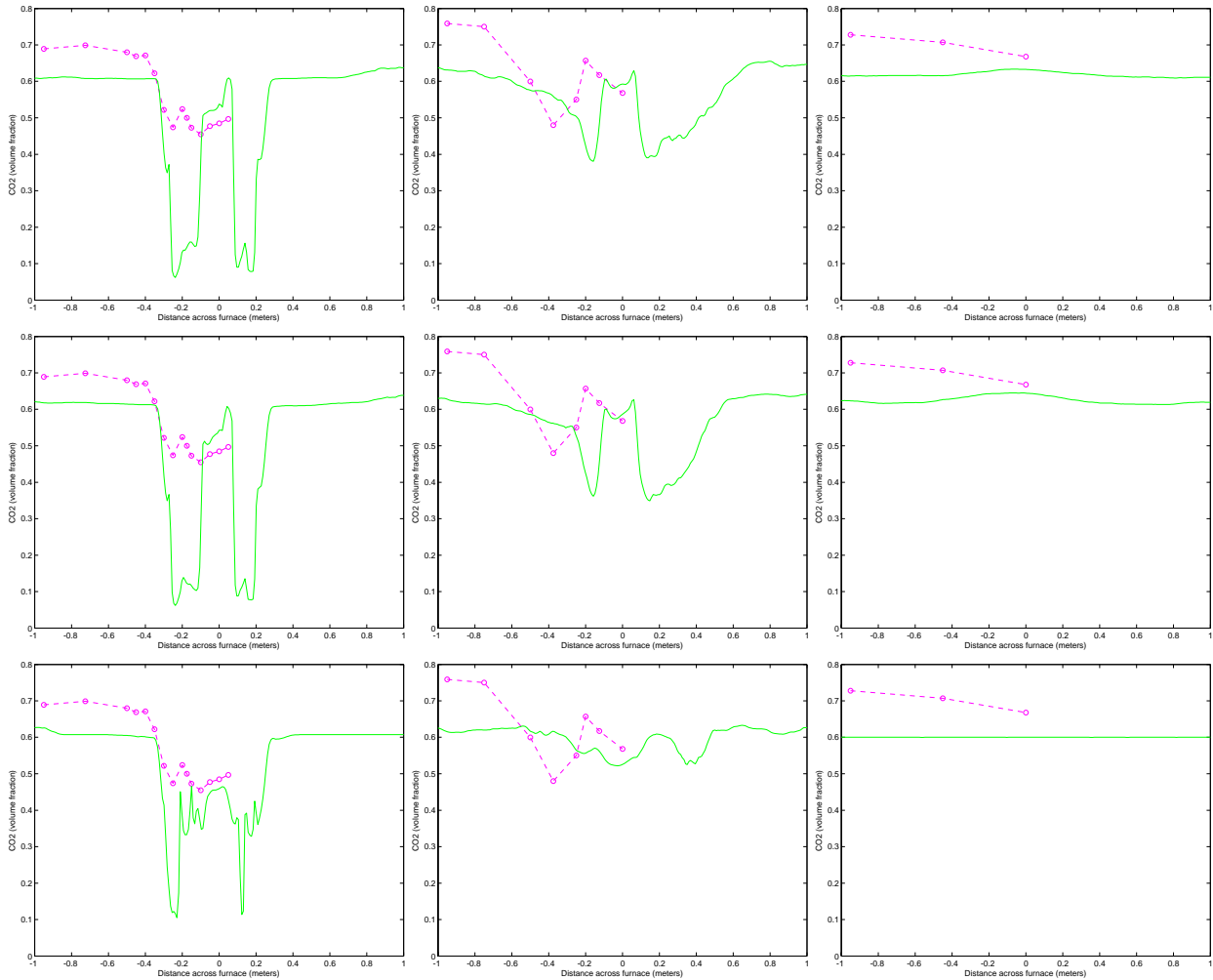
Figure 3: Comparison of CO_2 concentrations measured experimentally (purple circles) and computed from simulation of the oxy-fired IFRF furnace (green line). Axial locations (left to right) are 0.17 m, 1.04 m, and 3.84 m from the burner face. Cases (top to bottom) are base case, increased wall temperature, and secondary/tertiary oxidant split.
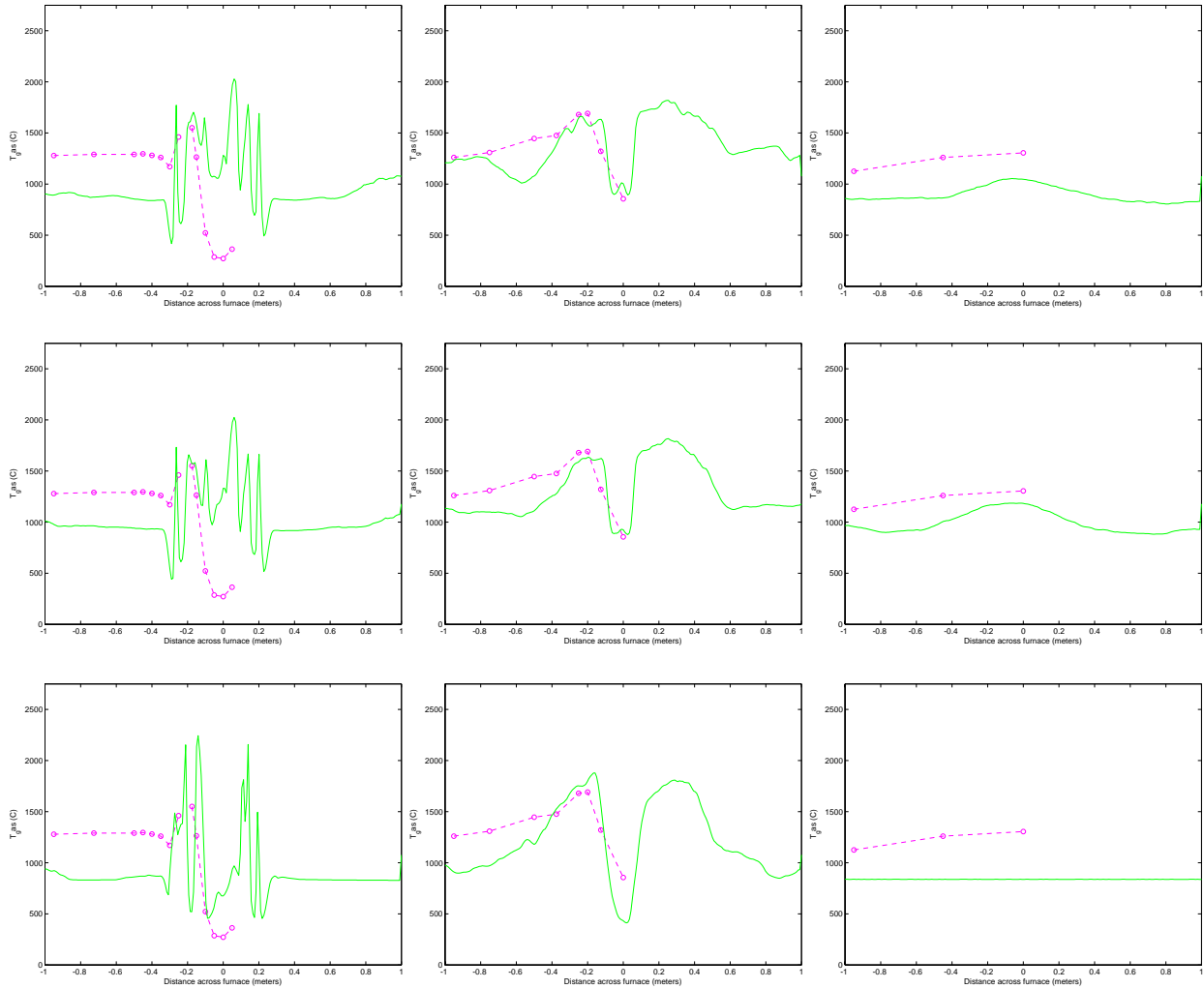
Figure 4: Comparison of gas temperatures measured experimentally (purple circles) and computed from simulation of the oxy-fired IFRF furnace (green line). Axial locations (left to right) are 0.17 m, 1.04 m, and 3.84 m from the burner face. Cases (top to bottom) are base case, increased wall temperature, and secondary/tertiary oxidant split.
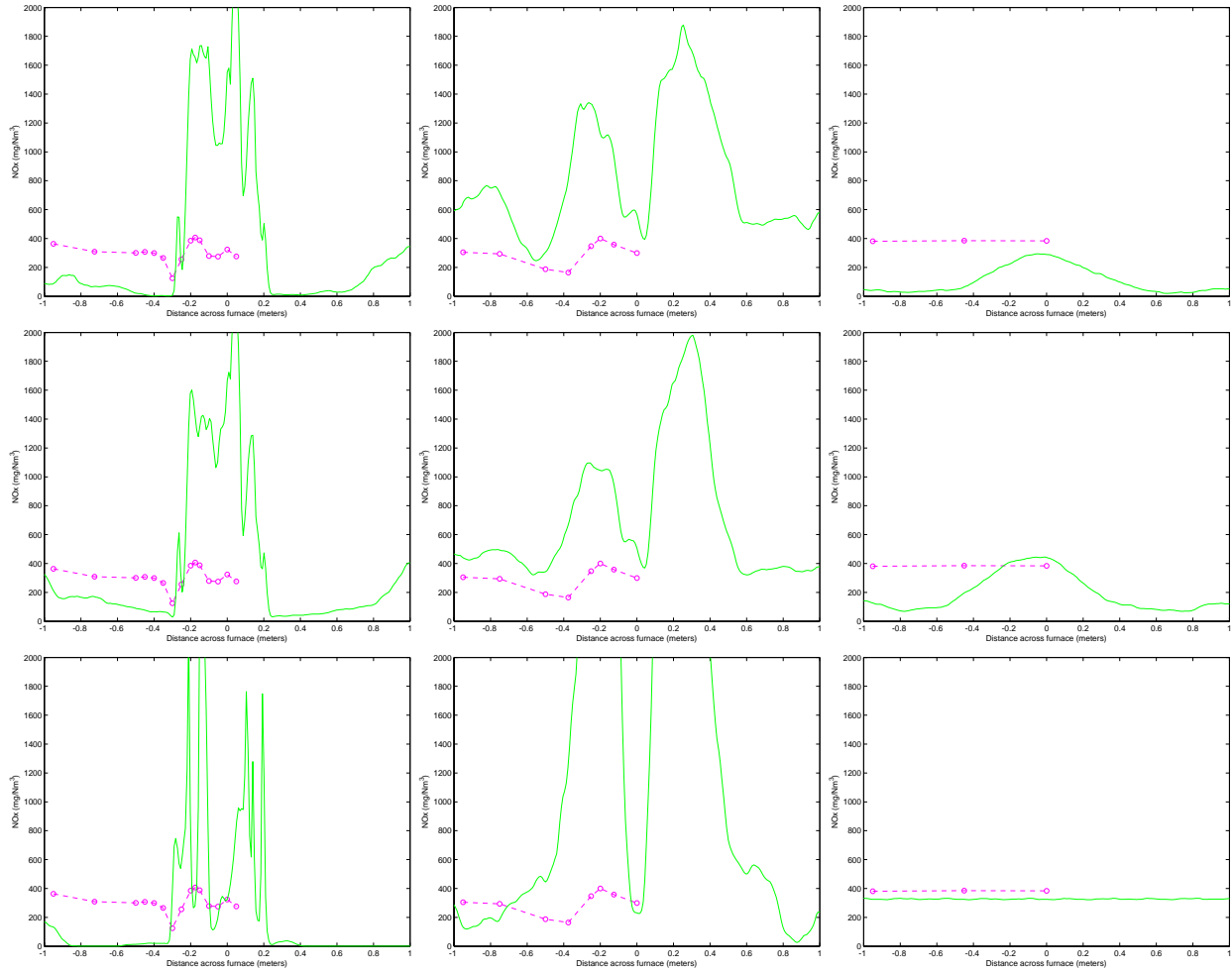
Figure 5: Comparison of NO$_x$ concentrations measured experimentally (purple circles) and computed from simulation of the oxy-fired IFRF furnace (green line). Axial locations (left to right) are 0.17 m, 1.04 m, and 3.84 m from the burner face. Cases (top to bottom) are base case, increased wall temperature, and secondary/tertiary oxidant split.

Several observations can be made from these figures. First, the CO$_2$ concentration profiles, while following the same trend as the experimental data, are consistently low; the corresponding O$_2$ concentration profiles (not shown) are consistently high. These results indicates that the parameter range spanned (air in-leakage, O$_2$ concentration in the RFG, and/or natural gas feed rate) need to be adjusted in the V/UQ study such that a drop in CO$_2$ concentrations is achieved. Second, the gas temperature profiles are in the range of the data at all axial locations except for the "outlet", so some adjustments may need to be made in the wall temperature profile near the outlet to reduce simulation temperatures there. Third, the NO$_x$ concentrations computed in the simulations are an order of magnitude higher than the experimental data except for near the "outlet." In the simulation, thermal NO$_x$ is the only NO$_x$ formation mechanism, so the NO$_x$ production rate is a function of the local N$_2$ and O$_2$ concentrations as well as the gas temperature. Analysis is ongoing to determine the root causes of these discrepancies so that the parameter space can be adjusted for the V/UQ analysis.

With a few additional simulations, the number of parameters can be narrowed (focusing on 2-3 that have the greatest effect on the output variables of interest) and the appropriate parameter space for the V/UQ analysis determined. The research team has dedicated time on a large

supercomputer in the next two months so that the remaining simulations and V/UQ analysis can be completed.

Subtask 3.3 - Development of Oil and Gas Production Modules for CLEAR_{uff} (PI: Terry Ring)

There was no work performed on this project during the quarter due to time commitments with Subtask 6.3 on the part of team members.

Subtask 3.4 - V/UQ Analysis of Basin Scale CLEAR_{uff} Assessment Tool (PI: Jennifer Spinti)

The project is on hold pending the completion of Subtask 6.3 and 3.2. The research team members are meeting in early August to define the next steps and assign tasks for the completion of milestones.

Task 4.0 - Liquid Fuel Production by In-situ Thermal Processing of Oil Shale/Sands

Subtask 4.1 (Phase I) - Development of CFD-based Simulation Tools for In-situ Thermal Processing of Oil Shale/Sands (PI: Philip Smith)

The Subtask 4.1 team submitted a topical report that details the heat transfer process inside the representative computational geometry. The report was approved by Robert Vagnetti during this quarter.

Subtask 4.1 (Phase II) - Development of CFD-based Simulation Tools for In-situ Thermal Processing of Oil Shale/Sands (PI: Philip Smith)

The Subtask 4.1 team has undergone personnel changes that have necessitated a refinement of the timetable for completion of the project deliverables. In the past year, the graduate student working on this project changed his research topic and was unable to continue with this research. The new graduate student responsible for completing this project had to go through a steep initial learning curve, both in using the simulation tool as well as the theoretical knowledge required for the completion of this project. This change delayed the implementation of the kinetic model into the high-performance computing (HPC) CFD-based simulations. Therefore, team researchers will complete their deliverables in conjunction with and within the time frame of Subtask 7.3. With this refinement of the deliverable date, the research team will have sufficient time to both implement the appropriate kinetic model as well as perform a V/UQ study of the process. The ultimate goal of the project is to develop simulation tools using the commercial software Star-CCM+ to study the thermal heating of oil shale inside the Red Leaf Resources' ECOSHALE capsule.

In the previous quarter, team researchers summarized several scientific papers that describe fundamentals of oil shale kinetics: Campbell et al. (1978), Sweeney et al. (1987), Granoff and Nuttall (1978), and Allred (1966). These papers have been used as a basis for the implementation of a kinetic model to study product yield as a function of temperature and oil shale properties.

The initial focus of model development reaction chemistry model implementation was the Campbell et al. (1978) paper as it provides experimental results for a simplified case of heating a solid block of oil shale. Results from a simulation to predict the oil yield from a specified block of shale have been analyzed during this quarter. The simulation results are not consistent with the experimental data in Campbell et al. (1978). The experimental initial and boundary conditions could be one reason for the inconsistencies since the paper does not provide an

exact description of what they are. Team researchers are continuing to analyze their simulation settings and results for additional sources of inconsistencies.

Based on this preliminary analysis, the Subtask 4.1 team has decided to include additional scientific papers in their study, Tiwari and Deo (2012) and Hillier and Fletcher (2010), and thus expand the knowledge base for coupling experiments with simulation. These papers are the result of research conducted for Subtask 4.3; they provide more detailed descriptions of their respective experiments, which is essential for a proper CFD simulation setup. Team members have met with the authors to obtain more detailed explanations of the experiments and have begun to incorporate these details into their simulation setup. These simulations will be run in the next quarter.

Subtask 4.2 - Reservoir Simulation of Reactive Transport Processes (PI: Milind Deo)

The Subtask 4.2 team completed the milestone to examine pore-level change models and their impact on production processes in both commercial and new reactive transport models

In 1980, the United States Office of Technology Assessment published *An Assessment of Oil Shale Technologies* (OTA, 1980). Only two in situ technologies were evaluated, true in situ (TIS) and modified in situ (MIS). TIS technology consisted of explosives being detonated underground to generate permeability. MIS technology consisted of the mining of a portion of the oil shale with underground mining techniques, followed by rubblization with explosives. A study of pilot scale processes in Wyoming (Goldstein, 1978) concluded that "calculations have shown that a minimum void volume of 10% is necessary to initiate and sustain in-situ combustion and retorting." If that void volume was not present, flow in the reservoir would not be possible. Current in situ retorting strategies by Shell, ExxonMobil, and AMSO do not include a rubblization step. Heating in these current processes is initially conductive, and permeable pathways are believed to be generated by solid kerogen conversion to fluids and by rock mechanical failure or fracturing. Understanding the geomechanics involved in such processes is essentail since oil shale resources are typically characterized by very low initial permeability.

In a paper by Tisot et al. (1970), the mechanical properties of oil shale while subjected to heat and stress were evaluated. This paper concluded that "...kerogen ... is the predominant contributor to [rich oil shales] properties and to their response to heat and stress." Fragments of oil shale were placed in a stress environment and heated. It was found that, "In most instances the induced permeability in the column of fragments was reduced to zero." A final conclusion stated, "This investigation shows that structural deformation in rich oil shales can be expected to occur ahead of the retorting zone." A study by Thomas et al. (1966) reported similar experiments with overburden pressure. The study concluded that thermal fracturing does not occur in an overburden environment, but some permeability is still generated by some other mechanism. Prats (1977) performed experiments, including field tests, where nahcolite was solution mined from the oil shale prior to retorting. Solution mining of nahcolite created free surfaces for oil shale rock to fail by "stress release at open faces, thermally induced stresses, and thermally induced pressures." (Prats, 1977). In *Oil Shale: A Solution to the Liquid Fuel Dilemma*, Burnham (2011), referring to the AMSO process, states "The shale ... will want to expand as it is heated, but since it is confined by the cool shale, it undergoes compressive failure and fills the high permeability conduit with rubble" and "... the thermomechanical fragmentation process is expected to propagate out to retort diameters of 100 or more feet ..." In the chapter of the same book describing the Shell ICP (Ryan et al., 2011) "... it was hypothesized that bulk heating with thermal conduction would generate permeability and that the gases generated during retorting will drive liquid oil from the pores of the shale." Finally ExxonMobil (Symington et al., 2011) states, "... hydrocarbons will escape from heated oil shale even under in situ stress. … [Our] set of experiments clearly indicates that, even under

conditions of overburden stress, the kerogen conversion and expulsion process creates porosity and permeability that was not present in the original oil shale." The current consensus by industry is that thermal stresses in oil shale will generate permeable pathways for fluids to flow.

Subtask 4.2 researchers used three different approaches to study thermally induced geomechanical changes:

- Material point method (MPM) in the Uintah Computation Framework (UCF) developed at the University of Utah

- Thermal geomechanical options in STARS – a commercial thermal simulator

- Addition of thermal geomechanical capabilities to the Advanced Reactive Transport Simulator (ARTS) at the University of Utah.

The MPM Method

MPM, implemented in the UCF developed at the University of Utah, has the capability of modeling thermal stresses, large material deformation, and mechanical failure due to stresses. Figure 6 shows Uintah MPM simulation results for a two-dimensional oil shale block (1 foot x 1 foot) where the bottom and side boundaries are confined. The top boundary is free to deform and move. The bottom boundary is suddenly subjected to 1000°C, and the thermal stress profiles can be seen traveling through the block. Failure criteria can be added to the simulation to approximate crack generation and propagation.
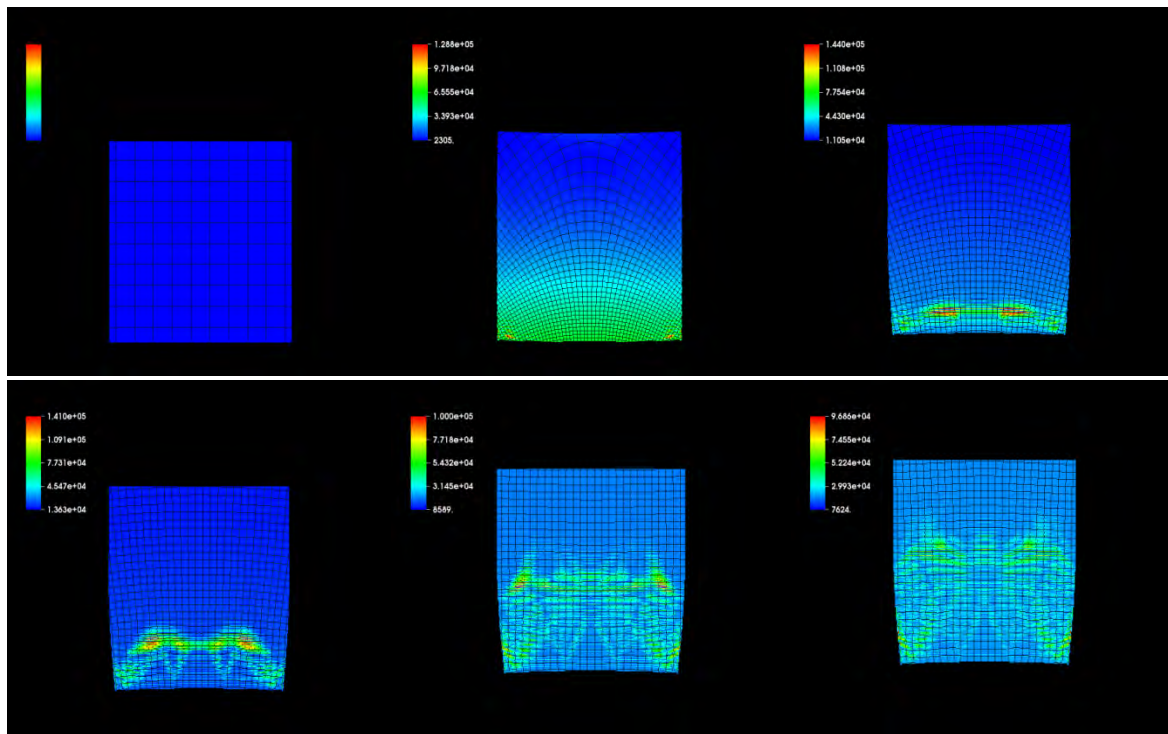
Figure 6: Thermal stress deformation observed in the MPM module of the UCF.

STARS Simulations

Simulations in STARS that included the geomechanical module and a permeability/fluid porosity relationship shown in Equation (1) were also explored.

$$k = k_0 \exp\left(k_{mul} \frac{\phi - \phi_0}{1 - \phi_0} \right)$$

(1)

In these simulations, a 900-foot horizontal heater supplies heat to the oil shale resource with a horizontal producer at the bottom. The simulated geometry is shown in Figure 7.
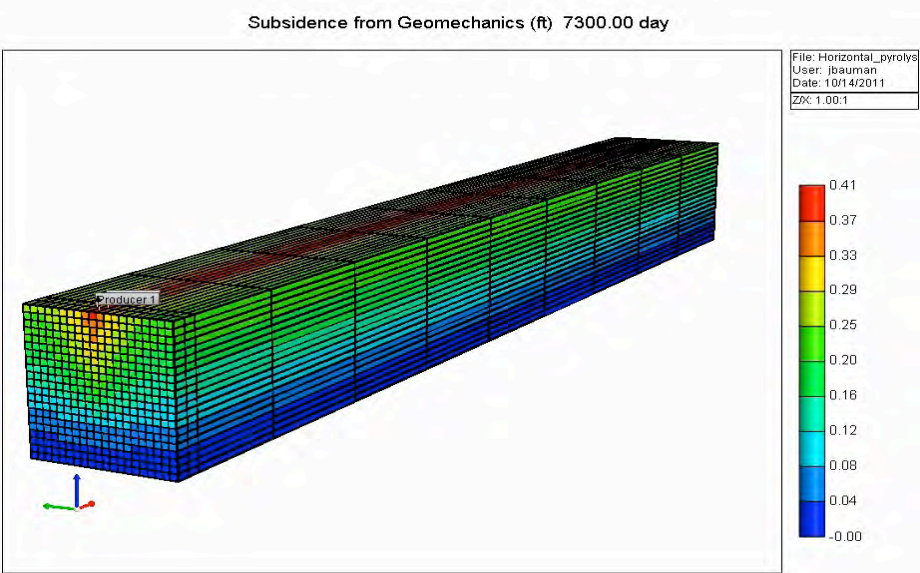
Figure 7: The geometry simulated in STARS.

The oil production results from sensitivity studies (with and without the geomechanics module and sensitivity to a parameter in Equation (1)) are shown in Figure 8. Changes in the geomechanics module and in the permeability model can make a significant difference in predicted results.
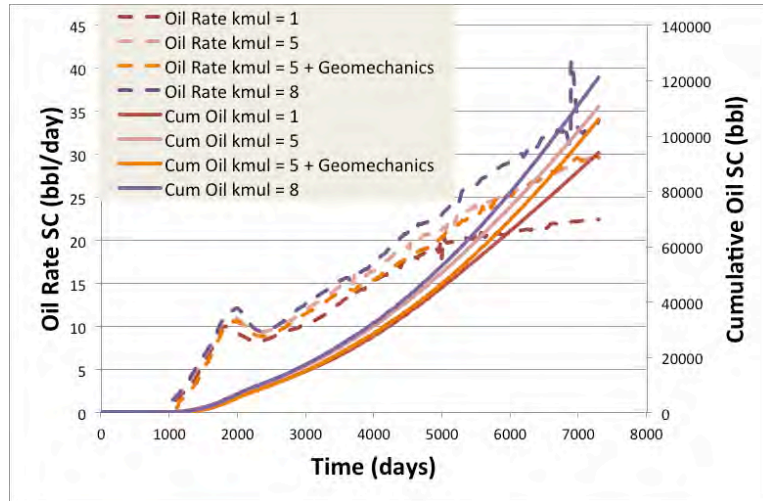
Figure 8: Effect of the "kmult" parameter and the geomechanics module on oil production.

Integration of Geomechanics with Thermal Reservoir Simulation

A geomechanical model was integrated with a K-value based thermal reservoir model in ARTS. A linear thermal poroelasticity stress constitutive law is used:

$$\sigma = \sigma' - \alpha P - 3\beta K_b T \tag{2}$$

where σ' is the effective stress, α is the Boit coefficient, β is the linear thermal expansion coefficient, K_b is the bulk modulus, P is the pore pressure and T is the temperature change in the reservoir.

In the ARTS framework, the K-value based thermal reservoir model and a geomechanical model with thermal stress constitutive relationship in Equation (2) are coupled to simulate a thermal recovery process. An iterative coupling scheme is used, and the coupling process is shown in Figure 9.

14
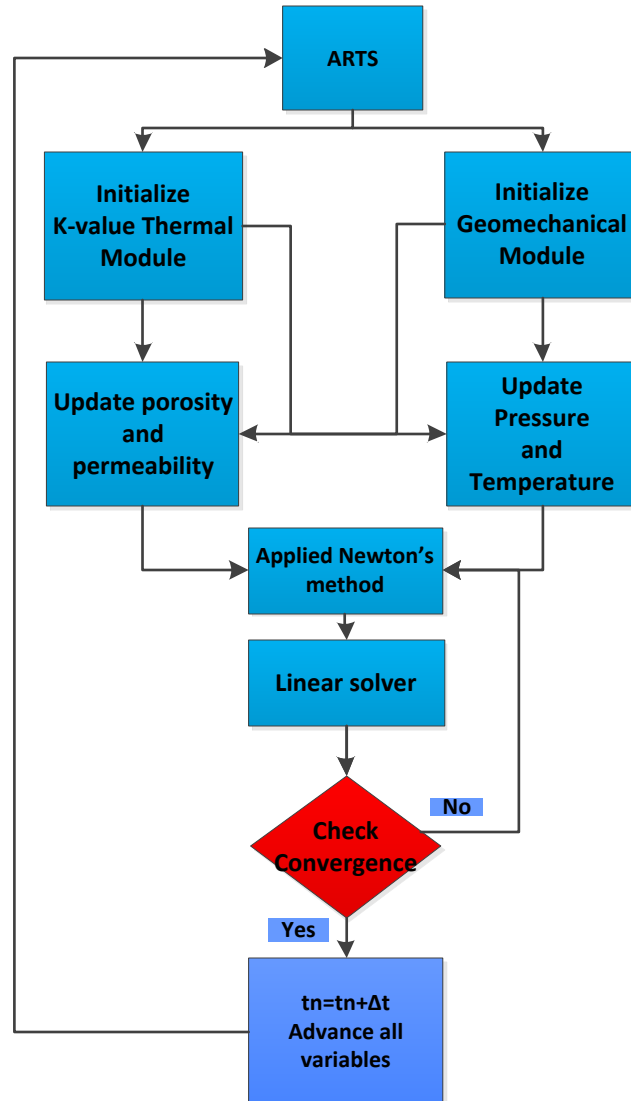
Figure 9: Geomechanical coupling process in ARTS with thermal stress model.

The thermal reservoir model and geomechanical model are both initialized in the beginning of the simulation. The temperature and pressure in the geomechanical model are updated by the thermal reservoir model, and the porosity and permeability in the thermal reservoir model are updated by the geomechanical model. With the updated information, the whole system is solved through a linear solver loop. Once convergence is achieved at a given time, iterations begin at the next time step.

In addition, ARTS has the capability of modeling complex fracture networks through the Discrete Fracture Network (DFN) model and the thermal model can model the complex kinetics that occur during the thermal recovery process. All these features give ARTS an advantage over the other codes for studying the thermal recovery process with geomechanics.

A simple demonstration case is presented to show the capability of ARTS in modeling a reservoir with geomechanics and a thermal stress model. A reservoir with a complex fracture network of almost 50 fractures is producing oil through a steam flooding process. Some key

parameters are listed in Table 1. The linear thermal expansion term is relatively small and does not show much impact in this case study; see Figure 10.

Table 1. Key parameters for ARTS reservoir simulation with geomechanical coupling and thermal stress.

Reservoir Geometry (feet)	1200*1200*200
Young's Modulus (psi)	1e6
Poisson's ratio	0.2
Linear thermal expansion coefficient (1/R)	1e-7
Initial pressure (psi)	400
Initial temperature (R)	620
Initial oil saturation	0.45
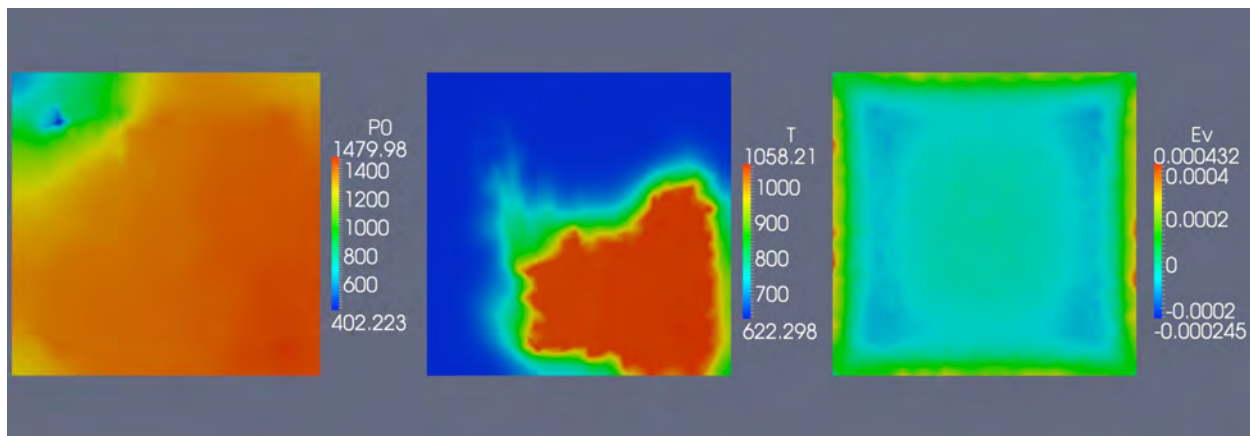
Figure 10: Oil pressure (left), temperature (middle), and volume change (right) distributions at 800 days.

Subtask 4.3 – Multiscale Thermal Processes (PI: Milind Deo, Eric Eddings)

Three project milestones are due or past due; of the three, one was completed in this quarter and two more are nearing completion as described below.

The milestone to develop a model that accounts for heat & mass transfer effects in predicting product yields & composition was completed. Detailed kinetic models based on the concepts of distribution of activation energies for the conversion of kerogen were derived using thermal gravimetric analyses (TGA). Equivalent algebraic expressions for these models were obtained. The kinetic models were then incorporated into a finite-element model in the COMSOL multiphysics framework. The COMSOL model consists of different modules as shown in Figure 11. The heat transfer consists of conduction and convection in a "grain model" concept. Additionally, different types of mass transfer representations were implemented.
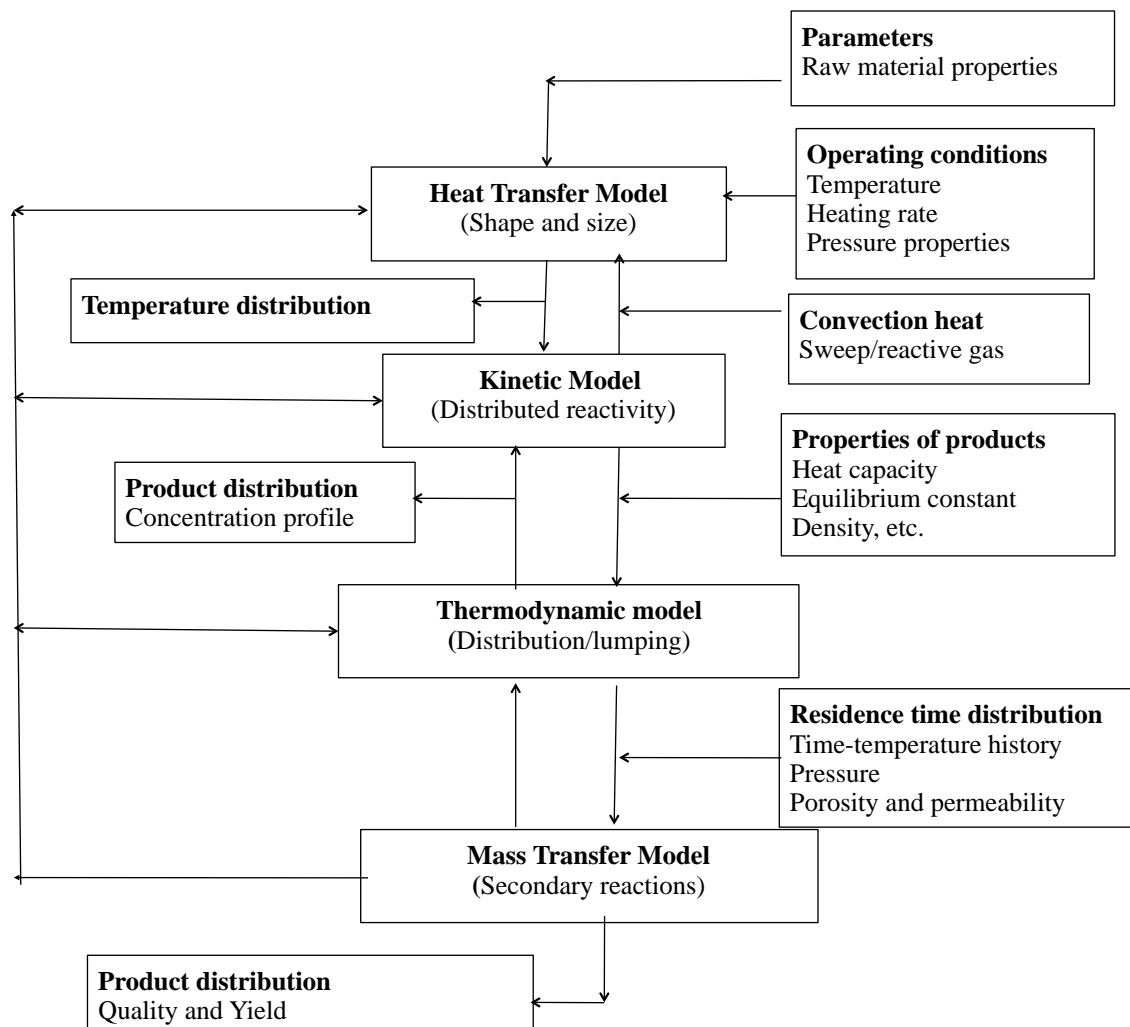
Figure 11: The COMSOL framework where the heat and mass transfer were combined with rigorous kerogen decomposition kinetics.

The models, their implementation and detailed results are provided in Chapter 10 the recently published dissertation of Pankaj Tiwari entitled "Oil Shale Pyrolysis: Benchscale Experimental Studies and Modeling" (2012). Chapter 10 is attached to this report as Appendix C.

The milestone to complete core sample pyrolysis at various pressures and to analyze product bulk properties and composition is nearing completion. Team researchers have completed the TGA pyrolysis set at three heating rates at atmospheric pressure with two runs at each condition to help with statistics. They are nearing completion on the pressurized samples after performing repairs on the TGA. They have also completed the kinetic rate analysis of the atmospheric samples, as per a previous method developed under James Hillier (Hillier et al., 2010; Hillier and Fletcher, 2011; Hillier, 2011). The bulk properties and composition have been completed by Pankaj Tiwari.

The milestone to collect and perform chemical analysis of condensable pyrolysis products from demineralized kerogen is also close to completion. All of the kerogen retort samples have been collected, and the tar and char samples have been sent to the NMR laboratory at the University of Utah for analysis. Dr. Mayne and Dr. Solum will complete this analysis during the next

quarter. Team members have also collected gases and performed the FTIR analysis at three temperature ranges. They are obtaining calibration gases to make this analysis more quantitative. The GC/MS has also been repaired and that analysis will be performed soon.

Pyrolysis of Demineralized Kerogen

Demineralized kerogen samples were pyrolyzed in a kerogen retort in order to collect sufficient quantities of gas, tar, and char for subsequent chemical analysis. This quarter additional experiments were performed to complete the data sets for the GR-2.9 and GR-3.9 demineralized kerogen samples. Samples were heated at a standard heating rate of 10 K/min to temperatures between 300°C and 575°C. Tars from each experiment were condensed on glass wool and then cooled using a dry ice/isopropanol mixture. Figure 12 shows a schematic of the reactor used to perform experiments.
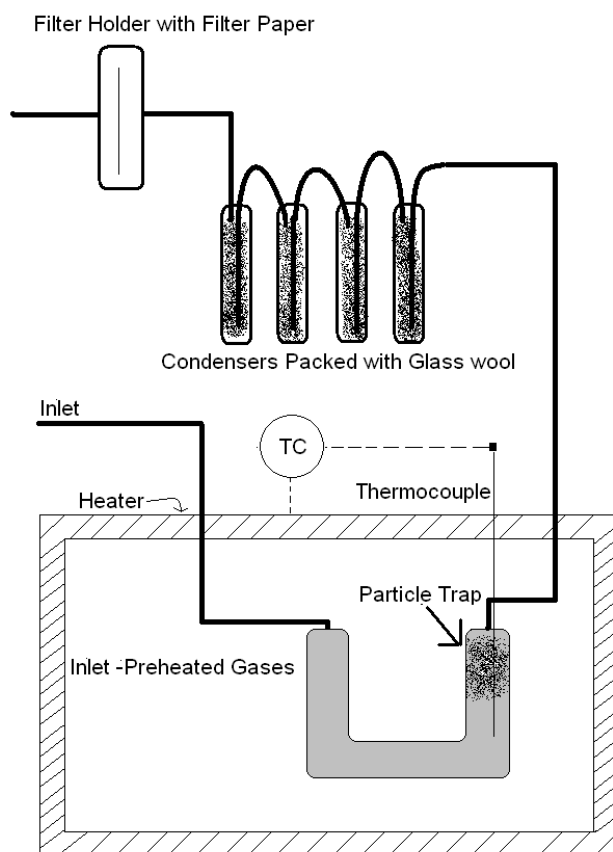
Figure 12. Schematic of the kerogen retort.

Masses of each individual section of the reactor were recorded both before and after each experiment to determine yields of char, tar, and light gases. All kerogen retort experiments have now been completed. Yields of gas, tar, and char at different temperatures are plotted in Figure 13.

18
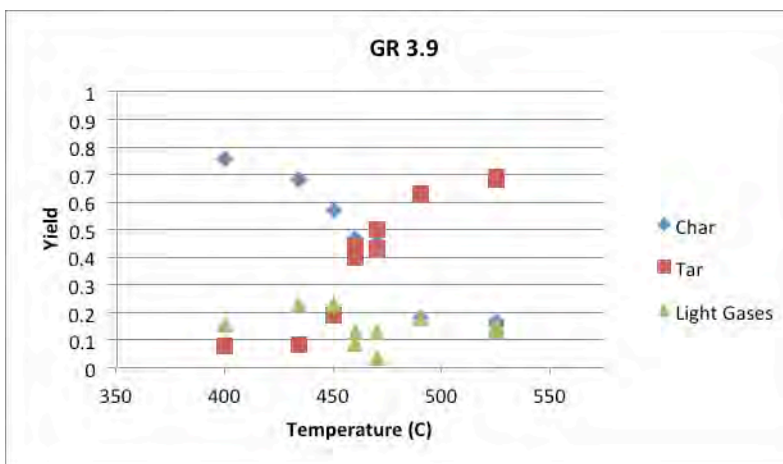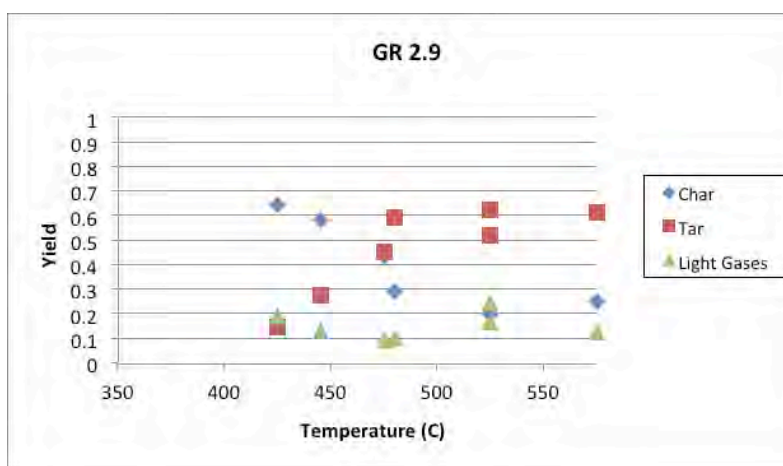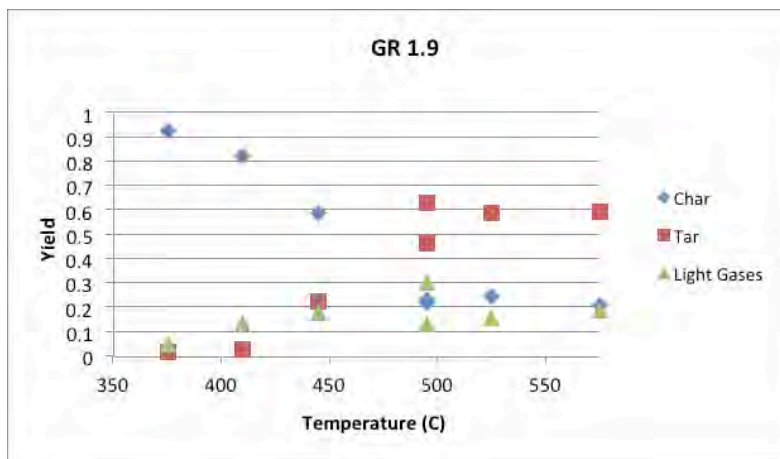
Figure 13: Complete results from retort of GR-1.9 (top), GR-2.9 (middle), and GR-3.9 (bottom).

Chemical Analysis of Pyrolysis Products

After tars were collected on glass wool packed into the cooled condensers, minimal amounts of dichloromethane were used to dissolve condensed tars for testing. Standard dichloromethane was used to prepare samples for analysis in the GC/MS. Deuterated dichloromethane was used

to dissolve tar samples to be analyzed using NMR spectroscopy. Deuterated samples were shipped to the University of Utah NMR lab along with corresponding char samples. Repeat pyrolysis experiments were run to collect enough char sample for analysis where char yield was low.

Also this quarter, a technician was called in to repair the broken GC/MS. The GC/MS power supply was repaired, and team researchers are preparing to analyze some of the tar samples obtained from the kerogen retort. They also began the quantitative analysis of the FTIR spectral data obtained for the gases from the kerogen retort experiments.

Pyrolysis Kinetics

The set of atmospheric TGA experiments was completed this quarter, including duplicate measurements for statistical analysis. Pulverized samples of oil shale were pyrolyzed in helium at heating rates of 1, 5, and 10 K/min. Determination of kinetic parameters was also performed for the atmospheric pyrolysis data, using (a) a first-order model, and (b) a distributed activation energy (DAEM) model. Mass release data from all three heating rates were fit simultaneously, along with the derivative of the mass vs. time curves (Hillier et al., 2010; Hillier and Fletcher, 2011; Hillier, 2011). Resulting kinetic parameters are shown in Table ** for the GR-1, GR-2, and GR-3 samples. Following repairs on the TGA, many of the pressurized (40 bar) TGA experiments have been completed. Results for the GR-1 sample are also reported in Table 2; only a few pressurized runs remain until GR-2 and GR-3 may be analyzed completely. The difference in activation energy between the samples is negligible and is consistent with results from previous experiments on Colorado oil shale samples.

Table 2. Kinetic coefficients determined from the atmospheric TGA experiments conducted at heating rates of 1, 5, and 10 K/min.

Sample		First-Order		DAEM	
		1 bar	40 bar	1 bar	40 bar
GR-1	A (s^{-1})	8.86×10^{13}	2.79×10^{13}	9.21×10^{13}	1.01×10^{14}
	E (kJ/mol)	221	219	223	215
	σ (kJ/mol)			4.0	2.6
GR-2	A (s^{-1})	4.48×10^{13}		2.63×10^{14}	
	E (kJ/mol)	217		228	
	σ (kJ/mol)			2.6	
GR-3	A (s^{-1})	9.52×10^{13}		9.35×10^{13}	
	E (kJ/mol)	220		222	
	σ (kJ/mol			4.6	

Subtask 4.4 - Effect of Oil Shale Processing on Water Compositions (PI: Milind Deo)

This project has been completed.

Subtask 4.5 - In Situ Pore Physics (PI: Jan Miller, Chen-Luh Lin)

The Subtask 4.5 team has one milestone and one deliverable that are due. However, their completion has been delayed by the lack of available samples under various loading conditions to be provided by Subtask 4.7. It is proposed the milestone and the final deliverable (listed below) be completed by Dec. 31, 2012.

- Complete pore network structures & permeability calculations of Skyline 16 core directional/anisotropic, mineral zones) for various loading conditions, pyrolysis temperatures, & heating rates
- Topical report summarizing results of pore network structures & permeability calculations on Skyline 16 cores

Subtask 4.6 - Atomistic Modeling of Oil Shale Kerogens and Oil Sand Asphaltenes (PI: Julio Facelli)

The only deliverable not completed for this project is the preparation of a paper on kerogen modeling. The project team is awaiting input from their colleagues at Argonne National Laboratory before submitting the paper to a journal for publication. A preliminary draft of the paper is attached to this report as Appendix D.

Subtask 4.7 - Geomechanical Reservoir State (PI: John McLennan)

The milestone to complete the experimental matrix is again delayed. The first test was postponed while some modifications were made to the system (see details below) and has been rescheduled for July 23, 2012. The nominal (subject to change) testing matrix is given in Table 3.

Table 3. Revised test matrix.

Test	Temperature (°C)	Confining Pressure (psi)	Comments
1	Ambient	0	Designed to determine any design modifications required, to ensure calibration of LVDTs and load cell (both already independently calibrated and to generate information on a White River oil shale sample. Measure the yield and other properties independently.
2	50	0	Duplication of AMSO testing on a White River oil shale sample, at a low temperature. Hook up the nitrogen lines to flow through the sample although no effluent is expected.
3	100	0	Idem. A separation system is being fabricated. This will be connected and debugged. We need to determine if there needs to be an external Plexiglas collection system purged with nitrogen around the sample.
4	200	0	Idem
5	400	0	Idem – precise temperature to be determined.
6	400	0	Idem - Using Skyline 16 parallel to bedding sample
7	400	0	Idem - Using Skyline 16 perpendicular to bedding sample
89			TBD – could be creep testing and/or undrained testing

During this quarter, the project team made final adjustments to the triaxial testing equipment following pre-test safety evaluations. These adjustments included the addition of mechanical (Bourdon tube) pressure gauges and additional pressure relief valves. A description of the fabricated equipment follows.

The vertical stress in-situ is simulated by a hydraulic jack. The original hydraulic jack is shown in Figure 14(a). It is designed for tests on four-inch samples. Since team members are currently testing Skyline and White River Mine samples that are 1.5-inches in diameter, a smaller jack has been substituted. At the top of the hydraulic jack is the load cell. The load cell and the pressure transducers for the pump that drives the jack will be used to determine the axial load.

Figure 14(b) shows the actual fixture. The "1" indicates the upper end cap which rests on top of the sample. The sample is jacketed in thinly machined, flexible copper tubing to prevent the confining fluid (N_2) from penetrating. Normally, shrink fit Teflon or polyurethane would be used for this purpose, but copper is chosen here because of the elevated temperature. The sample (1.5-inch diameter by 3-inches long in this case) is hidden by the electrical clamshell heater ("2") that is used to heat the sample to a controlled temperature up to 1000°F. The orange band keeps the two sides of the heating fixture taut. A black controller cable is seen at the upper left of the heater. Clamped to the upper ("1") and lower ("4") sample end caps is a fixture ("3") for mounting three linear variable differential transducers (LVDTs) at 120°. The LVDTs entail a slender, cylindrical ferromagnetic core that slides between solenoid coils. The induced current in two of the coils depends on the precise position of the coil. Hence, relative shortening or lengthening of the oil shale sample is reliably determined from these devices. Three LVDTs are used so that an average measurement can be made to account for nonuniform axial deformation. The shakedown testing will only use axial measurements. A supplementary system is being designed for radial strain measurements. Label "5" is an adaptor affixing to the load cell.

(a)   (b)
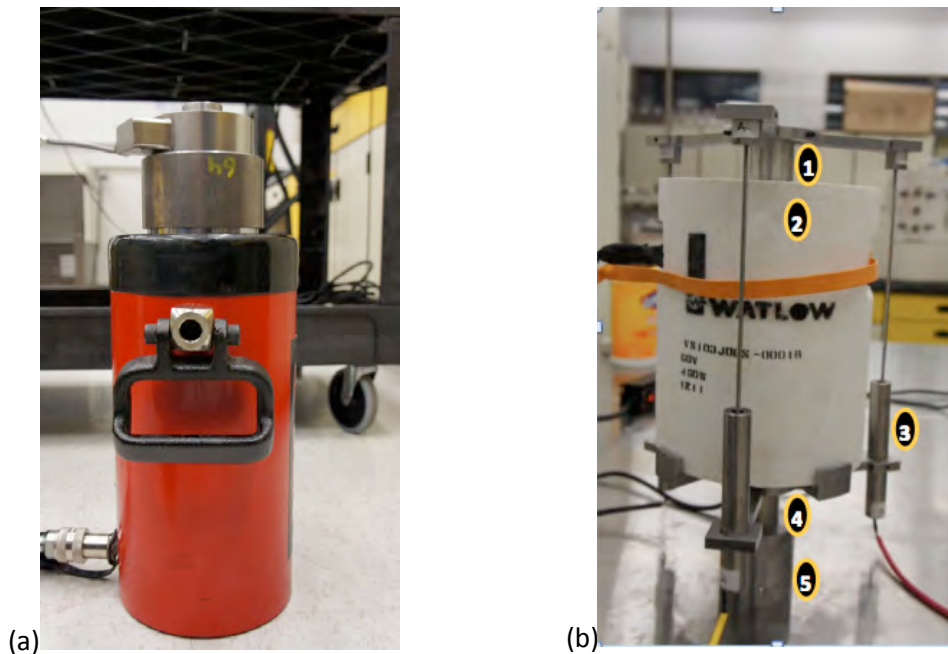
Figure 14: (a) Hydraulic jack with load cell on top. These will not be exposed to elevated temperature. (b) Heater and axial strain measuring devices.

Figure 15(a) shows the heater and Figure 15(b) shows a sample with its copper jacket and end caps.
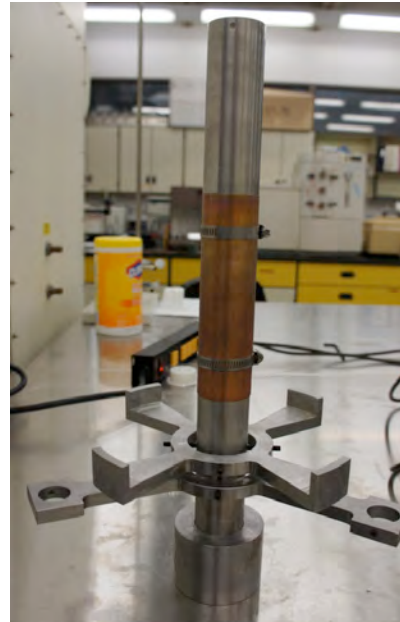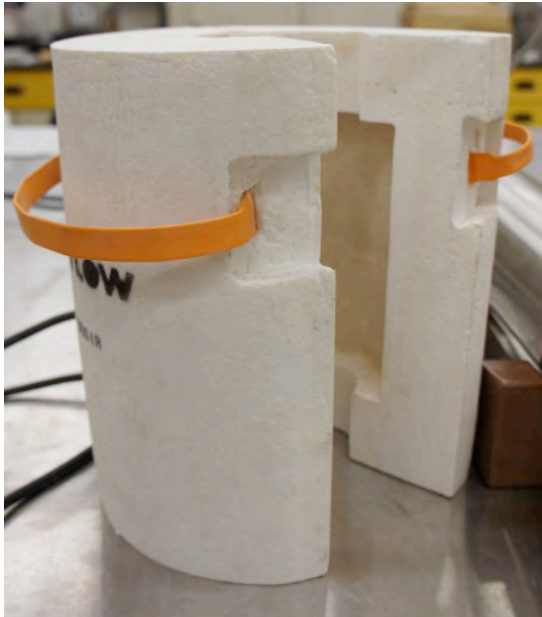
Figure 15: (a) Clamshell heater. (b) Sample with the upper end cap for axial load transfer, a copper jacket clamped to the end caps above and below the sample, and a lower end cap fitting into the load cell at the bottom. A four-armed holder for the heater is visible as is the lower 3-armed mount for the LVDTs.

Figure 16 (left) is a close-up of the axial load cell that is immediately below the fixture shown in Figure 15(b). To provide precise axial strain or stress rate control, the hydraulic jack is driven by an Isco pump, as shown in Figure 16 (middle).

Figure 16: (left) Load cell mounted on top of the hydraulic jack. (middle) Isco pumps for precise pressurization of the jack and controlled application of axial load. (right) Accumulator that separates hydraulic fluid in the pump from the hydraulic fluid in the flexble hose for the jack.

All data acquisition in the fixture uses Labview or Opto. The complete testing fixture (using the hydraulic jack for the four-inch diameter samples) is shown in Figure 17. The first testing is unconfined, i.e. there is no confining pressure applied to the sample. These tests are being run outside of the pressure vessel. All that is required is resistance to axial movement of the jack so that an axial load can be transferred to the sample. This resistance will be provided by a structural loading frame in the Civil Engineering Department at the University of Utah.
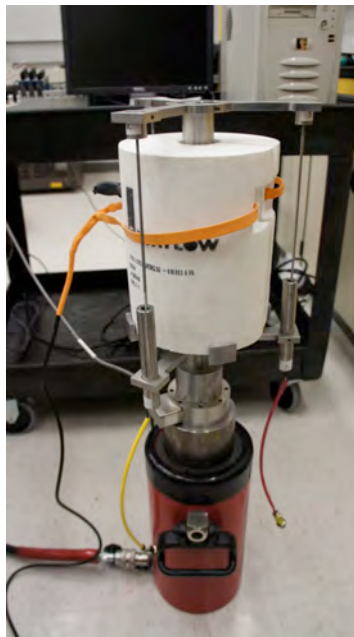
Figure 17: Complete sample configuration for shakedown testing.

After the unconfined measurements are carried out (axial stress only), measurements at confining pressure will be performed using the pressure vessel shown in Figure 18.
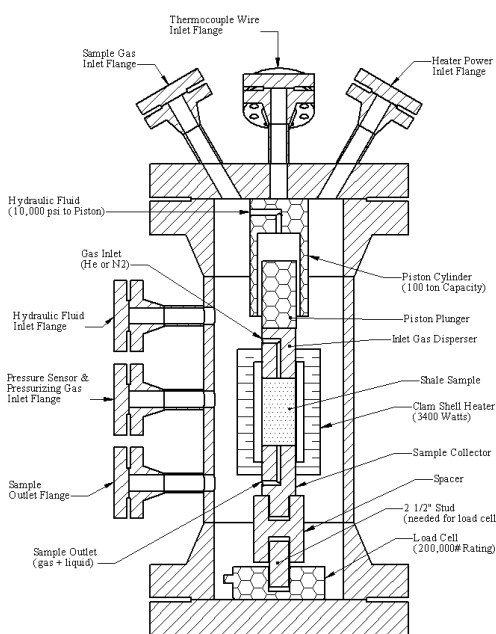
Figure 18: Schematic cross-sectional view and photograph of pressure vessel to be used for applying confining pressure.

Subtask 4.8 - Developing a Predictive Geologic Model of the Green River Oil Shale, Uinta Basin (PI: Lauren Birgenheier)

Subtask 4.8 researchers drafted the Asphalt Wash 1 core and calibrated, graphed and summarized elemental abundance (X-Ray Fluorescence) data. Additionally, L. Birgenheier and M. Vanden Berg are writing a manuscript to be published in a special edition book titled "Stratigraphy and Limnogeology of the Eocene Green River Formation" that documents regional and stratigraphic changes in the Green River Formation, Uinta Basin, Utah.

Subtask 4.9 - Experimental Characterization of Oil Shales and Kerogens (PI: Ronald Pugmire)

During this quarter, the milestone to develop a structural model of kerogen and bitumen was completed. The milestone goal was to use a variety of analytical techniques to obtain structural data on the kerogen isolated from oil shale. The structural model has been developed and the results of the studies outlined below are being gathered together for publication. Researchers have also started an early draft of one of two final deliverables, a paper on the chemical characterization of the oil shale and kerogen which will include the experimental data in the milestone. This paper will be submitted in the fall, so the July 2012 due date will need to be changed to October 2012.

Sample preparation/characterization

Kerogen and bitumen were isolated from each of the three one-foot shale segments which the oil shale team identified as the segments to be studied (named GR-1, GR-2 and GR-3). The one-foot segments were divided up according to the needs of the different research groups involved; the fragments left when the sampling was completed were crushed using a ceramic device to avoid introduction of metal to the sample and then sieved to 100 mesh. All the results listed below, unless explicitly stated otherwise, were obtained on either this 100 mesh ground shale or on the kerogen and bitumen extracted from this ground shale.

Ashing was performed on the oil shale at 505°C by Tom Fletcher's group to determine the organic content of each of the shale; results are shown in Table 4. Ashing was also performed on the isolated kerogen samples to determine the residual mineral matter in the kerogen samples: GR-1 – 5.0%; GR-2 (two samples) – 4.1% and 3.0%; GR-3 – 4.7%.

Table 4. Ashing test results for crushed oil shale samples.

		GR-1	GR-2	GR-3
Trial 1	Water %	0.47%	0.34%	0.39%
	Ash %	73.63%	85.46%	79.16%
	Organic %	25.90%	14.20%	20.45%
Trial 2	Water %	0.36%	0.19%	0.37%
	Ash %	73.65%	85.42%	79.06%
	Organic %	26.00%	14.39%	20.57%

The only reliable data for kerogen/bitumen yield from the extraction process, 17%, came from GR-3. Of this total yield, 88% was kerogen and the remainder was bitumen.

In addition, the isolated kerogen was sent to Huffman Laboratory for elemental analysis. Results of this analysis are shown in Table 5. On the dry ash free basis, this analysis results in the following molecular compositions: GR1 kerogen – $C_{100}H_{150}N_3O_8S_1$; GR2 kerogen – $C_{100}H_{153}N_3O_8S_1$; GR3 kerogen – $C_{100}H_{148}N_3O_8S_2$.

Table 5. Elemental analysis results for isolated kerogen samples.

SEQUENCE/ SAMPLE ID	01 GR1	02 GR2	03 GR3
Drying Loss---%- - -	0.77	0.39	0.54
Carbon--------%- - -	73.27	73.96	73.22
Hydrogen------%- - -	9.27	9.49	9.14
Nitrogen------%- - -	2.62	2.45	2.43
Oxygen (diff)-%- - -	7.64	7.64	7.78
Sulfur--------%- - -	1.90	1.87	3.57
Ash-----------%- - -	5.30	4.60	3.87

*Bitumen Analysis/Structural Model*

The bitumen samples from each of the segments were analyzed by solution ^{13}C NMR. The experiments were done in a quantitative manner. In addition, DEPT spectra, which differentiate between non-protonated, CH, CH$_2$, and CH$_3$ carbons, were recorded. The analysis of these spectra shows that the samples are 92±2% aliphatic. Using a comparison of the chemical shifts of the bitumen with known chemical shifts in wax, it was determined that the bitumen samples are composed mainly of long aliphatic chains with an average chain length of 23±3 carbons. In addition, there is very little branching observed.

Kerogen Analysis/Structural Model

Both the original shale and the isolated kerogen were analyzed by ^{13}C solid state NMR (ssNMR), small angle X-ray scattering (SAXS), and atomic pairwise distribution function (PDF) measurements. In addition, kerogen samples were provided to the Subtask 4.3 for pyrolysis and to Subtask 4.5 for CT analysis. The structural information was used to evaluate the atomistic models being developed in Subtask 4.9.

^{13}C ssNMR: Both the ground shale and the isolated kerogen were studied by ^{13}C ssNMR using procedures developed in the Pugmire/Grant group for the analysis of coals. Sample ssNMR spectra of the shales and the corresponding kerogens are seen in Figure 19. The ssNMR analysis results are presented in Table 6. The kerogen samples isolated from each of the three segments are very similar. Any differences measured are within the experimental error of the measurements. Using the data from the elemental analysis, average cluster molecular weights can be obtained.
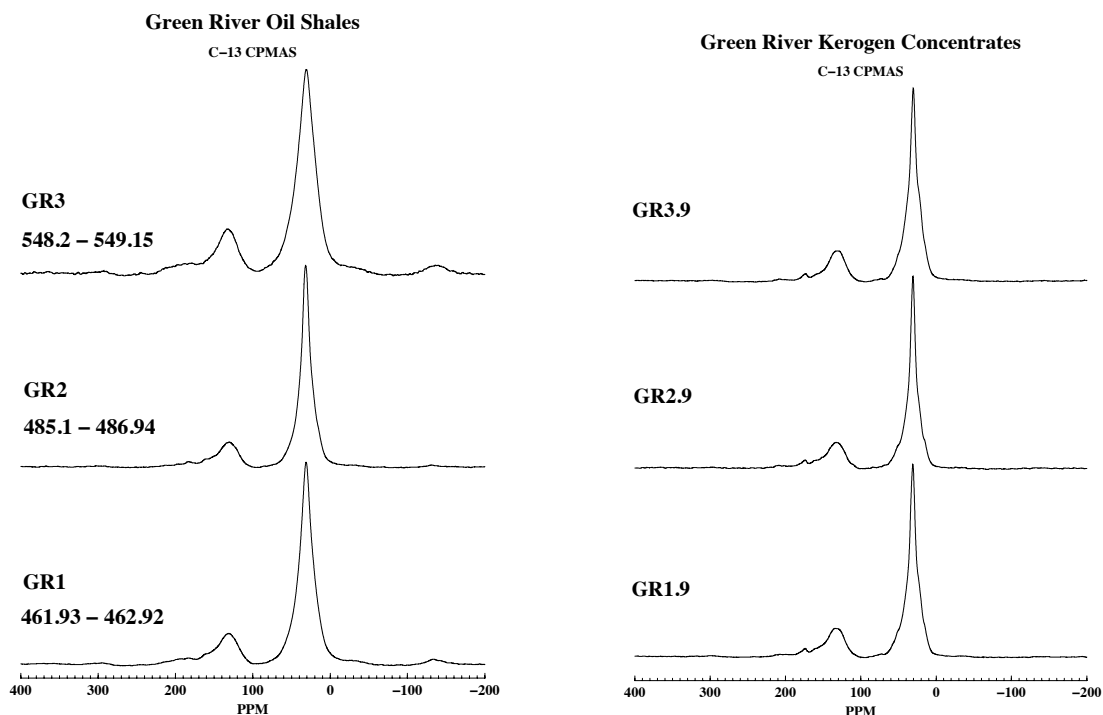
Figure 19: Sample ssNMR spectra of the GR-1, GR-2, and GR-3 oil shale samples and the corresponding kerogens.

Table 6. Green River shales and their kerogens from three cores.

Structural Parameters

Compound	f_a	f_a^C	f_a^O	f_a^{OO}	$f_{a'}$	f_a^H	f_a^N	f_a^P	f_a^S	f_a^B	f_{al}	f_{al}^H	f_{al}^*	f_{al}^O
GR1 (CP) cr	0.25	0.04	0.02	0.02	0.21	0.07	0.14	0.04	0.07	0.03	0.75	0.62	0.13	0.02
GR1.9 (CP) $C_{100}H_{150}N_3O_8S_1$	0.24	0.04	0.01	0.03	0.20	0.06	0.14	0.03	0.07	0.04	0.76	0.65	0.11	0.00
GR1.9 (SP)	0.25										0.75			
GR2 (CP) nc	0.22	0.04	0.02	0.02	0.18	0.06	0.12	0.03	0.06	0.03	0.78	0.65	0.13	0.00
GR2.9 (CP) $C_{100}H_{153}N_3O_8S_1$	0.23	0.05	0.02	0.03	0.18	0.06	0.12	0.03	0.06	0.03	0.77	0.66	0.11	0.01
GR2.9 (SP)	0.24										0.76			
GR3 (CP) cr	0.27	0.03	0.01	0.02	0.24	0.06	0.18	0.04	0.08	0.06	0.73	0.60	0.13	0.05
GR3.9 (CP) $C_{100}H_{148}N_3O_8S_2$	0.24	0.04	0.01	0.03	0.20	0.05	0.15	0.03	0.07	0.05	0.76	0.63	0.13	0.00
GR3.9 (SP)	0.25										0.75			

Lattice Parameters

| Compound	χ_b	C	$\sigma+1$	P_0	B.L.	S.C.	M.W.	M_δ
Gr1 (CP)	0.143	8.4	4.4	-0.18	--	--	--	--
Gr1.9 (CP)	0.200	10.0	5.0	-0.10	--	--	776	131
Gr2 (CP)	0.167	9.0	4.5	-0.44	--	--	--	--
Gr2.9 (CP)	0.167	9.0	4.5	-0.22	--	--	775	148
Gr3 (CP)	0.250	12.0	6.0	-0.08	--	--	--	--
Gr3.9 (CP)	0.250	12.0	5.9	-0.30			946	135

Average structural values for the three samples are listed below:

- Aromaticity ($f_{a'}$) = 0.193
- Aromatic Cluster Size (C) = 10.3 ~ (naphthalene)
- Aliphatic Chain Length (C_n) = 11.5
- Fraction of Aromatics with Attachments (FAA) = 0.5 (average of 5 attachments per aromatic cluster)
- Cluster molecular weight = 832 Dalton
- Attachment molecular weight = 138 Dalton

SAXS and PDF: SAXS studies were completed on the 11-ID-B beam line at the Advanced Photon Source (APS) at Argonne National Laboratory on whole rock slices (~4mm × 4mm × 0.5mm thick, with the 4 mm square being perpendicular to the sedimentary layering of the shale), ground shale and isolated kerogen from each of the three segments. Atomic PDF measurements were also recorded on ground shale and the isolated kerogen on the 12-ID-B beam line. The interpretation and analysis of this data is an ongoing collaboration with personnel with expertise in these techniques at the APS. The data has been shared with Subtask 4.9 personnel.

SAXS is a useful tool for studying the nanoscale structure of disordered porous materials. The exponent from the power law fitting of the SAXS scattering curve for the kerogen (see Figure 20) is between 3 and 4, indicative of a system of monodispersed surface fractals or similarly sized pores with convoluted or irregular surfaces. Further analysis indicates that the pores are in the 3-5 Å (diameter) range. Similar results were obtained from the analysis of the shale scattering curves. Analysis is continuing to obtain additional information about the nano and

microstructure of both the shale and the kerogen. The shape of the scattering curve is also indicative of particles that are not spherical in nature but are arranged in planes or sheets.
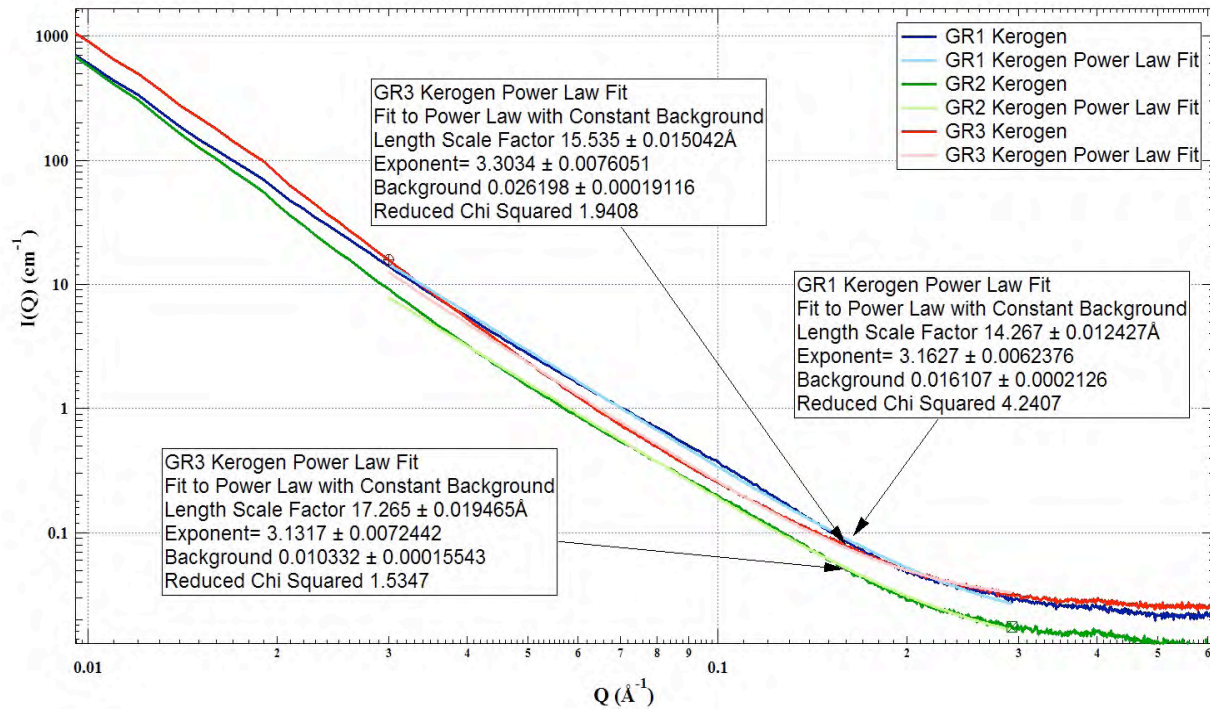
Figure 20: Power law fitting of the SAXS scattering curve for the isolated kerogen samples.

Finally, atomic PDF measurements were made on both the ground shale and the isolated kerogen of all three segments. This X-ray diffraction technique is used on amorphous systems to produce a trace of the probability of finding two atoms separated by a given distance. The PDF for the kerogen of each of the segments is shown below in Figure 21. As can be observed, the three plots are nearly identical. The peaks below 1 Å are artifacts of the experiment. The peaks between 1 and 2 Å are due to the C-H and the C-C bonds, whereas those between 2 and 4 Å are due to the nonbonding separation of two atoms across an angle. Finally, the peaks above 4 Å are due to the separation of atoms related by a dihedral or an even longer range interaction in the kerogen atomic structure.
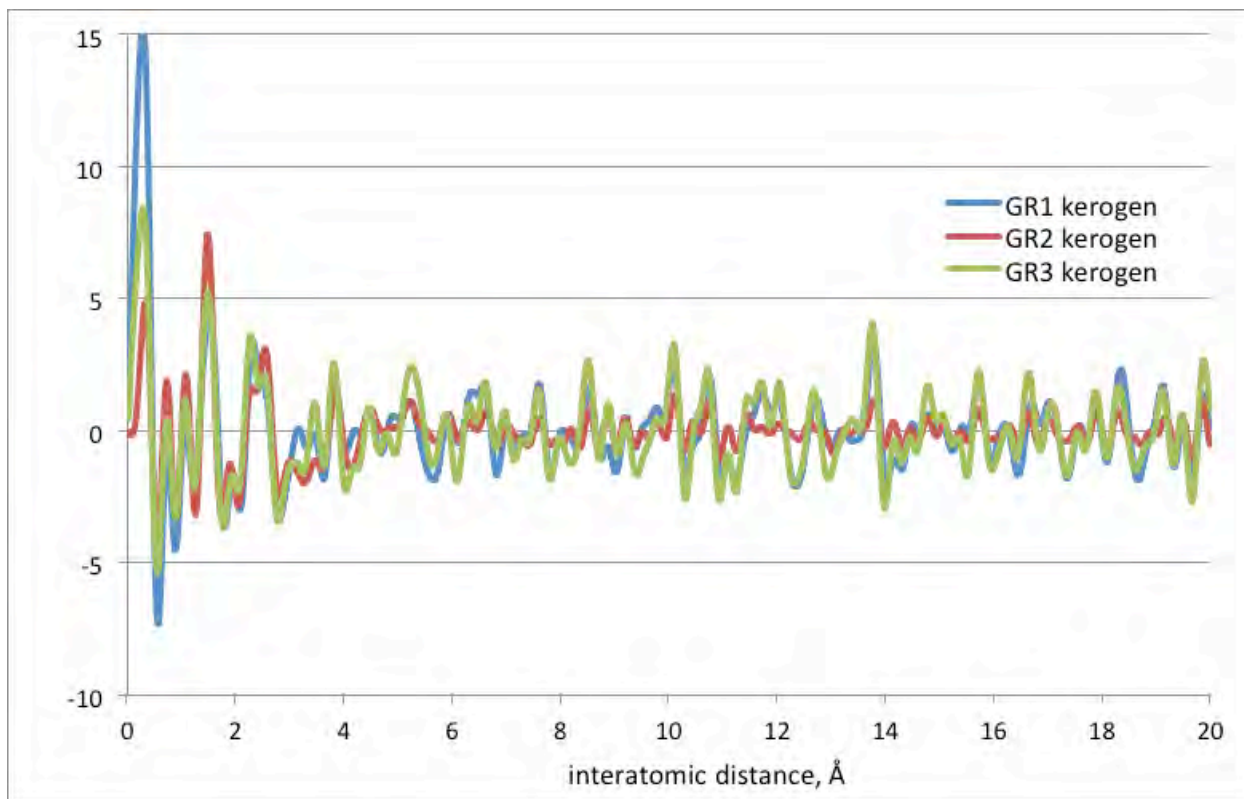
Figure 21: Atomic PDF measurements from the three isolated kerogen samples.

Task 5.0 - Environmental, Legal, Economic and Policy Framework

Subtask 5.1 – Models for Addressing Cross-Jurisdictional Resource Management (PI: Robert Keiter, John Ruple)

This project has been completed.

Subtask 5.2 - Conjunctive Management of Surface and Groundwater Resources (PI: Robert Keiter, John Ruple)

This project has been completed.

Subtask 5.3 - Police and Economic Issues Associated with Using Simulation to Assess Environmental Impacts (PI: Robert Keiter, Kirsten Uchitel)

Efforts this quarter were focused on preliminarily surveying the legal standards articulated by the Environmental Protection Agency in addressing the role and value of modeling in assessing environmental risks or harms.

6.0 – Economic and Policy Assessment of Domestic Unconventional Fuels Industry

Subtask 6.1 Engineering Process Models for Economic Impact Analysis (PI: Terry Ring)

A process model for in situ oil shale production was completed in this quarter and the model for in situ oil sands production is halfway finished. The milestone to provide models used and data collected to the ICSE repository will be completed by September 2012. Also, rather than duplicate the information that is in the Market Assessment report, the project team would like to modify the final deliverable to:

> •Provide a brief description of the inputs/outputs for the process models and how the models are run.

Subtask 6.2 - Policy analysis of the Canadian oil sands experience (PI: Kirsten Uchitel)

The topical report being prepared for this Subtask was delayed this quarter while the macroeconomic impact analysis for Subtask 6.3 was completed. Now that the economic portion of the report can be finalized, it is expected that the topical report for this Subtask will be completed in September 2012. In this quarter, the project team updated the policy analysis and discussion portions of the topical report so that the report is sufficiently current to be relevant and of analytic utility.

Subtask 6.3 – Market Assessment Report (PI: Jennifer Spinti)

The report is nearly complete. Only one section, Section 9 (in situ oil sands scenario), remains to be finalized. Draft copies of the report will be distributed in the next quarter to a small group of reviewers prior to releasing the report in electronic form.

7.0 – Strategic Alliance Reserve

The Task 7.0 project team is continuing to meet with its industrial partner, AMSO, on a regular basis. Team members worked together to prepare a presentation on Task 7.0 activities given by Dr. Alan Burnham of AMSO at the University of Utah Unconventional Fuels Conference held on May 15 on the University of Utah campus. A copy of Dr. Burnham's presentation is attached as Appendix E.

Subtask 7.1 – Geomechanical Model (PI: John McLennan)

The focus of the Subtask 7.1 team during this quarter has been on methods for reasonably representing the matrix of experimental data that has been generated by AMSO. The tactics are to:
> •Use hyperbolic relationships between stress and deformation to fit various constitutive behaviors – adopted from soil mechanics protocols
> •Use neural networking protocols to interrelate constitutive (stress-strain) behavior to the governing independent variables.

Summary of Analysis Protocols

Deformation, load bearing capacity, porosity, and permeability are required for numerical simulations and vary with grade, temperature, orientation, stress, and loading history. Methods are being developed for providing these data to the numerical simulations by interpreting performance from a sparse number of tests with different temperatures, grades, and orientations.

The basis for the hyperbolic fitting is as follows. Nonlinear stress-strain curves are approximated by hyperbolae (Equation (3)):

$$\sigma_1 - \sigma_3 = \frac{\varepsilon}{a + b\varepsilon} \tag{3}$$

where σ_1 and σ_3 are the major and minor principal stresses, ε is the axial strain, a is the reciprocal of initial tangent modulus, E_i, and b is the reciprocal of the asymptotic value of stress difference that the stress-strain curve approaches at infinite strain; the constants a and b are determined experimentally.

The raw stress strain data are then linearized using the relationship in Equation (4). An example of this fit is shown in Figure 22.

$$\frac{\varepsilon}{\sigma_1 - \sigma_3} = a + b\varepsilon \tag{4}$$
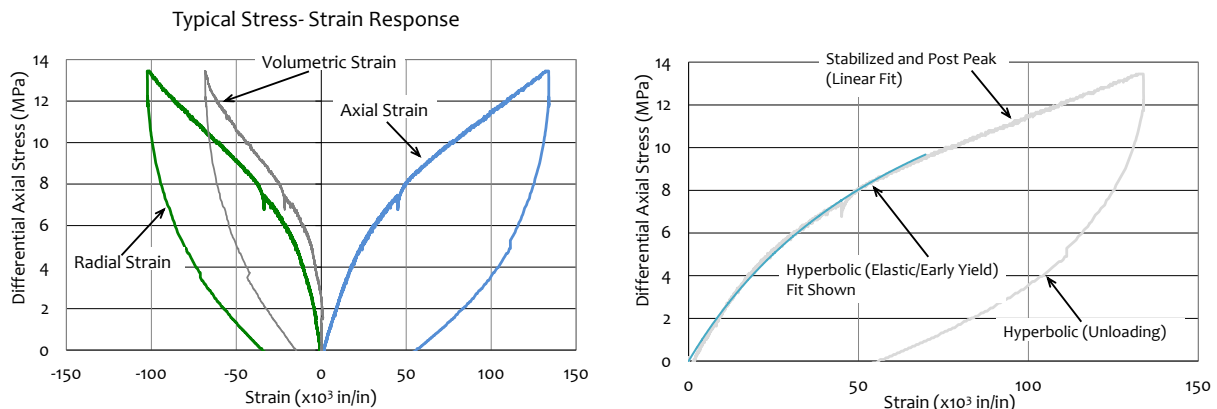
Figure 22: Conceptual fitting mechanism. (left) Raw stress strain data. (right) Proof of concept hyperbolic fit.

A MatLab code has been written for analyzing the data and automatically fitting the linear and the stabilized region. The unloading data are being transformed to also allow a hyperbolic fit. Load rate dependency is a complication that might be solved using rate type compaction methodology published by Shell some years ago de Waal and Smits (1988). Figure 23 shows the MatLab-automated hyperbolic plus linear fit for an example data set.
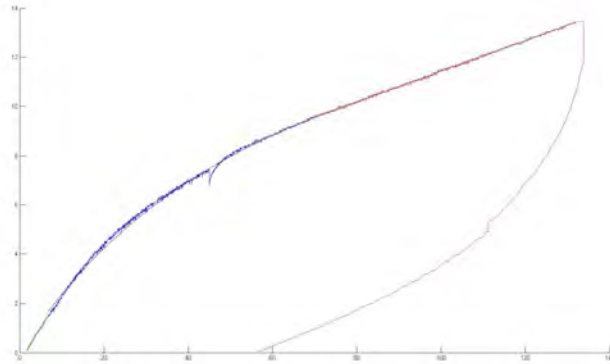
Figure 23: Automated curve fitting of experimental data (Zones I and II).

Once the characteristic parameters for each zone are determined (intercepts and slopes, starting and ending strains, etc.), the project team will attempt to use neural networking or similar technologies to interrelate the data and allow interpolation within a sparse data set.

Data Fitting

Triaxial testing data received from AMSO and generated by New England Research has been fitted in three generic regions as identified in Table 7. Unloading data are also being fitted, as are data from Metarock and Colorado School of Mines. The data output are summarized in Table 8. This table only shows the fits for the samples cored perpendicular to the bedding planes. Radial stress-strain data – where available – is also being fit.

Table 7. Loading regimes.

Region	Identifier	Description
Loading - 1	Elastic	During loading, there are finite loading regimes that have characteristics of linearity that researchers are labeling as elastic (linear elastic). Candidly, the linearity is no guarantee of elastic behavior.
Loading - 2	Hyperbolic	After the so-called elastic behavior, a hyperbolic fit is carried out – see previous section
Loading - 3	Post-Hyperbolic	Behavior after the hyperbolic zone was variable – covering strain hardening, perfect plasticity, and strain softening. At this time, a linear fit with no constitutive interpretation is carried out.

Table 8. Data fitting of AMSO data from samples cored perpendicular to the bedding planes (see next page).

AMSO ID		AMSO.CC.2072.3.C.1.041610	AMSO.CC.2072.3.D.1.041610	AMSO.CC.2072.8.C.1.041610	AMSO.CC.2072.8.D.1.041610	AMSO.CC.2074.35.C.1.070910	AMSO.CC.2129.0.C.1.041610	AMSO.CC.2132.1.C.1.041610	AMSO.CC.2132.1.D.1.041610	AMSO.CC.Multi.2073.8.A.1.050310
		NER1	NER2	NER3	NER4	NER6	NER10	NER11	NER12	NER14
Orientation		Perpen-dicular	Perpen-dicular	Perpen-dicular	Perpen-dicular	Perpen-dicular	Perpen-dicular	Perpen-dicular	Perpen-dicular	Perpen-dicular
Pre-test diameter	in	2	2	2	1.999	1.999	1.996	1.999	1.999	1.996
Pre-test Sample Area	in^2	3.1416	3.1416	3.1416	3.1385	3.1385	3.129	3.1385	3.1385	3.129
Depth	ft	2072.3	2072.3	2072.8	2072.8	2074.35	2129	2132.1	2132.1	2073.8
ID		C-1	D-1	C-1	D-1	C1	C-1	C-1	D-1	A-1
Grade	GOPT	34.1300	34.1300	57.4800	57.4800	57.0000??	25.0000	46.8200	46.8200	41.7000
Confined Pressure	MPa	0.0000	8.2000	11.7000	18.6000	8.2000	11.7000	8.2000	11.7000	11.7000
Pore Pressure	MPa	0.0000	4.8000	4.8000	4.8000	4.8000	4.8000	4.8000	4.8000	4.8000
Temperature	°C	150.0000	150.0000	150.0000	150.0000	237.0000	150.0000	150.0000	150.0000	150.0000
Elastic Section Initial Strain	millistrain	0.0101	1.4259	0.5576	3.2125	11.8938	2.3704	0.8744	3.6158	3.0679
Elastic Section Initial Stress	MPa	0.2330	0.2182	0.1492	0.3109	1.4773	0.3118	1.8723	0.1213	1.8404
Elastic Section Final Strain	millistrain	2.9541	9.1827	13.9095	16.5977	21.8415	8.6233	9.1347	14.5703	9.6414
Elastic Section Final Stress	MPa	1.0512	2.5008	3.1164	3.6045	2.5658	1.4598	3.7322	2.2456	3.6745
Elastic slope		0.2657	0.2943	0.2126	0.2462	0.1054	0.1781	0.2212	0.2098	0.2782
Elastic intercept		0.2726	-0.2014	0.2898	-0.3908	0.1961	-0.0476	1.7632	-0.8032	1.0202
Hyperbolic Section Initial Strain	millistrain	3.0268	9.2397	13.9095	16.6004	22.2739	8.7882	9.1839	14.5703	9.6414
Hyperbolic Section Initial Stress	MPa	1.0771	2.5176	3.1195	3.6169	2.5658	1.4691	3.7446	2.2487	3.6870
Hyperbolic Section Final Strain	millistrain	70.0040	80.9912	74.4749	66.5056	41.0880	105.1618	105.1128	80.2023	70.1176
Hyperbolic Section Final Stress	MPa	7.4151	10.0882	9.4886	9.2118	4.0430	8.5346	13.0840	9.5045	10.8585
Hyperbolic slope (transformed) - b		0.0965	0.0665	0.0552	0.0540	0.0623	0.0719	0.0584	0.0314	0.0675
Hyperbolic intercept (transformed) - a		2.7391	2.7087	3.7885	3.6194	7.2678	5.5193	2.5813	5.8595	2.1048
Post Hyperbolic Section Initial Strain	millistrain	70.0767	81.1366	74.6175	66.6333	41.3042	105.1618	105.3126	80.4207	70.3367
Post Hyperbolic Section Initial Stress	MPa	7.4203	10.0944	9.4948	9.2211	4.0430	8.5377	13.1089	9.5201	10.8678
Post Hyperbolic Section Final Strain	millistrain	73.5881	103.0299	132.3489	133.6610	80.6623	119.5971	129.9889	150.0504	114.3787

| AMSO ID		AMSO.CC.2072.3.C.1.041610	AMSO.CC.2072.3.D.1.041610	AMSO.CC.2072.8.C.1.041610	AMSO.CC.2072.8.D.1.041610	AMSO.CC.2074.35.C.1.070910	AMSO.CC.2129.0.C.1.041610	AMSO.CC.2132.1.C.1.041610	AMSO.CC.2132.1.D.1.041610	AMSO.CC.Multi.2073.8.A.1.050310
Post Hyperbolic Section Final Stress	MPa	7.3633	11.3031	12.8069	13.3266	0.2333	9.2176	14.9469	13.8150	13.6722
Post hyperbolic slope		-0.0137	0.0540	0.0568	0.0609		0.0469	0.0727	0.0551	0.0632
Post hyperbolic intercept		8.4220	5.7581	5.2969	5.2212		3.6216	5.5463	5.3996	6.5456
Note		Jacket Failed				Softening				

Regression for Interpolation

All data above were regressed with multivariate linear regression so that a composite curve for each region could be inferred. Individual regressions were done based on the measured properties as a function of grade, confining pressure, pore pressure and temperature; mineralogy needs to be added. The dependent variables are shown in gray shading in Table 8. Perpendicular and parallel to bedding regression have been done separately. R^2 values ranged from good to poor for the regression, which is not surprising given the limited data. An example is shown in Equation (5) and Table 9; the regression routine was elementary and the significance is not considered. Figure 24 shows a fit to one of the data sets. Few other alternatives exist currently for analysis of this type of data.

$$\varepsilon_a \left(\text{Hyperbolic, Initial}\right) = -19.8042 + 0.1499 \times Grade + 0.4657 \times \sigma_3 + \\ + 0.35943 \times P_o + 0.1181 \times Temperature$$

(3)

Table 9. Multivariate linear regression on the start of the axial strain that can be fitted by hyperbolic relationships.

| SUMMARY OUTPUT								
Regression Statistics								
Multiple F	0.977215							
R Square	0.95495							
Adjusted	0.909899							
Standard	1.674129							
Observati	9							
ANOVA								
	df	*SS*	*MS*	*F*	*gnificance F*			
Regressio	4	237.64	59.40999	21.19735	0.005906			
Residual	4	11.21084	2.802709					
Total	8	248.8508						
	Coefficients	*andard Err*	*t Stat*	*P-value*	*Lower 95%*	*Upper 95%*	*ower 95.0%*	*pper 95.0%*
Intercept	-19.8042	3.708127	-5.34076	0.005922	-30.0996	-9.5088	-30.0996	-9.5088
Grade (GC	0.149937	0.065635	2.284416	0.084375	-0.03229	0.332167	-0.03229	0.332167
Confined	0.465714	0.224381	2.075553	0.106558	-0.15727	1.088695	-0.15727	1.088695
Pore Press	0.35943	0.620111	0.579622	0.593249	-1.36228	2.081135	-1.36228	2.081135
Temperat	0.118091	0.026078	4.52836	0.010591	0.045687	0.190496	0.045687	0.190496
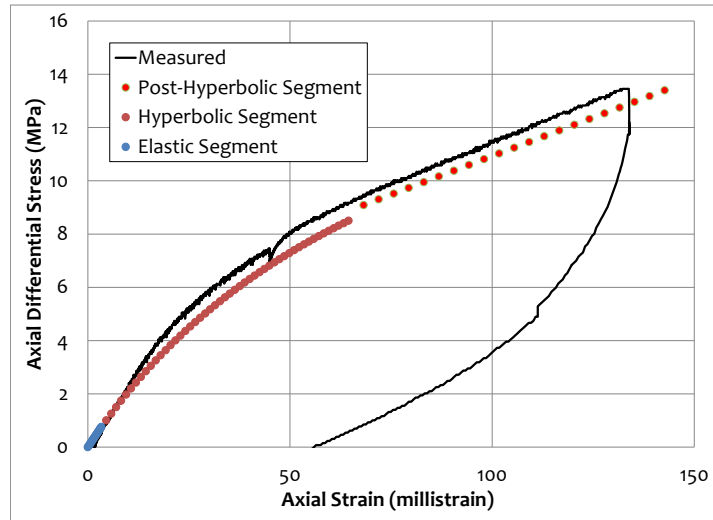
Figure 24: Regression fit to experimental dataset. The black curve is data from AMSO.CC. 2072.8.D.1.032910. The dots are three regressed values to make a synthetic curve with the only input being the four independent variables (grade, confining pressure, pore pressure, and temperature).

Not all of the fits are as good as in Figure 24 (and it is being improved by forcing continuity in slope where one region transitions to another), but the predictive capabilities seem reasonable even if they are not sophisticated.

Figure 25 shows forecasted behavior as a function of grade. While promising, the data fits require further refinement as shown in Figure 26. While trends are intuitively reasonable, the discontinuous behavior needs to be resolved. The project team is also uncomfortable extrapolating outside of the available range of data and is proceeding with incorporation of the Metarock data to determine if these issues can be resolved. Also, team members will try some more sophisticated statistical evaluations and see if there is any value from neural network analysis.
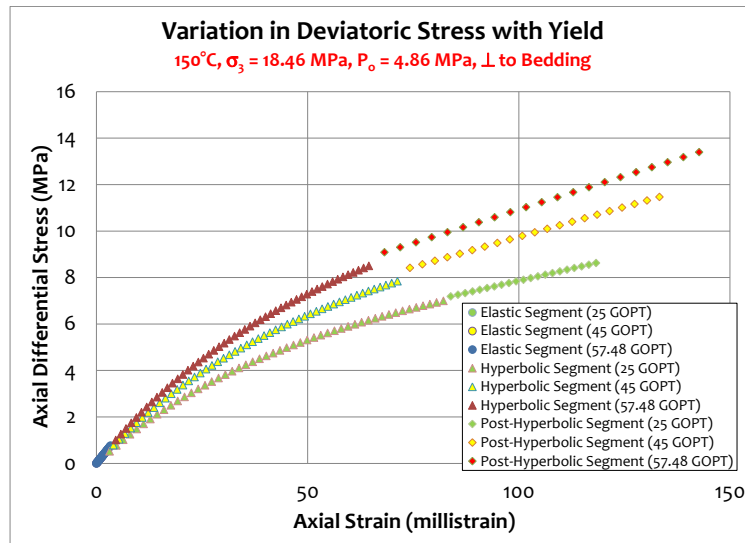
Figure 25: Reconstructed data for three samples at 150°C with grades between 25-57 GOPT.
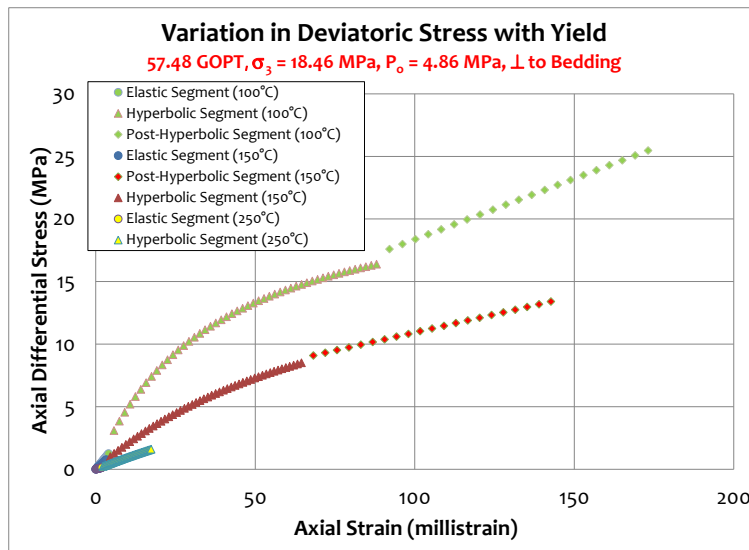
Figure 26: Reconstructed data for three high-grade samples (57.48 GOPT) with temperatures between 100-250°C.

<u>Subtask 7.2 – Kinetic Compositional Models and Thermal Reservoir Simulators (PI: Milind Deo)</u>

In this subtask, researchers are implementing the tools developed in Subtask 4.2 to study the ongoing AMSO pilot test. During this quarter, the milestone to incorporate chemical kinetics into thermal reservoir simulators was completed. Specifically, the rigorous kinetic model described below has incorporated into the thermal reservoir simulator STARS.

The reaction mechanism used is a relatively low complexity series of reactions representing seven pseudo components. A distribution of activation energy model is used for conversion of kerogen to products.

Reaction 1   Kerogen -> HO + LO + gas + CH_4 + char
Reaction 2   HO -> LO + gas + CH_4 + char
Reaction 3   LO -> gas + CH_4 + char
Reaction 4   gas -> CH_4 + char
Reaction 5   char -> CH_4 + gas + coke

Team researchers also investigated multiple ways of including geomechanics in reservoir models, including a study of geomechanics in the Uintah framework, a study of adding fractures in STARS as a function of thermal stress and a geomechanics model in the ARTS. Both Uinta and ARTS were developed at the University of Utah.

This project is currently in transition. Three of the senior students working on various components of the project (Pankaj Tiwari, Jacob Bauman and Nan Zhao) all graduated with Ph.D. degrees in the last three months. Post-doctoral fellows in the group are expected to assume responsibility for this task.

<u>Subtask 7.3 – Rubblized Bed High Performance Computing Simulations (PI: Philip Smith)</u>

In the past quarter, Subtask 7.3 researchers have completed simulations of the initial geometric representation of the process used by the project's industrial partner, AMSO. They continue to work closely with AMSO through teleconferences and frequent on-site visits by AMSO's lead scientist to redesign the geometric representation of their process based on these initial simulation results. They also completed the milestone to collect background knowledge from AMSO about characteristics & operation of the heated wells as described below.

The computational domain created by the project team for the set of preliminary simulations is shown in Figure 27. This geometry was used to simulate the heater test conducted by AMSO. However, results from the initial simulations showed an unusually high heating rate inside the domain, as can be seen in Figure 28. This high heating rate occurred because the size of cracks that were implemented in the geometry were significantly larger than those present in the actual experiment. The size of the cracks allowed increased flow circulation (e.g. convective currents), which then heated the domain much faster than observed in the experiment.
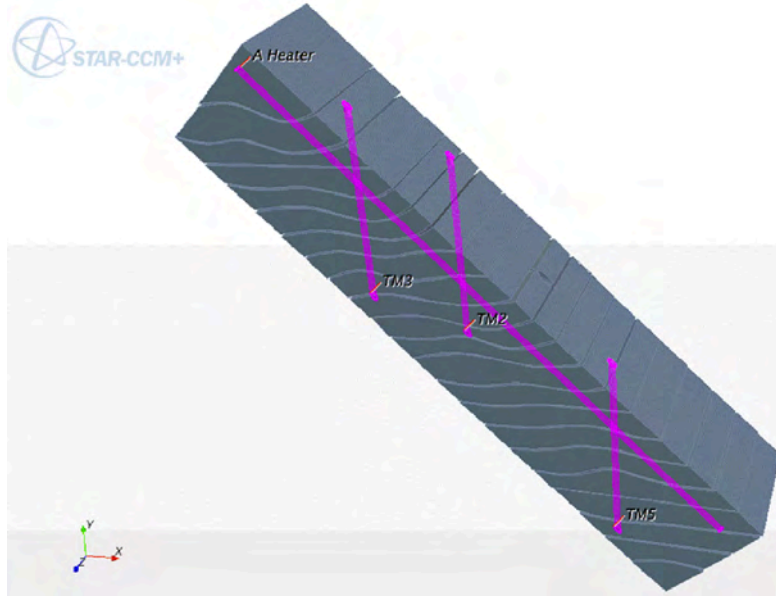
Figure 27: Initial computational representation of the AMSO process.
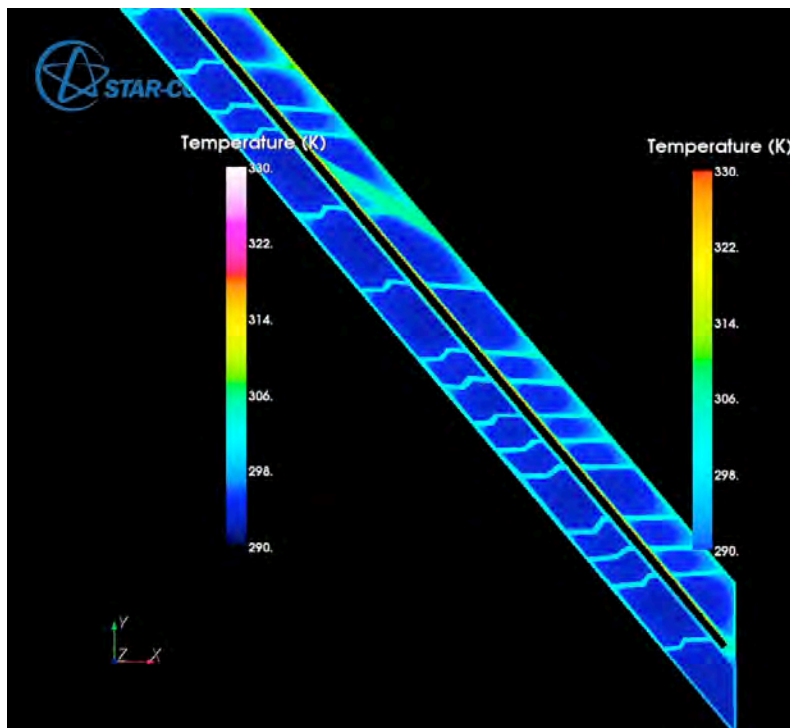

Figure 28: Temperature distribution from the preliminary simulation of the AMSO heater test.

Based on the simulation results and feedback from AMSO, the research team has redesigned the representative AMSO heater test geometry as shown in Figure 29. In this geometry, the shale representation has been extended further from the heating well to allow for sufficient

volume for heat dissipation from the heater into the shale. The number of convective channels has been reduced as well. Additionally, team members have made adjustments in input parameters and models to properly capture conductive heating in the simulation, which is the predominant mode of heat transfer for this stage of the AMSO process.
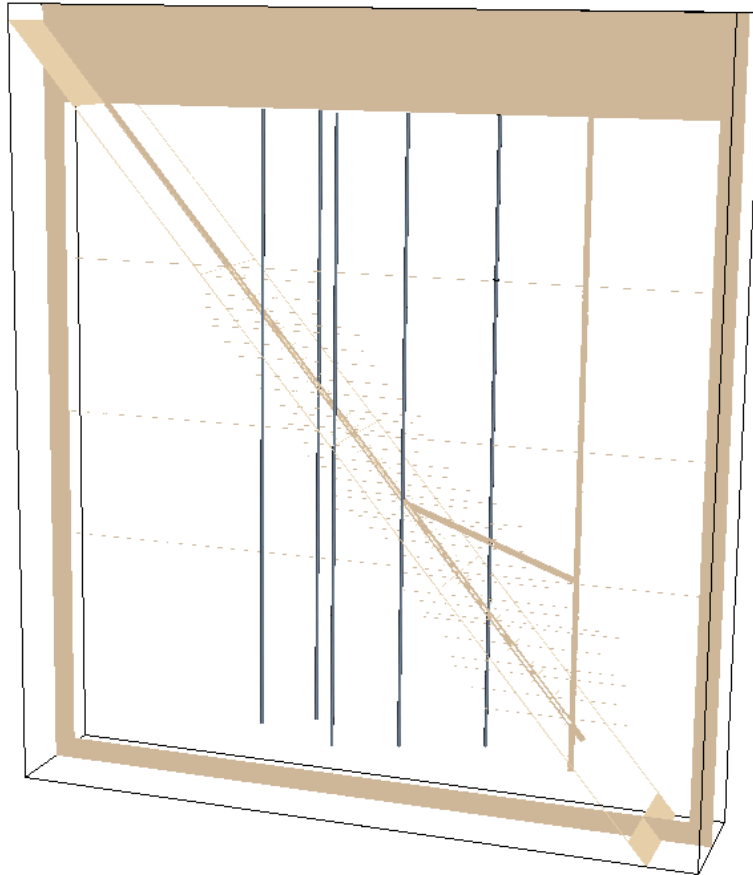
Figure 29: Redesigned geometry of the AMSO process.

Soon after completion of this geometry and a follow-up AMSO review, team members were contacted by a third-party geologist contracted by AMSO. The geologist provided the project team with actual field gyro surveys of all of the drilled wells. Using this extraordinary collection of data, the project team recreated the simulation geometry once again. Further review of the gyro surveys showed some discrepancies compared with a magnetic well proximity survey. However, given that the depth of all wells is 2,000+ feet below the surface, these errors of few feet are very common. The most up-to-date geometry of the AMSO process is shown in Figure 30. Team members are continuing to work with AMSO to adjust this geometry so that it matches the magnetic well proximity surveys.
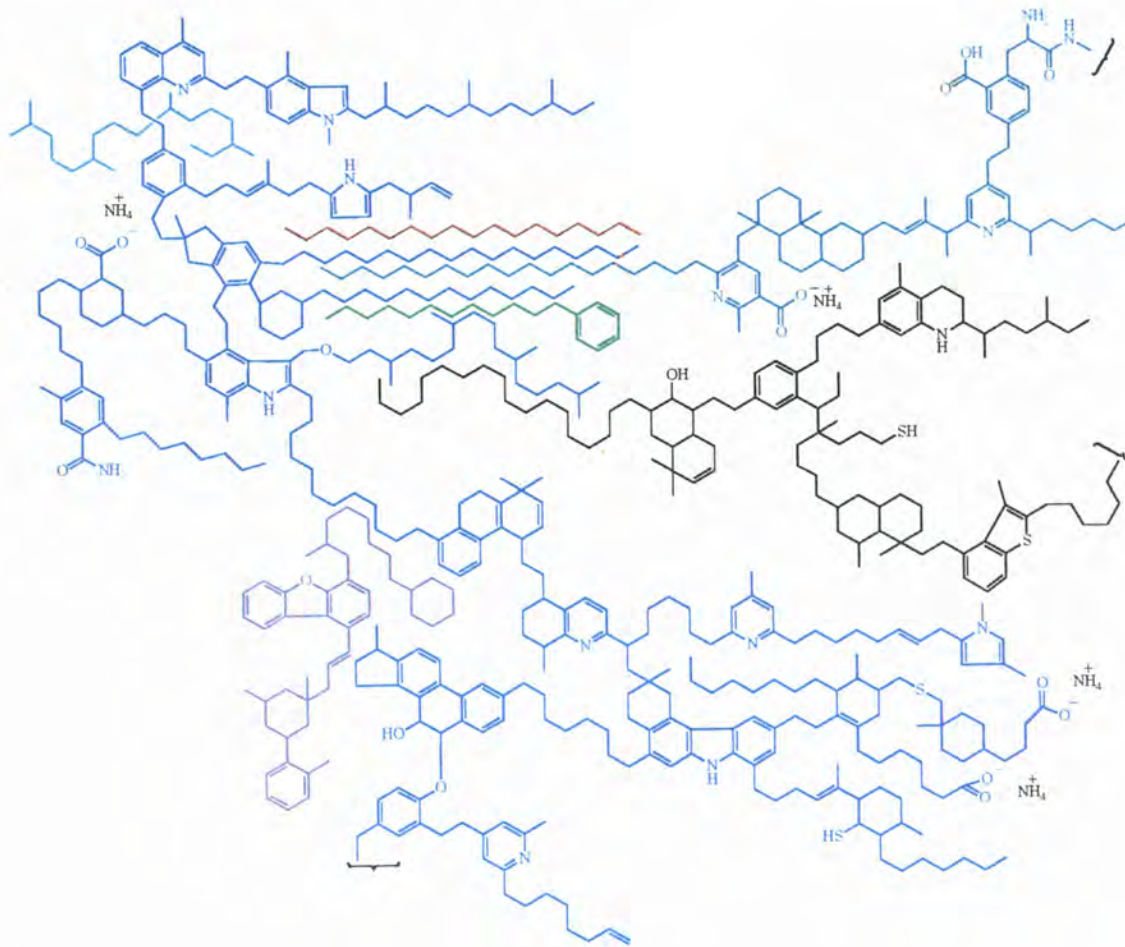
Figure 30: The most up to date geometry representing the AMSO heater test. The wells were constructed from the actual field gyro surveys.

Team members continued to gather information from AMSO scientists on the characteristics and operation of the heated wells. They have also processed and converted the temperatures measured during the heater test to an appropriate format usable by Star-CCM+ , the HPC simulation tool used in this project.

CONCLUSIONS

Several subtasks are nearing completion, including 4.6, 4.9, 6.1, 6.2, and 6.3. ICSE continues to expand it's efforts to collaborate with industry, including a tight collaboration with AMSO on Task 7.0 and an opportunity to present a short course to and develop a PhD project with Statoil.

COST PLAN/STATUS

Baseline Reporting Quarter - PHASE I	Yr. 1								Yr. 2			
	Q1		Q2		Q3		Q4		Q5		Q6	
	7/1/09 - 12/31/09		1/1/10 - 3/31/10		4/1/10 - 6/30/10		7/1/10 - 9/30/10		10/1/10 - 12/31/10		1/1/11 - 3/31/11	
	Q1	Total	Q2	Total	Q3	Total	Q4	Total	Q5	Total	Q6	Total
Baseline Cost Plan												
Federal Share	484,728	484,728	484,728	969,456	484,728	1,454,184	484,726	1,938,910	323,403	2,262,313	798,328	3,060,641
Non-Federal Share	121,252	121,252	121,252	242,504	121,252	363,756	121,254	485,010	80,835	565,845	199,564	765,409
Total Planned	605,980	605,980	605,980	1,211,960	605,980	1,817,940	605,980	2,423,920	404,238	2,828,158	997,892	3,826,050
Actual Incurred Cost												
Federal Share	420,153	420,153	331,481	751,634	547,545	1,299,179	428,937	1,728,116	593,386	2,321,502	307,768	2,629,270
Non-Federal Share	29,456	29,456	131,875	161,332	151,972	313,304	100,629	413,933	191,601	605,534	45,101	650,635
Total Incurred Costs	449,609	449,609	463,356	912,966	699,517	1,612,483	529,566	2,142,049	784,987	2,927,036	352,869	3,279,905
Variance												
Federal Share	64,575	64,575	153,247	217,822	-62,817	155,005	55,789	210,794	-269,983	-59,189	490,560	431,371
Non-Federal Share	91,796	91,796	-10,623	81,172	-30,720	50,452	20,625	71,077	-110,766	-39,689	154,463	114,774
Total Variance	156,371	156,371	142,624	298,994	-93,537	205,457	76,414	281,871	-380,749	-98,878	645,023	546,145

Note: Q5 and Q6 reflect both CDP 2009 and CDP 2010 SF424a projections as the award periods overlap.

Baseline Reporting Quarter - PHASE II	Yr. 2				Yr. 3							
	Q7		Q8		Q9		Q10		Q11		Q12	
	04/01/11 - 06/30/11		07/01/11 - 09/30/11		10/01/11 - 12/31/11		01/1/12 - 03/31/12		04/01/12 - 06/30/12		07/01/12 - 09/30/12	
	Q7	Total	Q8	Total	Q9	Total	Q10	Total	Q11	Total	Q12	Total
Baseline Cost Plan												
Federal Share	712,385	3,773,026	627,423	4,400,449	147,451	4,547,900	147,451	4,695,351	147,451	4,842,802	245,447	5,088,249
Non-Federal Share	178,100	943,509	156,854	1,100,363	36,863	1,137,226	36,863	1,174,089	36,863	1,210,952	58,906	1,269,858
Total Planned	890,485	4,716,535	784,277	5,500,812	184,314	5,685,126	184,314	5,869,440	184,314	6,053,754	304,353	6,358,107
Actual Incurred Cost												
Federal Share	449,459	3,078,729	314,813	3,393,542	271,897	3,665,439	267,784	3,933,223	191,438	4,124,661		4,124,661
Non-Federal Share	48,902	699,537	48,835	748,372	105,695	854,067	40,652	894,719	33,092	927,811		927,811
Total Incurred Costs	498,361	3,778,266	363,648	4,141,914	377,592	4,519,506	308,436	4,827,942	224,530	5,052,472		5,052,472
Variance												
Federal Share	262,926	694,297	312,610	1,006,907	-124,446	882,461	-120,333	762,128	-43,987	718,141		963,588
Non-Federal Share	129,198	243,972	108,019	351,991	-68,832	283,159	-3,789	279,370	3,771	283,141		342,047
Total Variance	392,124	938,269	420,629	1,358,898	-193,278	1,165,620	-124,122	1,041,498	-40,216	1,001,282		1,305,635

Baseline Reporting Quarter - PHASE II	Yr. 4											
	Q13		Q14		Q15		Q16					
	10/01/12 - 12/31/12		01/01/13 - 03/31/13		04/01/13 - 06/30/13		07/01/13 - 09/30/13					
	Q13	Total	Q14	Total	Q15	Total	Q16	Total		Total		Total
Baseline Cost Plan												
Federal Share	146,824	5,235,073	146,824	5,381,897	146,824	5,528,721	133,794	5,662,515				
Non-Federal Share	36,705	1,306,563	36,705	1,343,268	36,705	1,379,973	35,906	1,415,879				
Total Planned	183,529	6,541,636	183,529	6,725,165	183,529	6,908,694	169,700	7,078,394				
Actual Incurred Cost												
Federal Share		4,124,661		4,124,661		4,124,661		4,124,661				
Non-Federal Share		927,811		927,811		927,811		927,811				
Total Incurred Costs		5,052,472		5,052,472		5,052,472		5,052,472				
Variance												
Federal Share		1,110,412		1,257,236		1,404,060		1,537,854				
Non-Federal Share		378,752		415,457		452,162		488,068				
Total Variance		1,489,164		1,672,693		1,856,222		2,025,922				

MILESTONE STATUS

ID	Title/Description	Planned Completion Date	Actual Completion Date	Milestone Status
1.0	Project Management			
2.0	Technology Transfer and Outreach			
	Advisory board meeting	Jun-12		
	Hold final project review meeting in format determined jointly by DOE/NETL and ICSE	Jun-13		
3.0	Clean Oil Shale & Oil Sands Utilization with CO2 Management			
3.1	Lifecycle greenhouse gas analysis of conventional oil & gas development in the Uinta Basin			
	Complete modules in CLEAR$_{uff}$ for life-cycle CO2 emissions from conventional oil & gas development in the Uinta Basin	Jun-12		Project on hold pending completion of Subtask 6.3
3.2	Flameless oxy-gas process heaters for efficient CO2 capture			
	Preliminary report detailing results of skeletal validation/uncertainty quantification analysis of oxy-gas combustion system	Sep-12		CFD code is now working; preliminary matrix of cases has been run
3.3	Development of oil & gas production modules for CLEAR$_{uff}$			
	Develop preliminary modules in CLEAR$_{uff}$ for conventional oil & gas development & produced water management in Uinta Basin	Oct-11	Dec-11	Discussed in Jan. 2012 quarterly report
3.4	V/UQ analysis of basin scale CLEAR$_{uff}$ assessment tool			
	Develop a first generation methodology for doing V/UQ analysis	Oct-11	Nov-11	Discussed in Jan. 2012 quarterly report
	Demonstrate full functionality (integration of all modules) of V/UQ methodology for conventional oil & gas development in Uinta Basin	Apr-12		Project on hold pending completion of Subtask 6.3
4.0	Liquid Fuel Production by In-Situ Thermal Processing of Oil Shale/Sands			
4.1	Development of CFD-based simulation tool for in-situ thermal processing of oil shale/ sands			

ID	Title/Description	Planned Completion Date	Actual Completion Date	Milestone Status
	Expand modeling to include reaction chemistry & study product yield as a function of operating conditions	Feb-12	Mar-12	
4.2	Reservoir simulation of reactive transport processes			
	Incorporate kinetic & composition models into both commercial & new reactive transport models	Dec-11	Dec-11	Discussed in this quarterly report
	Complete examination of pore-level change models & their impact on production processes in both commercial & new reactive transport models	Jun-12		Discussed in this quarterly report
4.3	Multiscale thermal processes			
	Complete thermogravimetric analyses experiments of oil shale utilizing fresh "standard" core	Sep-11	Sep-11	Discussed in Oct. 2011 quarterly report
	Complete core sample pyrolysis at various pressures & analyze product bulk properties & composition	Dec-11		Equipment problems have been fixed; tests nearly complete
	Collection & chemical analysis of condensable pyrolysis products from demineralized kerogen	May-12		Discussed in this quarterly report; nearly complete
	Complete model to account for heat & mass transfer effects in predicting product yields & compositions	Jun-12	Jun-12	Discussed in this quarterly report
4.5	In situ pore physics			
	Complete pore network structures & permeability calculations of Skyline 16 core (directional/anisotropic, mineral zones) for various loading conditions, pyrolysis temperatures, & heating rates	Mar-12	Mar-12	Discussed in April 2012 quarterly report for 1 loading condition; add'l loading condition by Dec. 2012
4.6	Atomistic modeling of oil shale kerogens & oil sand asphaltenes			
	Complete web-based repository of 3D models of Uinta Basin kerogens, asphaltenes, & complete systems (organic & inorganic materials)	Dec-11	Dec-11	Discussed in Jan. 2012 quarterly report
4.7	Geomechanical reservoir state			
	Complete high-pressure, high-temperature vessel & ancillary flow system design & fabrication	Sep-11	Sep-11	Discussed in Oct. 2011 quarterly report
	Complete experimental matrix	Feb-12		Revised test matrix presented in this report
	Complete thermophysical & geomechanical property data analysis & validation	Apr-12		Experimental apparatus still undergoing final testing

ID	Title/Description	Planned Completion Date	Actual Completion Date	Milestone Status
4.8	Developing a predictive geologic model of the Green River oil shale, Uinta Basin			
	Detailed sedimentologic & stratigraphic analysis of three cores &, if time permits, a fourth core	Dec-12		
	Detailed mineralogic & geochemical analysis of same cores	Dec-12		
4.9	Experimental characterization of oil shales & kerogens			
	Characterization of bitumen and kerogen samples from standard core	Jan-12	Feb-12	Email sent to R. Vagnetti
	Development of a structural model of kerogen & bitumen	Jun-12		Discussed in this quarterly report
5.0	Environmental, legal, economic, & policy framework			
5.1	Models for addressing cross-jurisdictional resource management			
	Identify case studies for assessment of multi-jurisdictional resource management models & evaluation of utility of models in context of oil shale & sands development	Jun-11	Jul-11	Discussed in Oct. 2011 quarterly report
5.2	Conjunctive management of surface & groundwater resources			
	Complete research on conjunctive surface water & groundwater management in Utah, gaps in its regulation, & lessons that can be learned from existing conjunctive water management programs in other states	Aug-11	Aug-11	Discussed in Oct. 2011 quarterly report
5.3	Policy & economic issues associated with using simulation to assess environmental impacts			
	White paper describing existing judicial & agency approaches for estimating error in simulation methodologies used in context of environmental risk assessment and impacts analysis	Dec-12		
6.0	Economic & policy assessment of domestic unconventional fuels industry			
6.1	Engineering process models for economic impact analysis			
	Upload all models used & data collected to repository	Oct-11		New completion data of Sept. 2012

ID	Title/Description	Planned Completion Date	Actual Completion Date	Milestone Status
7.0	Strategic Alliance Reserve			
	Conduct initial screening of proposed Strategic Alliance applications	Mar-11	Mar-11	
	Complete review and selection of Strategic Alliance applications	Jun-11	Jul-11	Discussed in Oct. 2011 quarterly report
	Implement new Strategic Alliance research tasks	Sep-11	Sep-11	Discussed in Oct. 2011 quarterly report
7.1	Geomechanical model			
	Infer permeability-porosity-temperature relationships, develop model that can be used by other subtasks	Dec-12		
	Make experimental recommendations	Aug-13		
7.2	Kinetic compositional models & thermal reservoir simulators			
	Incorporate chemical kinetics into thermal reservoir simulators	Jun-12		Discussed in this quarterly report
	Demonstrate reservoir simulation of AMSO process	Sep-12		
	Incorporate poroelastic & geomechanical models into reservoir simulator	Jun-13		
7.3	Rubblized bed HPC simulations			
	Collect background knowledge from AMSO about characteristics & operation of heated wells	Jun-12		Discussed in this quarterly report
	Perform generation 1 simulation - DEM, CFD & thermal analysis of characteristic section of AMSO rubblized bed	Sep-12		
	Perform generation 2 simulation that incorporates kinetic compositional models from subtask 7.2 and/or AMSO	Jun-13		

NOTEWORTHY ACCOMPLISHMENTS

The methodologies being explored in Subtask 7.1 for the representation of stress-strain data have applications well beyond this project. They will be of great interest in many areas of geoscience and geo-engineering – for example, wellbore stability, subsidence/ compaction prediction, sand production. The project team remains very optimistic and encouraged.

PROBLEMS OR DELAYS

Several project milestones and deliverables from Subtasks 3.1 (Phase I), 3.2, 3.3, 3.4, 6.1, and 6.2 continue to be delayed by work on the Market Assessment. However, work is wrapping up on the final section of the Assessment, so the delayed projects will be completed or brought back on track in the next quarter. A change in graduate students on the Subtask 4.1 research team has delayed the deliverables for that project. It will be completed in the same time frame as the Subtask 7.3 deliverables as team members work together to complete both subtasks. The pressurized TGA needed in Subtask 4.3 has been repaired and researchers have been collecting pyrolysis kinetics data at pressure. However, the test matrix won't be complete until the next quarter. Subtask 4.5 researchers are still waiting on samples from Subtask 4.7 before completing a permeability analysis of pyrolyzed samples under different loading conditions. The Subtask 4.7 project team, after experiencing long delays with equipment fabrication, is now finishing up test runs and has proposed a nominal testing matrix in this report. Lastly, Subtasks 4.6 and 4.9 are waiting on collaborators to draft/revise papers that will then be submitted as the final deliverables for those projects.

RECENT AND UPCOMING PRESENTATIONS/PUBLICATIONS

List of publications/presentations

Ruple, J. (2011). Clear law and murky facts: Utah's approach to conjunctive surface and groundwater management. *Idaho Law Review, 47*, 217-254.

Bauman, J. H., Bhide, R. & Deo, M. D. (2011, October). An evaluation of porosity and permeability changes in oil shale due to thermal stresses. Paper presented at the 31st Oil Shale Symposium, Colorado School of Mines, Golden, CO.

Orendt, A., Facelli, J. C. & Pugmire, R. (2011, October). Atomistic modeling of oil shale kerogens and asphaltenes. Paper presented at the 31st Oil Shale Symposium, Colorado School of Mines, Golden, CO.

Orendt, A., Pugmire, R., Facelli, J. C. & Birgenheier, L. (2011, October). Structural characterization of segments of a Green River oil shale core and the kerogen isolated from these segments. Paper presented at the 31st Oil Shale Symposium, Colorado School of Mines, Golden, CO.

Orendt, A., Pugmire, R., Facelli, J. C. & Birgenheier, L. (2011, October). Detailed analytical data from select segments of a Green River oil shale core. Poster presented at the 31st Oil Shale Symposium, Colorado School of Mines, Golden, CO.

Tran, T. Q., McLennan, J. D., Deo, M. &and Okerlund, R. (October, 2011). Evaluation of transport properties of in-situ processed oil shale. Poster presented at the 31st Oil Shale Symposium, Colorado School of Mines, Golden, CO.

Vanden Berg, M. & Birgenheier, L. (2011, October). Not all rich zones are created equal: Geologic characterization results of Green River formation core descriptions from Utah's Uinta Basin, including the newly drilled Skyline 16 core. Paper presented at the 31st Oil Shale Symposium, Colorado School of Mines, Golden, CO.

Wilkey, J. (2011, December). Evaluation of the economic feasibility of heavy oil production processes for West Sak Field. MS Thesis, University of Utah, Salt Lake City, UT.

R. Keiter, J. Ruple, H. Tanana and R. Holt. (2012, January). Conjunctive surface and groundwater management in Utah: Implications for oil shale and oil sands development. Submitted to the Department of Energy under DOE Award No. DE-FE0001243.

Tiwari, P. & Deo, M. (2012, February). Detailed kinetic analysis of oil shale pyrolysis TGA data. *AICHE Journal*, *58(2*), 505-515.

Spinti, J. (2012, February 15). Presenter/panelist - *Oil sands: How Utah can improve on the Alberta model.* Utah Governor's Energy Development Summit, Salt Lake City, UT.

Deo, M. (2012, February 15). Presenter/panelist - *Oil sands: How Utah can improve on the Alberta model.* Utah Governor's Energy Development Summit, Salt Lake City, UT.

Tiwari, P. & Deo, M. (2012, April). Compositional and kinetic analysis of oil shale pyrolysis using TGA-MS. *Fuel*, *94*, 333-341.

Rosenberg, M., Birgenheier, L. & Vanden Berg, M. (2012, April) Outcrop examination and sequence stratigraphy of the lacustrine Green River Formation, Uinta Basin, Utah: Implications for conventional and unconventional oil and gas development. Poster presented at the annual meeting of the American Association of Petroleum Geologists Annual Convention, Long Beach, CA, April 22-25, 2012.

Eby, D., Chidsey, T., Vanden Berg, M. & Laine, M. (2012, April). Microbial carbonates from core and outcrop, Tertiary (Eocene) Green River Formation, Uinta Basin, Utah. Paper presented at the American Association of Petroleum Geologists Annual Convention, Long Beach, CA, April 22-25, 2012.

Badu, S., Pimienta, I. S. O., Orendt, A. M. Facelli, J. C. & Pugmire, R. J. (2012). Modeling of asphaltenes: Assessment of sensitivity of ^{13}C SSNMR to molecular structure. Submitted to *Energy & Fuels, 26(4),* 2161-2167.

Fletcher, T. H., Orendt, A. M., Facelli, J. C., Solum, M. S., Mayne, C. L. & Deo, M. (2012, May 15). Kinetics of Uinta Basin oil shale pyrolysis. Presentation at the 2012 University of Utah Unconventional Fuels Conference, Salt Lake City, UT.

Ruple, J. (2012, May 15). Wilderness quality lands and unconventional fuel development. Presentation at the 2012 University of Utah Unconventional Fuels Conference, Salt Lake City, UT.

Tiwari, P. (2012). Oil shale Pyrolysis: Benchscale experimental studies and modeling. Ph.D. dissertation, Department of Chemical Engineering, University of Utah.

Lin, C. L., Miller, Hsieh, C. H., Tiwari, P. & Deo, M. D. (2012, May). Characterization of core pore structure before and after pyrolysis using X-ray micro CT. Paper submitted to *Fuel*.

Tiwari, P., Deo, M., Lin C. L. & Miller, J.D. (2012, October). Characterization of the oil shale core pore structure before and after pyrolysis. Paper accepted for presentation at the 2012 AICHE Annual Meeting in Pittsburgh, PA, October 28-November 2, 2012.

Vanden Berg, M. D., Birgenheier, L. P. & Rosenberg M. J. (2012, September). Core-based sedimentologic, stratigraphic, and geochemical analysis of the lacustrine upper Green River Formation, Uinta Basin, Utah: Implications for conventional and unconventional petroleum development. Poster to be presented at the 2012 AAPG-RMS Meeting in Grand Junction, CO.

Rosenberg, M.J., Birgenheier, L.P, & Vanden Berg, M.D. (2012, October). Sedimentology and Sequence Stratigraphy of the Green River Formation, eastern Uinta Basin, Utah. Submitted abstract to the 32nd Oil Shale Symposium in Golden, CO.

Birgenheier, L. & Vanden Berg, M. (n.d.). manuscript that documents regional and stratigraphic changes in the Green River Formation, Uinta Basin, Utah. To be published in a special edition book titled *Stratigraphy and Limnogeology of the Eocene Green River Formation*.

Bauman. J. H. & Deo, M. D. (n.d.) Simulation of a conceptualized combined pyrolysis, in situ combustion, and CO_2 storage strategy for fuel production from Green River oil shale. Submitted to *Energy and Fuels*.

Pimienta, I. S. O., Orendt, A. M., Pugmire, R. J., Facelli, J. C., Locke, D. R., Winans, R. E., Chapman, K. W. & Chupas, P. J. (n.d.). Three-dimensional structure of the Siskin Green River oil shale kerogen model: A computational study. Manuscript in final draft form and will be submitted to a journal in August.

Orendt, A. , Pimienta, I. S. O., Badu, S., Solum, M., Pugmire, R. J., Facelli, J. C., Locke, D. R., Winans, R. E., Chapman, K. W. & Chupas, P. J. (n.d.). Three-dimensional structure of the Siskin Green River oil shale kerogen model: A comparison between calculated and observed properties. Manuscript in draft form.

REFERENCES

Allred, V. D. (1966). Kinetics of oil shale pyrolysis. *Chemical Engineering Progress, 62(8)*.

Burnham, A. K., Day, R. L., Hardy, M. P. & Wallman, P. H. (2011). AMSO's novel approach to in-situ oil shale recovery. In Ogunsola, O. I., Hartstein, A. M. & Ogunsola, O. (Eds.), *Oil shale: Solutions to the liquid fuel dilemma*. Washington, D.C.: American Chemical Society.

Campbell, J. H., Koskinas, G. H., & Stout, N. D. (1978, June). Kinetics of oil generation from Colorado oil shale. *Fuel, 57*.

Coraggio, G. & Laiola, M. (2009). *Combustion of NG and pulverized coal in a mixture of oxygen and RFG* (IFRF. Doc. No F110/y/01). Pisa, Italy: International Flame Research Foundation.

de Waal, J. A. & Smits, R. M. M. (1988, June). Prediction of reservoir compaction and surface subsidence: Field application of a new model, SPE 14214. *SPE Formation Evaluation, 3(2)*, 347-356.

Goldstein, K. M. & Goldstein, L. F. (1979). *Final field results of true in situ oil shale retorting demonstration project in the green river formation of southwestern Wyoming*, SPE 8445. Paper presented at the SPE Annual Technical Conference and Exhibition, 23-26 September 1979, Las Vegas, NV.

Granoff, B. & Nuttall, H. E. (1977, July). Pyrolysis kinetics of oil-shale particles. *Fuel, 56*.

Hillier, J. L. (2011). *Pyrolysis kinetics and chemical structure considerations of a Green River oil shale and its derivatives*. Ph.D. dissertation, Chemical Engineering Department, Brigham Young University.

Hillier, J., Bezzant, T. & Fletcher, T. H. (2010). Improved method for determination of kinetic parameters from non-isothermal TGA data. *Energy & Fuels, 24,* 2841-2847.

Hillier, J. L. & Fletcher, T. H. (2011). Pyrolysis kinetics of a Green River Oil Shale using a pressurized TGA. *Energy & Fuels*, *25,* 232-239.

Office of Technology Assessment Materials Program Staff. (1980, June). *An assessment of oil shale technologies.* Washington, D.C.: U.S. Government Printing Office.

Prats, M., Closmann, P. J., Ireson, A. T. & Drinkard, G. (1977). Soluble-salt processes for in-situ recovery of hydrocarbons from oil shale. *Journal of Petroleum Technology, 29*, 1078-1088.

Ryan, R. C., Fowler, T. D., Beer, G. L. & Nair, V. (2011). Shell's In situ Conversion Process - From laboratory to field pilotsCarbon dioxide emissions from oil shale derived liquid fuels. In Ogunsola, O. I., Hartstein, A. M. & Ogunsola, O. (Eds.), *Oil shale: Solutions to the liquid fuel dilemma*. Washington, D.C.: American Chemical Society.

Sweeney, J. J., Burnham, A. K., & Braun, R. L. (1987, August). A model of hydrocarbon generation from type I kerogen: Application to Uinta Basin, Utah. *The American Association of Petroleum Geologists Bulletin, 71(8)*.

Symington, W. A., Kaminsky, R. D., Meurer, W. P., Otten, G. A., Thomas, M. M. & Yeakel, J. D. (2011). ExxonMobil's Electrofrac process for in situ oil shale conversion. In Ogunsola, O. I., Hartstein, A. M. & Ogunsola, O. (Eds.), *Oil shale: Solutions to the liquid fuel dilemma*. Washington, D.C.: American Chemical Society.

Thomas, G. W. (1966). Some effects of overburden pressure on oil shale during underground retorting. *Society of Petroleum Engineers Journal*, *6(1)*, 1-8.

Tisot, P. R. & Sohns, H. W. (1970). Structural response of rich Green River oil shales to heat and stress and its relationship to induced permeability. *Journal of Chemical and Engineering Data*, *15(3)*, 425-434.

Tiwari, P. (2012). Oil shale Pyrolysis: Benchscale experimental studies and modeling. Ph.D. dissertation, Department of Chemical Engineering, University of Utah.

Tiwari, P. & Deo, M. (2012, February). Detailed kinetic analysis of oil shale pyrolysis TGA data. *AICHE Journal*, *58(2*), 505-515.

APPENDIX A. Agenda for the 2012 University of Utah Unconventional Fuels Conference

UNIVERSITY OF UTAH
UNCONVENTIONAL FUELS CONFERENCE
Unconventional Fuels in the State   2012
& National Energy Portfolios

AGENDA

Session 1 - Welcome & Opening Remarks

8:30 a.m.   **Philip J. Smith**, Director, Institute for Clean and
Secure Energy, Professor, Department of Chemical
Engineering, University of Utah

8:50 a.m.   **David W. Pershing**, President, University of Utah

Session 2 - Energy Policy at the State Level

9:15 a.m.   **Utah's 10-Year Strategic Energy Plan**
L. Douglas Smoot, Professor/Dean Emeritus,
Brigham Young University and Senior Consultant,
Combustion Resources, Inc.

9:40 a.m.   **Impact of New State Laws on Utah's
Unconventional Fuel Development**
James Holtkamp, Partner, Holland & Hart

10:05 a.m.   **Unconventional Fuels Development in Utah**
John Nowoslawski, Manager of Unconventional
Energy Development, State of Utah

10:30 a.m.   **Break & Display of Skyline 16 oil shale core**

Session 3 - What Can We Learn from Research?

10:50 a.m.   **First Results and Simulation of AMSO's RD&D
Process Tests**
Alan Burnham, Chief Technology Officer,
American Shale Oil LLC

11:15 a.m.   **Kinetics of Uinta Basin Oil Shale Pyrolysis**
Thomas Fletcher, Professor, Chemical Engineering
Department, Brigham Young University

Institute for
CLEAN AND SECURE ENERGY
THE UNIVERSITY OF UTAH

State of Utah
Office of Energy Development
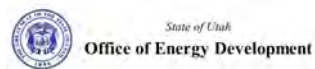
| 11:40 a.m. | **Wilderness Quality Lands and Unconventional Fuel Development**
John Ruple, Wallace Stegner Center for Land, Resources and the Environment, SJ Quinney College of Law, University of Utah |
| 12:05 p.m. | **Lunch & Display of Skyline 16 oil shale core** |

Session 4 - Energy Development Impacts & Mitigation

| 1:00 p.m. | **Sage Grouse Habitat & Unconventional Fuels Development**
John Harja, Senior Counsel on Detail to the Public Lands Office |
| 1:25 p.m. | **Uinta Basin Air Quality Study**
Seth Lyman, Director of Eastern Utah Operations, Energy Dynamics Laboratory |

Session 5 - Unconventional Fuels Development in the Western U.S.

1:50 p.m.	**US Oil Sands 2013 Project Start-up: Economic, Repeatable & Environmentally Responsible** Cameron M. Todd, Chief Executive Officer, US Oil Sands
2:15 p.m.	**Progress Update for Enefit American Oil** Rikki Hrenko, Chief Executive Officer, Enefit American Oil
2:40 p.m.	**Red Leaf Resources, Inc.: Overview and Update** Laura Nelson, Vice President, Energy and Environmental Development, Red Leaf Resources
3:05 p.m.	**Break & Display of Skyline 16 oil shale core**

Session 6 - Plenary Address

| 3:30 p.m. | **Former U.S. Senator Robert F. Bennett**, Chairman, The Bennett Consulting Group |
| 4:00 p.m. | Wrap-up & Adjourn |

Institute for
CLEAN AND SECURE ENERGY
THE UNIVERSITY OF UTAH

State of Utah
Office of Energy Development

APPENDIX B. Examples of articles published about 2012 University of Utah Unconventional Fuels Conference.

Outlet: Casper Star-Tribune
Title/Program: Oil shale companies tout research projects
Publication Date: 5/16/2012
Publicity Value:
Unique Visitors Per Month: 12,115
Snippet: ... process Tuesday at an unconventional fuels conference at the **University** of **Utah**. It's the latest in nearly a century ...
Link to Article

Outlet: Connecticut Post
Title/Program: Oil-shale companies tout research projects
Publication Date: 5/16/2012
Publicity Value:
Unique Visitors Per Month: 286,911
Snippet: ... process Tuesday at an unconventional fuels conference at the **University** of **Utah**. It's the latest in nearly a century ...
Link to Article

Outlet: Republic
Title/Program: Colorado oil shale company to pump hot fuel gas underground to release petroleum
Publication Date: 5/16/2012
Publicity Value:
Unique Visitors Per Month: 270,452
Snippet: ... process Tuesday at an unconventional fuels conference at the **University** of **Utah**. It's the latest in nearly a century ...
Link to Article

Outlet: Salt Lake Tribune

APPENDIX C. Chapter 10 from *Oil Shale Pyrolysis: Benchscale Experimental Studies and Modeling* **(see attached).**

APPENDIX D. Kerogen modeling paper (see attached).

APPENDIX E. Presentation give by Dr. Alan Burnham at the 2012 University of Utah Unconventional Fuels Conference.

10. MATHEMATICAL MODELING OF OIL SHALE PYROLYSIS

The process of transforming solid kerogen to liquid and gaseous products is complex. Several interrelated physical and chemical phenomena occur simultaneously. Products are formed and exit the mineral matrix at definitive velocities through permeable paths. A pore network is created and the pressure changes during the gaseous product formation due to decomposition of the organic matter. A model created with COMSOL multiphysics for oil shale thermal retorting has been developed. The general kinetic model was integrated with some of the important physical processes which occur during pyrolysis. The effect of the process conditions was also investigated.

10.1. Modeling Framework

The main components of the oil shale pyrolysis process, in a logical sequence are depicted in Figure 10-1. A mathematical representation of the physical phenomena during oil shale pyrolysis is modeled in COMSOL multiphysics simulation suite. COSMOL multiphyics uses finite element method to solve the coupled equations simultaneously. The data visualization is relatively simple. It has the capability to include problem specific equation with existing simulation modules. The purpose of developing this model was to understand the coupling of various phenomena in oil shale pyrolysis and to estimate the effect of operational parameters on product distribution. The model developed in this study includes heat transfer due to conduction and mass transformation due to reaction kinetics. Further, porosity and permeability models were included in the

Parameters
Raw material properties

Operating conditions
Temperature
Heating rate
Pressure properties

Heat Transfer Model
(Shape and size)

Temperature distribution

Convection heat
Sweep/reactive gas

Kinetic Model
(Distributed reactivity)

Properties of products
Heat capacity
Equilibrium constant
Density, etc.

Product distribution
Concentration profile

Thermodynamic model
(Distribution/lumping)

Residence time distribution
Time-temperature history
Pressure
Porosity and permeability

Mass Transfer Model
(Secondary reactions)

Product distribution
Quality and Yield

Figure 10- 1: Schematic of the model design to simulate the coupled multiphysics involved in the thermal treatment of oil shale.

framework and convective phenomena in heat and mass balance equations were included. In a shrinking core model, the particle size changes. Hence a grain model concept was applied. It was assumed that the physics vary only in the radial direction. Figure 10-2 shows the geometric representation of simplified simulation scheme adopted in this study. The coupled governing equations were solved simultaneously. Appropriate changes in the physical properties of the material were taken into account as the decomposition process evolved. For example, the propagation of heat conduction within

Figure 10- 2: Schematic of experimental approach and identical simulation environment. The variation is in the r direction only.

10.2. Governing Equations and Solution Methodology

The governing equations included in the basic model are shown below.

- Heat transfer equation

$$\rho \cdot Cp \frac{\partial T}{\partial t} + \nabla\left(-k\nabla T\right) = Q - \rho \cdot Cp \cdot \vec{u}\nabla T \qquad (10.1)$$

- Mass transfer equation

$$\frac{\partial c_i}{\partial t} + \nabla\left(-D_{AB}\nabla c_i\right) = r_i - \vec{u}\nabla c_i \qquad (10.2)$$

- Rate equation

$$ri = -A \times e^{\left(-\frac{E}{R \times T}\right)} \times Ci \qquad (10.3)$$

the particle changes the basic physical properties such as density, thermal conductivity, and heat capacity used in the heat transport governing equation. The changes in the physical properties ρ_{OS}, Cp and K of raw material were adopted from the literature [37, 52] and allowed to be changed as the reaction progressed using the following expressions;

- Density of the raw material- function of organic composition (org)

$$\rho os = \frac{\text{Rho\_org} \times \text{Rho\_rock}}{(\text{Org} \times (\text{Rho\_rock} - \text{Rho\_org}) + \text{Rho\_org})} \tag{10.4}$$

- Heat capacity of the raw material- function of oil yield and temperature

$$Cp = 4186.8383 \times [0.172 + (0.067 + 0.00162 \times \text{Grade\_OS} \times cO) \times (10^{-3} \times \tfrac{9}{5} \times T)] \tag{10.5}$$

- Thermal conductivity of the raw material –function of oil yield and temperature

$$K = 1.73074 \times [(a'_1 \times (1 - b'_1 \times (\tfrac{9}{5} \times (T - 273.15) - 53) - b'_2 \times (\tfrac{9}{5} \times (T - 273.15) - 53)^2 \times \exp (a'_2 \times \text{Grade\_OS} \times cO)] \tag{10.6}$$

a_1', b_1, a_2` and $b_2$` are constants. Three reaction mechanisms were examined- a single step mechanism which does not account for the secondary reactions and a two-step mechanism in which oil produced during the process participates in the secondary reaction. The mass coefficients in the reactions were adopted from the literature and were modified based on the observation in the laboratory [121]. The third mechanism is a multistep mechanism proposed by Burnham and Braun [121] and modified by Bauman and Deo [153] for mass stoichiometric coefficients as to match the mass and elemental balances. The mass coefficients (equation 10-7 to 10-9) are assumed constant, though reaction temperature affects the distribution of product.

Table 10-1 shows the molecular weight (MW) and elements, carbon and hydrogen data for the multistep mechanism. The data up to three decimal points are required to conserve the

mass balance. The mass coefficients were calculated balancing the elements and conserving the mass. The products of the primary reaction from kerogen decomposition are classified as HO (heavy oil), LO (light oil), Gas, Char and Methane. Methane is not included in the Gas fraction and does not go through the secondary processes. All other products participate in further pyrolysis and produce solid and fluid products by cracking or coking.

- Single step mechanism

$$\text{Kerogen} \longrightarrow 0.63\,\text{Oil} + 0.24\,\text{Gas} + 0.13\,\text{Coke} \qquad (10.7)$$

- Two step mechanism

$$\text{Kerogen} \longrightarrow 0.63\,\text{Oil} + 0.24\,\text{Gas} + 0.13\,\text{Coke}$$

$$\text{Oil} \longrightarrow 0.80\,\text{Gas} + 0.20\,\text{Coke} \qquad (10.8)$$

- Multistep mechanism

$$\text{Kerogen} \longrightarrow a_1 \cdot \text{HO} + a_2 \cdot \text{LO} + a_3 \cdot \text{Gas} + a_4 \cdot \text{Char} + a_5 \cdot \text{CH}_4$$

$$\text{HO} \longrightarrow b_2 \cdot \text{LO} + b_3 \cdot \text{Gas} + b_4 \cdot \text{Char} + b_5 \cdot \text{CH}_4$$

$$\text{LO} \longrightarrow c_3 \cdot \text{Gas} + c_4 \cdot \text{Char} + c_5 \cdot \text{CH}_4 \qquad (10.9)$$

$$\text{Gas} \longrightarrow d_4 \cdot \text{Char} + d_5 \cdot \text{CH}_4$$

$$\text{Char} \longrightarrow e_3 \cdot \text{Gas} + e_5 \cdot \text{CH}_4 + e_6 \cdot \text{Coke}$$
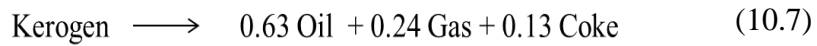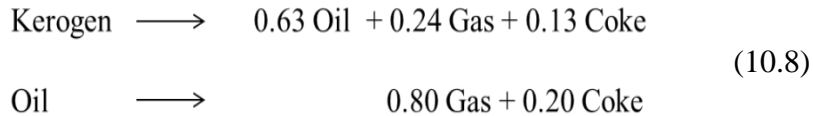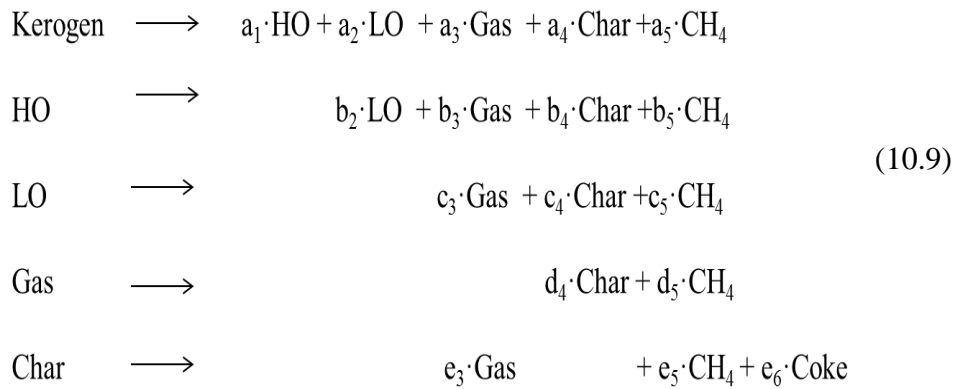
Table 10- 1: Elements and molecular weight data used in constructing the multistep step reaction mechanism.

Component	Kerogen	HO	LO	Gas	Char	Methane	Coke
C	1479.000	31.751	11.189	3.354	1.004	1.000	1.185
H	2220.000	42.818	17.510	11.634	0.546	4.000	0.316
Ratio	1.501	1.349	1.565	3.468	0.544	4.000	0.267
MW	20000.550	424.492	152.034	52.011	12.604	16.042	14.552

The kinetic parameters for kerogen decomposition were taken from Tiwari and Deo [148]. The distributions of activation energy and preexponential factor as decomposition reaction progresses were used for the first step. The kinetic expressions for secondary reactions were fixed, $E = 200$ kJ/mol and $A = 1E10$ S^{-1}. The heat of the reaction was assigned a value of 370 kJ/kg [154]. All the species concentrations were converted to mass units and the equations were solved keeping the overall mass conserved.

The model was simulated first for a single particle, TGA analysis of a fine powder. The convection terms from heat and mass equations were omitted. To understand the effect of the scale (large size) the model was modified by including flow. Convective heat transfer as well as convective flow of the products was introduced in the governing equations using Darcy's law and the continuity equation assuming fluid follows the ideal gas law. Continuity equations coupled with the Darcy flow generates the velocity data. Ideal gas law was used to account for the change in pressure because of density (ρ) variation. Velocity field (u) is determined by the pressure gradient (∇p), the fluid viscosity (μ), and the structure of the porous medium permeability (K_p).

- Darcy law
$$u = \frac{Kp}{\mu} \nabla p \qquad \qquad (10.10)$$

- Continuity equation
$$\frac{\partial}{\partial t}(\rho\varepsilon) + \nabla \cdot (\rho u) = Q_m \qquad \qquad (10.11)$$

- Ideal gas law
$$\rho = \frac{pM}{RT} \qquad \qquad (10.12)$$

An empirical formula for the porosity generated due to kerogen conversion was used [155]. The relationship of porosity and permeability was established using standard Kozney-Carman equation by assuming the average pore diameter of 50×10^{-6} meter.

- Porosity of oil shale as a function of conversion

$$\varepsilon = 0.003 + (0.0146 + 0.0129 \times (\text{Grade\_OS} \times xK) - 0.000046 \times (\text{Grade\_OS} \times xK)^2)$$

$$(10.13)$$

- Permeability of oil shale

$$K_p = D_p^2 \times \varepsilon^3 / (150 \times (1 - \varepsilon)^2) \qquad \qquad (10.14)$$

The model was calculated with the physical and chemical conditions mentioned above. The initial and boundary conditions were assigned according to the geometry and simulation conditions. For temperature, the initial condition was room temperature and boundary conditions were the pyrolysis temperatures (isothermal and nonisothermal). The boundary was set at atmospheric pressure. The mesh size in the geometry was generated and optimized for each simulation to achieve fast and reliable results.

Following assumptions were applied to develop the model

- It is assumed that the material was a 30 gal/ton grade oil shale contains 18% organic matter that was uniformly distributed. The physical properties expressions (ρos, Cp, K) were reported for this grade in the literature.

- The material was heated in the radial direction and it was assumed that the system is symmetrical with respect to z and theta direction.

- Mass transfer through diffusion was not considered. A very small value 10^{-50} [m^2/s] was used for all the species

- Mass transfer equation was solved for each species involved in the reaction network. Kerogen, char and coke were considered as the solid phase, while the oils and gases were the fluid phase.

- Single phase fluid behavior was applied assuming propane as a model fluid to compute the flux of each species. Model built follows the ideal gas law.

10.3. Model Results and Observations

The model developed was simulated with several conditions. A single particle model was examined for all three mechanisms to understand the kinetics and product distribution. This simulation scheme did not include the convective terms and it used the intrinsic kinetics parameters like in the TGA experiments and in a closed system. Figure 10-3 shows the kerogen decomposition and product formation for a single step mechanism for isothermal (400°C) and nonisothermal (10°C/min) boundary conditions. The two step and multistep mechanisms were simulated for the identical conditions and the results are shown in Figure 10-4 and Figure 10-5, respectively.

It can be observed from the results of single particle simulation that the kinetics used for the kerogen decomposition is able to simulate the process effectively. The kerogen decomposition followed the similar trend as TGA analysis. The products formed are in accordance with the mechanisms and associated mass stoichiometry. The results also suggest the effects of the secondary reactions on the final products. To achieve the
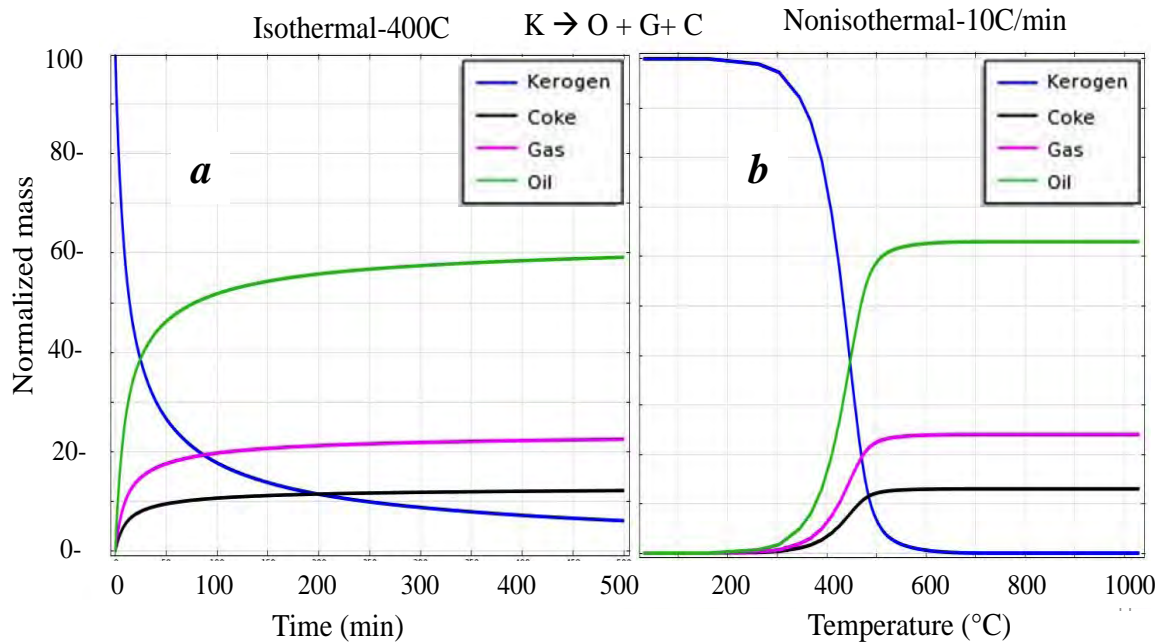
Figure 10- 3: Kerogen decomposition (single particle) and product formation profiles using single step mechanism under (a) isothermal (400°C) and (b) nonisothermal (10°C/min).
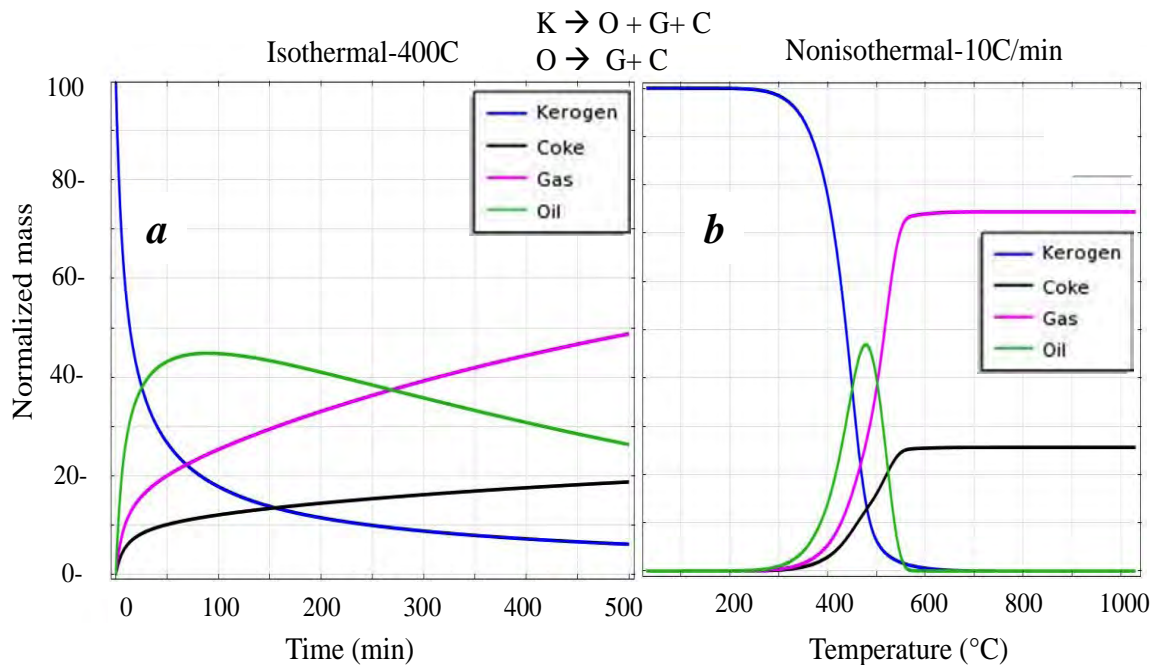
Figure 10- 4: Kerogen decomsposition (single particle) and product formation profiles using two step mechanism under (a) isothermal (400°C) and (b) nonisothermal (10°C/min).
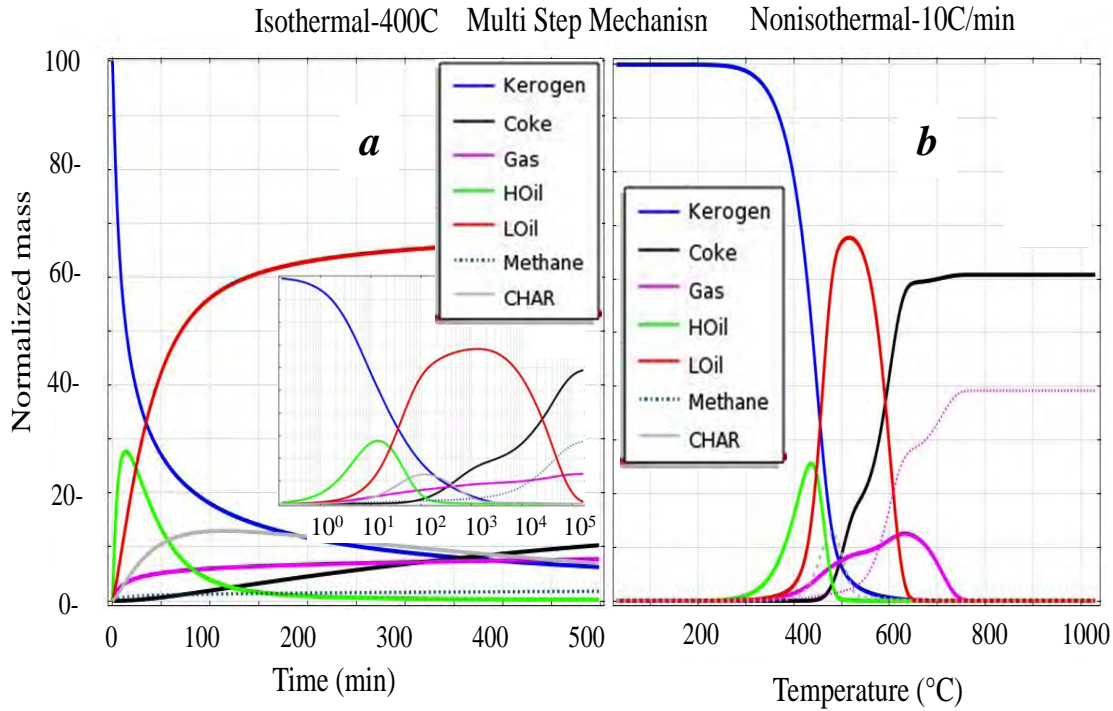
Figure 10- 5: Single particle (TGA scheme in batch mode) of kerogen decomposes to different products using multiple step reactions mechanism under (a) isothermal (400°C) and (b) nonisothermal (10°C/min) pyrolysis. The small window shows the material profiles at long time scale (a log scale).

maximum yield of the desired products, the material needs to be in a pyrolysis environment for a certain time and temperature. Increasing the temperature and heating rate reduced the optimal time. However, it is clear from the results that if the products are heated for a longer time (isothermal) or to higher temperatures (nonisothermal) the final result will be coke and gases. Thus, it is important to sweep the products out.

The reaction mechanism is an important factor to control the product distribution. The multistep mechanisms showed that products are dominated by light oil fractions if the process is shutdown when kerogen decomposition is about 90% at 400°C (isothermal) and 10°C/min (nonisothermal) cases. This value was observed to decrease with an increase in temperature and heating rate for the maximum production of light oil. These are results of the secondary

reactions. The two step mechanism which describes oil degradation as secondary reaction shows that maximum oil yield occurs at 80% and 95% kerogen conversion at 400°C isothermal and 10°C/min nonisothermal conditions respectively.

The next logical step in understanding the product formation rates and distributions was simulating the process with open boundary conditions with a large sample size. The fluid products generated were allowed to travel within the sample by the pressure gradient generated due to gas and methane formation. Core geometry of 10 cm radius was selected. The material was heated in two different configurations which were surface heating and heating from the center of the core. The schematic of the geometries for this simulation scheme is shown in Figure 10-6. In case of heat source at the center of the core a boundary with a radius of 1cm was created inside to act as a heater. There is a temperature distribution across the material in heating schemes. Temperature distribution

Surface heating
Lab scale experiments

Center heating
Reservoir thermal treatment
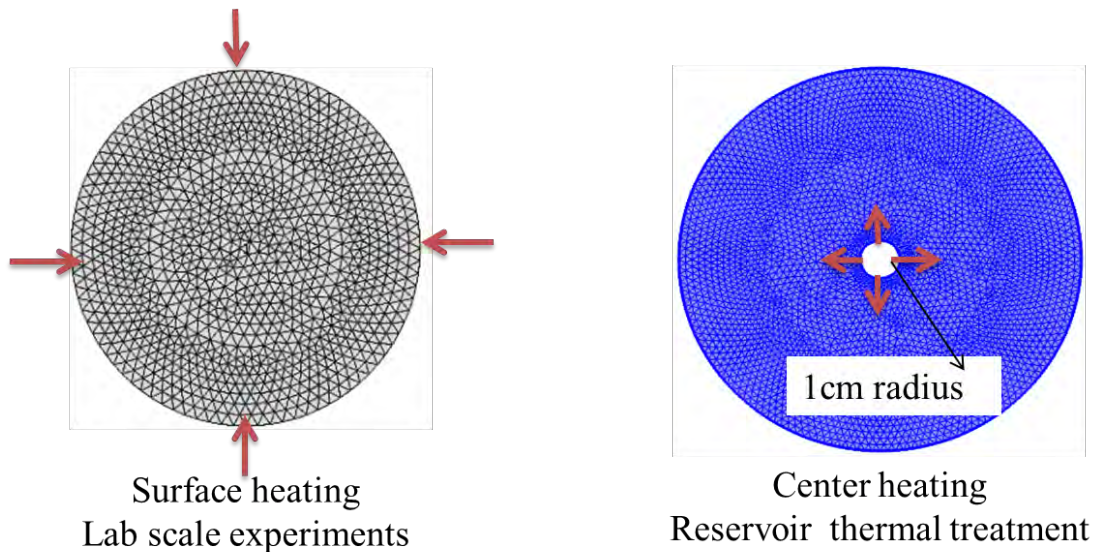
Figure 10- 6: Schematic of the application of the heat to the source material via surface heating and center heating.

controls the kinetics, and hence the product distribution. The temperature distribution across the sample due to heat conduction and resulting rates of heavy oil formation in different sections in case of isothermal (400°C) surface heating are shown in Figure 10-7. The formation and degradation of products occur in a manner similar to single particle simulations. The temperature at the surface is higher thus the formation and degradation of heavy oil occur earlier. And, if the desired products (oils) are not collected at specific time/temperature they participate in the secondary reaction network resulting in formation of more coke and gases.

Further, other physical processes such as convective heat, convective mass transport, and creation of porous media to flow were included in the model. The simulations were carried out when the pressure generated due to the product formation regulated the flow behavior of the fluid products.
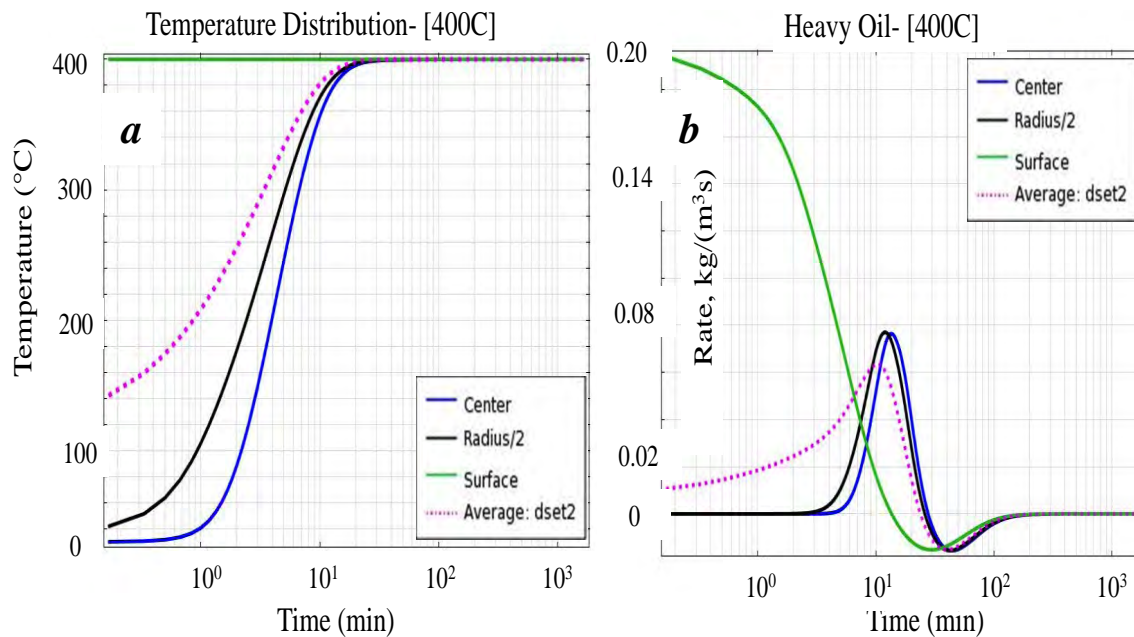
Figure 10- 7: Isothermal (400°C) surface heating, (a) distribution of temperature and (b) rate of heavy oil formation in different sections of the core.

A single phase flow by using propane as a model fluid, for gas and methane fractions with Darcy's law was incorporated in the model. The convection terms in heat and mass equations were included. All fluid products were assumed to follow the velocity of model fluid. The comparison of the rates of product formation at the surface with convection and no convection under nonisothermal heat input at the surface (10°C/min) is shown in Figure 10-8. The rates of fluid products are comparatively higher with convection. This indicates that the convective source in heat and mass transport equations influences the product rates.

When the material is heated from surface, the products form faster at the outer zone and are released. Temperature propagates from the outer surface to inner zone. The product formation creates a porous network. The products at the inner zone form and are transported from a cold to a hot zone. The high temperature in this path favors the secondary reactions, but fluid spends less time due to high porosity. In the case of central
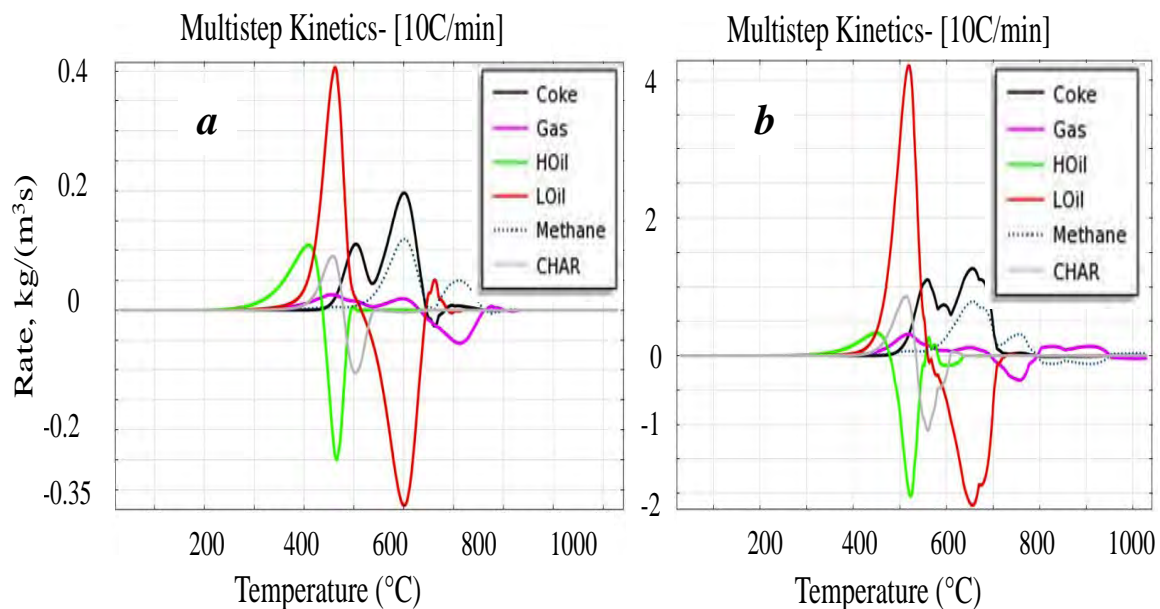
Figure 10- 8: Effect of convection on product formation rates.

heating, the products hit the low temperature and less permeable zone. These conditions restrict the flow and products spend more time within the sample. The condensation reactions due to local thermodynamic conditions may occur. The thermodynamic behavior of the fluid products is not taken into consideration in this model. In both the cases, kinetic conversion experienced a combined isothermal and nonisothermal temperature history. Figure 10-9 shows the average total flux $(kg/m^2.s)$ of the fluid products from the surface of 10cm radius core samples in the surface heating and center heating schemes under isothermal (400°C) heat supply to the material. The comparison of these two plots shows that due to different time/temperate history the material is exposed, average outward fluxes of the products from the surface varies significantly in the distribution. In case of the center heating products come out with a time delay and lighter oil is produced.
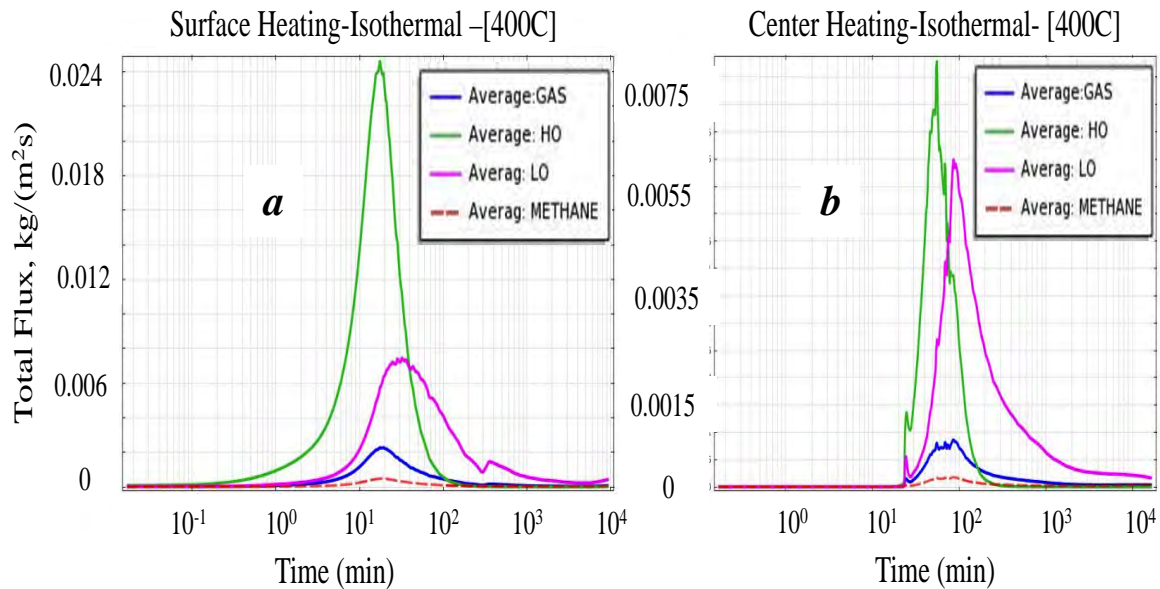
Figure 10- 9: Average total flux of the fluid products from the surface of the core during (a) surface heating and (b) center heating schemes.

10.4. Summary of the Model Results

The model is able to capture the effect of operation conditions and influence of secondary reactions on the distribution of products. The secondary reactions of coking and cracking in the product phase were addressed and their formation kinetics were included. The product distribution is constrained by elemental and product mass balances. The model is capable of predicting compositional information for generated and collected products at different scales. The simulation was designed to understand the effects of the temperature and heating rate on product distribution when additional physics involved in the process are applied. Surface and center heating schemes replicate two different boundary conditions of the core. The heat transfer through a large block experienced both isothermal and nonisothermal behavior simultaneously. The heat distribution regulates the kerogen conversion to product and formation rates. The secondary reactions in the process control the final product distribution. Each physical and chemical process included in this study influences the results. Additional processes which are not considered in this model may alter the product distribution such as thermodynamics of the phase equilibria, multiphase flow behavior, contributions of mineral reactions to the reaction network and the gas pressure generation, etc. The measurement study of the fracture and expansion during the pyrolysis at various temperature and compressive loads was reported [156-158]. These physical processes may also be important in developing a model. The model needs validation against experimental data.

REFERENCES

[1]   George JH, Harris HG. Mathematical modeling of insitu oil shale retorting. Siam J Number Anal 1977;14.

[2]   Bartis JT, LaTourrette T, Dixon L, Peterson DJ, Cecchine G. OIl shale development in the United States- Prospective and policy issues. In: Rand Corporation, Santa Monica, CA, 2005.

[3]   Engler C. Die chemie und physik des erdols. Das Erdol 1913;1:1-37.

[4]   ZNuttall HE, Guo T, Schrader S, Thakur DS. Pyrolysis kinetics of several key world oil shales. In: F.P. Miknis, J.F. McKay (Eds.) Geochemistry and chemistry of oil shales, American Chemical Society;1983, p. 269-300.

[5]   Burham AK, Richardson JH, Coburn TT. Pyrolysis kinetics for western and eastern oil shale. In proceedings of the 17th intersociety energy conversion engineering conference, IEEE publishing: New York, 1982, pp. 912-7.

[6]   Torrente MC, Galan MA. Kinetics of the thermal decomposition of oil shale from puertollano (Spain). Fuel 2001;80:327-34.

[7]   Burnham AK. Oil evolution from a self purging reactor: Kinetic and composition at 2C/min and 2C/h. Energy Fuels 1991;5:205-14.

[8]   Charlesworth JM. Oil shale pyrolysis. 1. Time and temperature dependence of product composition. Ind Eng Chem Process Des Dev 1985;24:1117-25.

[9]   Burnham AK, Singleton MF. High-pressure pyrolysis of green river oil shale. in: F.P. Miknis, J.F. McKay (Eds.) Geochemistry and Chemistry of Oil Shales;1983, p. 335-51.

[10] Sohn HY, Yang HS. Effect of reduced pressure on oil shale retorting. 1. Kinetics of oil generation. Ind Eng Chem Process Des Dev 1985;24:265-70.

[11] Yang HS, Sohn HY. Mathematical analysis of the effect of retorting pressure on oil yield and rate of oil generation from oil shale. Ind Eng Chem Process Des Dev 1985;24:274-80.

[12] Stainforth JG. Practical kinetic modeling of petroleum generation and expulsion. Mar Petrol Geol 2009;26:552-72.

[13] Burnham AK, Happe JA. On the mechanism of kerogen pyrolysis. Fuel 1984;63:1353-6.

[14] Burnham AK. Relationship between hydrous and ordinary pyrolysis. In: NATO advanced study institute on composition, geochemistry and conversion of oil shales conference Akcay, Turkey, 1995 pp. 211–28.

[15] Pan C, Geng A, Zhong N, Liu J, Yu L. Kerogen pyrolysis in the presence and absence of water and minerals. 1. Gas components. Energy Fuels 2008;22:416-27.

[16] Lewan MD, Ruble TE. Comparison of petroleum generation kinetics by isothermal hydrous and non-isothermal open system pyrolysis. Org Geochem 2002;33:1457-75.

[17] Michels R, Landaisa P, Torkelsonb BE, Philpc RP. Effects of effluents and water pressure on oil generation during confined pyrolysis and high pressure hydrous pyrolysis. Geochim Cosmochim Acta 1995;59:1589-604.

[18] Hill GR, Johnson DJ, Miller L, Dougan JL. Direct production of low pour point high gravity shale oil. Ind Eng Chem Prod Res Dev 1967;6:52-9.

[19] Haung ETS. Retorting of single oil shale blocks with nitrogen and air. Soc Petrol Eng J 1977;17:331-6.

[20] Jaber JO, Probert SD. Nonisothermal thermogravimetry and decomposition kinetics of two Jordian oil shales under different processing conditions. Fuel Process Technol 2000;63:57-70.

[21] Kavianian HR, Yesavage VF, Dickson PF, Peters RW. Kinetic simulation model for steam pyrolysis of oil shale feedstock. Ind Eng Chem Res 1990;29:527-34.

[22] Fathoni AZ, Batts BD. A literature review of fuel stability studies with a particular emphasis on shale oil. Energy Fuels 1992;6:681–93.

[23] A technical, economical and legal assesment of North American heavy oil, oil sands, and oil shale resources; In responce to Energy Policy Act of 2005 Section 369(p); Prepared by Utah heavy oil program, 2007.

[24] Survey of energy resources. In: World Energy Council, 2007, pp. 93-115.

[25] Smith JW. Oil shale resources of the United States. CSM Mineral and Energy Resources Series 1980;23.

[26] Dyni JR. Geology and resources of some world oil shale deposits. Oil Shale 2003;20:193-252.

[27] Campbell JH, Kokinas GJ, Stout ND. Kinetics of oil generation from Colorado oil shale. Fuel 1978;57:372-6.

[28] VandenBerg MD. Basin wide evaluation of the uppermost green river formation's oil shale resource, Unita Basin, Utah and Colorado. In: Utah Geological Survey, 2008.

[29] Heistand RN. The Fishcer Assay, a standard method? in: Symposium on oil shale, tar sands, and related materials- production and utilization of sinfuels, San Francisco, 1976.

[30] Wellington SL, Berchenko IE, P. RE, Fowler TD, Ryan RC, Shalin GT, Stegemeier GL, Vinegar HJ. U.S. Patent 6,880,633, 2005.

[31] Symington WA, Olgaard DL, Phillps TC, Thomas MM, Yeakel JD. ExxonMobile's electrofrac[TM] process for in situ oil shale conversion. In: 26th Oil Shale Symposium, Colorado Energy Research Institute, Colorado, 2006.

[32] Kasevich RS, Kolker M, Dwyer AS. U.S. Patent 4,140,179, 1979.

[33] Hubbard AB, Robinson WE. A thermal decomposition study of Colorado oil shale. in, U.S. Bureau of Mine:Report of investigation #4744, 1954.

[34] Pan Z, Feng HY, Smith JM. Rates of pyrolysis of colorado oil shale. AIChE J 1985;31:721-8.

[35] Allred VD. Kinetics of oil shale pyrolysis. Chem Eng Prog 1966;62:55-60.

[36] Braun RL, Rothman AJ. Oil shale pyrolysis: Kinetics and mechanism of oil production. Fuel 1975;54:129-31.

[37] Gregg ML, Campbell JH, Taylor JR. Laboratory and modelling investigation of a Colorado oil shale block heated to 900C. Fuel 1981;60:179-88.

[38] McKee RH, Lyder EE. Thermal decomposition of shales. Ind and Eng Chem 1921;13:613-8.

[39] Maier CG, Zimmerly SR. The chemical dynamics of the transformation of organic matter to bitumen in oil shale. Utah Eng Exper Sta Bull 1924;14:62-81.

[40] Franks AJ, Goodier BD. Preliminary study of the organic matter of Colorado oil shales. Quarterly of the Colorado School of Mines 1922;17:3-16.

[41] Bae JH. Some effects of pressure on oil shale retorting. Soc Petrol Eng J 1969;9:287-92.

[42] Parker JC, Zhang F. Efficient formulation of heat and mass transfer in oil shale retort models. In: 26th Oil Shale Symposium, Coloarodo School of Mines, 2006.

[43] Rajeshwar K, Nottenburg N, Dubow J. Review: Thermophysical properties of oil shales. J Mater Sci 1979;14:2025-52.

[44] Fausett DW, Mikinis FP. Simplified kinetics of oil shale pyrolysis. In: Colorado School of Mines Press, Golden, CO;1981.

[45] Campbell JH. The kinetics of decomposition of Colorado oil shale II. Carbonate minerals. Lawrence Livermore Laboratory Rep 1978;UCRL-52089-2.

[46] Jeong KM, Patzer IJF. Indigenous mineral matter effects in pyrolysis of Green River oil shale. In: F.P. Miknis, J.F. McKay (Eds.) Geochemistry and Chemistry of Oil Shales, Americal Chemical Society;1983, p. 529–42.

[47] Marshall CP, Kannangara GSK, Wilson MA, Guerbois JP, Hartung-Kagi B, Hart G. Potential of thermogravimetric analysis coupled with mass spectrometry for the evaluation of kerogen in source rocks. Chem Geol 2002;184:185-94.

[48] Galan MA, Smith JM. Pyrolysis of oil shale: Experimental study of transport effects. AIChE J 1983;29:604-10.

[49] Charlesworth JM. Oil shale pyrolysis. 2. Kinetics and mechanism of hydrocarbon evolution. Ind Eng Chem Process Des Dev 1985;24:1125-32.

[50] Burnham AK, Ward RL. A possible mechanism of alkene/alkane production. in: H.C. Stauffer (Ed.) Oil Shale, Tar Sands, and Related Materials, American Chemical Society, Washington DC;1981, p. 79-92.

[51] Burnham AK. Chemistry of shale oil cracking. in: H.C. Stauffer (Ed.) Oil Shale, Tar Sands, and Related Materials, American Chemical Society, Washington DC;1981, p. 79-92.

[52] Campbell JH, Koskians GJ, Coburn TT, D.Stout N. Oil shale retorting: The effects of particle size and heating rate on oil evolution and intraparticle oil degradation. InSitu 1978;2:1-47.

[53] Rajeshwar K. The kinetics of the thermal decomposition of green river oil shale kerogen by nonisothermal thermogravimetry. Thermochim Acta 1981;45:253-63.

[54] Hillier J, Fletcher J, Orgill J, Isackson C, Fletcher TH. An improved method for determination of kinetic parameters from constant heating rate TGA oil shale pyrolysis data. Am Chem Soc, Div Fuel Chem 2009;54:155-7.

[55] Li S, Yue C. Study of pyrolysis kinetics of oil shale. Fuel 2003;82:337-42.

[56] Li S, Yue C. Study of different kinetic models for oil shale pyrolysis. Fuel Process Technol 2003;85:51-61.

[57] Qing W, Baizhong S, Aijuan H, Jingru B, Shaohua L. Pyrolysis charactristic of Huadian oil shale. Oil Shale 2007;24:147-57.

[58] William PT, Ahmad N. Influence of process conditions on the pyrolysis of Pakistani oil shale. Fuel 1999;78:653-62.

[59] Thakur DS, Nuttal HE. Kinetics of pyrolysis of Moroccan oil shale by thermogravimetry. Ind Eng Chem Process Des Dev 1987;26:1351-6.

[60] Shin SM, Sohn HY. Nonisothermal determination of the intrinsic kinetics of oil generation from oil shale. Ind Eng Chem Process Des Dev 1980;19:420-6.

[61] Campbell JH, Koskinas GH, D SN. Kinetics of oil generation from Colorado oil shale Fuel 1978;57:372-6.

[62] Leavitt DR, Tyler AL, Kafesjiant AS. Kerogen decomposition kinetics of selected green river and eastern U.S. oil shales from thermal solution experiments. Energy Fuels 1987;1:520-5.

[63] Brown ME, Maciejewski M, Vyazovkin S, Nomen R, Sempere J, Burnham A, Opfermann J, Strey R, Anderson HL, Kemmeler A, Janssens J, Desseyn HO, Li CR, Tang TB, Roduit B, Malek J, Mitsuhasshi T. Computational aspects of kinetic analysis: Part A: The ICTAC kinetics project data, methods and results. Thermochim Acta 2000;355:125-43.

[64] Burnham AK. Computaional aspects of kinetic analysis. Part D: The ICTAC kinetic project multi thermal history model fitting methods and their relation to isoconversion methods in: Thermochim. Acta, 2000, pp. 165-70.

[65] Maciejewski M. Computational aspects of kinetic analysis: Part B- The ICTAC project- The decomposition kinetics of calcium carbonate revisited, or some tips on survival in the kinetic minefield. Thermochim Acta 2000;355:125-43.

[66] Roudit B. Computational aspects of kinetic analysis: Part E- Numerical techniques and kinetics of solid state processes. Thermochim Acta 2000;35:171-80.

[67] Vyazovkin S. Computational aspects of kinetic analysis: Part C- The ICTAC project- The light at the end of the tunnel? Thermochim Acta 2000;355:155-63.

[68] Burnham AK, Braun RL. Global kinetic analysis of complex materials. Energy Fuels 1999;13:1–22.

[69] Burnham AK, Dinh LN. A comparision of isoconversional and model fitting kinetic parameter estimation and application predictions. J Therm Anal Calorim 2007;89:479-90.

[70] Vyazovkin S. Reply to "What is meant by the term 'variable activation energy' when applied in the kinetics analyses of solid state decompositions (crystolysis reactions)?". Thermochim Acta 2003;397:269-71.

[71] Burnham AK. Chemistry and kinetics of oil shale retorting. In: Oil shale: A solution to the liquid fuel dilemma, ACS symposium series;2010, p. 115–34.

[72] Braun RL, Burnham AK. Analysis of chemical reaction kinetics using a distribution of activation energies and simpler models. Energy Fuels 1987;1:153-61.

[73] Burnham AK, Braun RL. General kinetic model of oil shale pyrolysis. InSitu 1985;9:1-23.

[74] Burnham AK, Braun RL, Coburn TT, Sandvik EI, Curry DJ, Schmidt BJ, Noble RA. An appropriate kinetic model for well-preserved algal kerogen. Energy Fuels 1996;10:49-59.

[75] Starink MJ. The determination of activation energy from linear heating rate experiments: A comparison of the accuracy of isoconversion methods. Thermochim Acta 2003;404:163-76.

[76] Sundararaman P, Merz PH, Mann RG. Determination of kerogen activation energy distribution. Energy Fuels 1992;6:793-803.

[77] Al-Ayed OS, Matouq M, Anbar Z, Khaleel AM, Abu-Nameh E. Oil shale pyrolysis kinetics and variable activation energy principle. Appl Energ 2010;87:1269-72.

[78] Friedman HL. Kinetics of thermal degradation of charforming plastics from thermogravimetry. In: Application to a phenolic plastic. J Polym SciPart C 1964;6:183–95.

[79] Vyazovkin S, Wight CA. Estimating realistic confidence intervals for the activation energy determined from thermoanalytical measurements. Anal Chem 2000;72:3171-5.

[80] Vyazovkin S, Wight CA. Isothermal and nonisothermal kinetics of thermally stimulated reactions of solids. Int Rev Phys Chem 1998;17:407-33.

[81] Vyzovkin SV, Lesnikovich AL. Practical application of isoconversional methods. Thermochim Acta 1992;203:177-85.

[82] Vyazovkin S, Wight CA. Kinetics in solids. Annu Rev Phys Chem 1997;48:125-49.

[83] Espitalie J, Ungerer P, Irwin I, Marquis F. Primary cracking of kerogens. Experimenting and modeling C_1, C_2–C_5, C_6–C_{15} and $C_{15}+$ classes of hydrocarbons formed. Org Geochem 1988;13.

[84] Huizinga BJ, Aizenshtat ZA, Peters KE. Programmed pyrolysis gas chromatography of artificially matured Green River kerogen. Energy Fuels 1988;2:74-81.

[85] Morandi JR, Jensen HB. Comparison of porphyrins from shale oil, oil shale, and petroleum by absorption and mass spectroscopy. J Chem Eng Data 1966;11:80-8.

[86] Wood KV, Narayan R, Stringham KR, Huang SL, Leehe H. Characterization of the oil extract of an Indiana shale. Fuel Process Technol 1990;26:73-81.

[87] Lee S. Oil shale technology. CRC Press Inc, Boca Raton, Florida, USA; 1991.

[88] Greenwood PF, George SC. Mass spectral characteristic of C_{19} and C_{20} tricylcic terpanes detected in Latrobe Tasmanite oil shale. Eur J Mass Spectrom 1999;5:221-30.

[89] Steck SJ, Muenow DW, Margrave JL. Mass spectrometric volatilization studies of oil shale. in: Division of Fuel Chemistry, American Chemical Society, Chicago, 1970.

[90] Chakravarty T, Windig W, Taghizadeh K, Meuzelaar HLC, Shadle LJ. Computer-assisted interpretation of pyrolysis mass spectra of two oil shales and their corresponding kerogens. Energy Fuels 1988;2:191-6.

[91] Campbell JH, Kokinas GJ, Gallegos G, Gregg M. Gas evolution during oil shale pyrolysis 1: Nonisothermal rate measurements. Fuel 1980;59:718-26.

[92] Campbell JH, Gallegos G, Gregg M. Gas evolution during oil shale pyrolysis 2: Kinetic and stoichiometric analysis. Fuel 1980;59:727-32.

[93] Huss EB, Burnham AK. Gas evolution during pyrolysis of various Colorado oil shales. Fuel 1982;61:1188-96.

[94] Burnham AK, Huss EB, Singleton MF. Pyrolysis kinetics for Green River oil shale from the saline zone. Fuel 1983;62:1199-204.

[95] Oh MS, Coburn TT, Crawford RW, Burnham AK. Study of gas evolution during oil shale pyrolysis by TQMS. Lawrence Livermore National Laboratory, UCRL 98233, 1988.

[96] Reynolds JG, Crawford RW, Burnham AK. Analysis of oil shale and petroleum source rock pyrolysis by triple quadrupole mass spectrometry: Comparisons of gas evolution at the heating rate of 10^0C/min. Energy Fuels 1991;5:507-23.

[97] Burnham AK, Braun RL, Gregg HR, Samoun AM. Comparison of methods for measuring kerogen pyrolysis rates and fitting kinetic parameters. Energy Fuels 1987;1:452-8.

[98] Burnham AK, Samoun AM, Reynolds JG. Characterization of petroleum source rocks by pyrolysis-mass spectroscopy gas evolution profiles. Lawrence Livermore National Laboratory, UCRL 111012, 1992.

[99] Burnham AK. Pyrolysis kinetics for the Bakken shale. Lawrence Livermore National Laboratory, UCRL 109622, 1992.

[100] Braun RL, Burnham AK, Reynolds JG. Oil and gas evolution kinetics for oil shale and petroleum source rocks determined from pyrolysis-TQMS data at two heating rates. Energy Fuels 1992;6:468-74.

[101] Oh MS, Taylor RW, Coburn TT, Crawford RW. Ammonia evolution during oil shale pyrolysis. Energy Fuels 1988;2:100-5.

[102] Oh MS, Fostera KG, Alcaraza A, Crawforda RW, Taylora RW, Coburna TT. Thermal decomposition of buddingtonite in oil shales. Fuel 1993;72:517-23.

[103] Wong CM, Crawford RW, Burnham AK. Determination of sulfur-containing gases from oil shale pyrolysis by triple quadrupole mass spectrometry. Anal Chem 1984;56:390-5.

[104] Wong CM, Crawforda RW. Application of a self-adaptive detector system on a triple quadrupole MS/MS to high explosives and sulfur-containing pyrolysis gases from oil shale. Int J Mass spectrom 1984;60:107-16.

[105] Meuzelaa HLC, Windig W, Futrell JH, Harper AM, Larter SR. Pyrolysis mass spectrometry and multivariable analysis of several key world oil shale kerogens and some recent alginites. In: T. Aczel (Ed.) Mass Spectrometric Characterization of Shale Oils: A Symposium;1986, p. 81-108.

[106] Khan MR. Influence of weathering and low-temperature preoxidation on oil shale and coal cevolatilization. Energy Fuels 1987;1:366-76.

[107] Stout ND, Koskinas GJ, Raley JH, Santor JD, Opila RL, Rothman AJ. Pyrolysis of oil shale, the effects of thermal history on oil yiled. In: 9th Oil Shale Symposium, Colorado School of Mines, 1976, pp. 153-72.

[108] Miknis FP, Maclel GE. In: 14th Oil Shale Symposium, 1981, pp. 270.

[109] Nazzal JM. Influnce of heating rate on the pyrolysis of Jordon oil shale. J Anal Appl Pyrolysis 2002;62:225-38.

[110] Nazzal JM. The influence of grain size on the products yiled and shale oil composition from the pyrolysis of Sultani oil shale. Energy Convers Manage 2008;49:3278-86.

[111] Litster J, Newell RB, Bhell PRF. Pyrolysis of Rundle oilshale in a continuous fluidized bed retort. Fuel 1988;67:1327-30.

[112] Yang HS, Sohn HY. Effect of reduced pressure on oil shale retorting. 2. Oil yield. Ind Eng Chem Process Des Dev 1985;24:271-3.

[113] Noble RD, Harris HG, Tucker WF. Isothermal oil shale pyrolysis. 2. Kinetic of product formation and composition at various pressure. Fuel 1981;60:573-6.

[114] Voge HH, Good GM. Thermal cracking and high paraffins. J Am Chem Soc 1949;71:593.

[115] Hillier JL, Fletcher TH. Pyrolysis kinetics of a Green River oil shale using a pressurized TGA. Energy Fuels 2011;25:232-9.

[116] Symington WA, Spiecker PM. Heat conduction modeling tools for screening insitu oil shale conversion processes. In: 28th Oil Shale Symposium, Colorado School of Mines, Colorado, 2008.

[117] Computer Modeling Group. STARS User Manual. 2007.

[118] Huang CK. Development of a general thermal oil reservoir simulator under a modularized framework. In: University of Utah, Salt Lake City, Utah, 2009.

[119] Granoff B, Nuttall HE. Pyrolysis kinetics for oil Shale particles Fuel 1977;56.

[120] Braun RL, Burnham AK. Mathematical model of oil generation, degradation, and expulsion. Energy Fuels 1990;4:132-46.

[121] Braun RL, Burnham AK. PMOD: A flexible model of oil and gas generation, cracking and expulsion. In: 15th International Metting on Organic Geochemistry, Manchester, England, 1991.

[122] Braun RL, Burnham AK. Chemical reaction model for oil and gas generation from type I and II kerogens. LLNL 1993.

[123] Stainforth JG. Practical kinetic modeling of petroleum generation and expulsion. Marine and Petroleum Geology 2009;26:552-72.

[124] Coburn TT, Oh MS, Crawford RW, Foster KG. Water generation during pyrolysis of oil shale. 1. Sources. Energy Fuels 1989;3:216-23.

[125] ASTM E1582-04 Standard Practice for Calibration of Temperature Scale for Thermogravimetry. ASTM International.

[126] Neer LA, Deo MD. Simulated distillation of oils with a wide carbon number distribution. J Chromatogr Sci 1995;33:133-8.

[127] ASTM D5307-97, Standard test method for determination of boiling range distribution of crude oils by gas chromatography. ASTM International 2002.

[128] Roehner RM, Hanson FV. Determination of wax precipitation temperature and amount of precipitated solid wax versus temperature for crude oils using FTIR spectroscopy. Energy and Fuels 2001;15:756—63.

[129] ASTM D1298-99, Standard test method method for density, relative density (specific gravity), or API gravity of crude petroleum and liquid petroleum products by hydrometer methods. ASTM International.

[130] ASTM D1217-93, Standard test method for density, relative density (Specific gravity) of liquids by Bingham pycnometer. ASTM International.

[131] ASTM D4052-96, Standard test method for density and relative density of crude oils by digital density analyzer. ASTM International.

[132] ASTM D5002-99, Standard test method for density and relative density of crude oils by digital density analyzer. .

[133] ASTM D2983-04, Standard test method for low-temperature viscosity of lubricants measured by brookfield viscometer. ASTM International.

[134] Hutton A, Bharati S, Robl T. Chemical and petrographical classification of kerogen/macerals. Energy Fules 1994;8:1478-88.

[135] Araújo HD, Silva NFD, Acchar W, Gomes UU. Thermal decomposition of illite. Mat Res 2004;7:359-61.

[136] Johnsona DR, Younga NB, Robb WA. Thermal characteristics of analcime and its effect on heat requirements for oil shale retorting. Fuel 1975;54:249-52.

[137] Behar F, Vandenbroucke M. Chemical modelling of kerogens. Org Geochem 1987;11:15-24.

[138] Vandenbroucke M, Largeau C. Kerogen origin, evaluation and structure. Org Geochem 2007;38:719-833.

[139] Blazek A. Thermal analysis. In: J.F. Tyson (Ed.) Thermal analysis, Van Nostrand Reinhold, London;1973.

[140] Vyazovkin S, A LL. Estimation of the pre-exponential factor in the isoconversional calculation of effective kinetic parameters. Thermochimica Acta 1988;128:297-300.

[141] Vyazovkin S, Linert W. Detecting isokinetic relationships in nonisothermal systems by the isoconversional method Thermochim Acta 1995;269/270:61-72.

[142] Vyazovkin S, Sbirrazzuoli N. Confidence intervals for the activation energy estimated by few experiments. Anal Chim Acta 1997;355:175-80.

[143] Doyle CD. Estimating isothermal life from thermogravimetric data. J Appl Polym Sci 1962;6:639-42.

[144] Senum GI, Yang RT. Rational approximations of the integral of the Arrhenius function. J Therm Anal Calorim 1977;11:445-7.

[145] Constable FH. The mechanism of catalytic decomposition. In: Proceedings of the Royal Society of London, The Royal Society, 1923, pp. 355-78.

[146] Boudreau BP, Ruddick BR. On a reactive continuum representation of organic matter diagenesis. Am J Sci 1991;291:507-38.

[147] Lakshmanan CC, White N. A new distributed activation energy model using weibull distribution for the representation of complex kinetics. Energy Fuels 1994;8:1158-67.

[148] Tiwari P, Deo M. Detailed kinetic analysis of oil shale pyrolysis TGA data. AIChE J 2011;57: n/a. doi: 10.1002/aic.12589.

[149] Galan MA, Smith JM. Pyrolysis of oil shale: Experimental study of transport effects. AIChE 2006 Spring National Meeting 1983;29.

[150] Brown ME, Maciejewski M, Vyazovkin S, Nomen R, Sempere J, Burnham A, Opfermann J, Strey R, Anderson HL, Kemmeler A, Janssens J, Desseyn HO, Li CR, Tang TB, Roduit B, Malek J, Mitsuhasshi T. Computational aspects of kinetic analysis: Part A-The ICTAC kinetics project-data, methods and results. Thermochim Acta 2000;355:125-43.

[151] Lewan MD. Water as a source of hydrogen and oxygen in petroleum formation by hydrous pyrolysis. Amer Chem Soc Div Fuel Chem 1992;37:1643-49.

[152] Vandergrift GF, Winans RE, Scott RG, Horwitz EP. Quantitative study of the carboxylic acids in Green River oil shale Bitumen. Fuel 1980;59:627-33.

[153] Bauman JH, Deo MD. Parameter space reduction and sensitivity analysis in complex thermal subsurface production processes. Energy Fuels 2011;25:251-9.

[154] Camp DW. Oil shale heat capacity relations and heats of pyrolysis and dehydration. LLNL. In: 20th Oil shale symposium, Golden, CO, 1987.

[155] Baughman GL. Synthetic fuels data handbook : U.S. oil shale, U.S. coal, oil sands. Denver : Cameron Engineers 1978

[156] Duvall EWF, Sohn HY, Pitt CH. Physical behaviour of oil shale at various temperatures and compressive loads: 2. Thermal expansion under various loads. Fuel 1985;64:184-8.

[157] Duvall EWF, Sohn HY, Pitt CH. Physical behaviour of oil shale at various temperatures and compressive loads: 3. Structure failure under loads. Fuel 1985;64:938-40.

[158] Duvall EWF, Sohn HY, Pitt CH, Bronson MC. Physical behavior of oil shale at various temperatures and compressive loads: 1. Free thermal expansion. Fuel 1983;62:1455-61.

[159] Chen WJ, Nuttall HE. Paper presented at the 86th AIChE National Meeting, Houston, Texas. 1979.

[160] Coats AW, Redfern JP. Kinetic parameters from thermodynamic data. Nature (London) 1964;201:68-9.

[161] Kissinger HE. Reaction kinetics in differential thermal analysis. Anal Chem 1957;29:1702-6.

Three-Dimensional Structure of the Siskin Green River Oil Shale Kerogen Model: A Comparison between Calculated and Observed Properties

Anita M. Orendt,[1] Ian S.O. Pimienta,[1,2] Shyam R. Badu,[1] Mark S. Solum,[3] Ronald J. Pugmire,[4] and Julio C. Facelli[1,5]

[1]Center for High Performance Computing and [3]Departments of Chemistry, [4]Chemical and Fuels Engineering, and [5]Biomedical Informatics University of Utah, Salt Lake City, Utah 84112

[2]Department of Chemistry and Physics, Troy University, Troy, Alabama 36082

Darren R. Locke,[6] Karena W. Chapman,[6] Peter J. Chupas,[6] and Randall E. Winans[6]

[6]X-ray Science Division, Advanced Photon Source, Argonne National Laboratory, 9700 S. Cass Avenue, Lemont, Illinois 60439

Abstract

Three-dimensional (3D) structural models of the Green River kerogen based on the two-dimensional (2D) structure proposed by Siskin were generated using a combination of *ab initio* and molecular mechanics calculations. Several initial monomer conformations were generated using the simulated annealing procedure, followed by minimization via quantum mechanical calculations. ^{13}C solid state nuclear magnetic resonance (SSNMR) spectra and pair distribution function (PDF) plots were calculated based on these 3D models and compared to experimental results obtained on a Green River kerogen sample. The results show reasonable good agreement between calculated and experimental results.

Introduction

Kerogen is defined as the insoluble organic component of the organic matter in sedimentary rocks. This organic matter is usually mixed with minerals during its deposition which contributes to the difficulty in its physical isolation. Kerogen is not soluble in normal organic solvents because of the large molecular weight up to several thousand Daltons.[1–4] Kerogen is found in rocks such as shale, as oil shale deposits and upon heating in the Earth's crust, some types release hydrocarbons in the form of crude oil or natural gas.

As kerogen is a mixture of organic material, its chemical composition varies from one sample to another. According to the van Krevelen diagram, kerogens can be classified based on the ratios of H/C and O/C.[5] Type I kerogens have H/C ratio greater than 1.25 and O/C ratio less than 0.15. This class is derived primarily from cyanobacteria or various Chlorophyta and dinoflagellates. Type II kerogens, derived from marine planktonic organisms, have H/C ratio less than 1.25 and O/C ratio of 0.03 to 0.18. Type II kerogens can be enriched in organic sulfur; in this case they are further classified as belonging to Type IIS kerogens. Type III kerogens are derived primarily from higher plant remains in coals and coaly shales; they possess a low hydrogen count (H/C < 1, O/C ≡ 0.03−0.3) because of the extensive ring and aromatic character in these systems. Finally, type IV kerogens are comprised of mostly polycyclic aromatic hydrocarbons with H/C ratio less than 0.5. They contain mostly decomposed organic matter and have no potential to produce hydrocarbons.

Source rocks in the Green River formation, one of the most extensive oil shale reserves in the world, contains hydrogen-rich algal kerogen (type I) with up to ~20 wt% organic matter in the form of amorphous kerogen solid integrated in a silicate- and carbonate-based mineral matrix.[6,7] In the past few years, investigators have employed different methods to separate organic kerogen from inorganic minerals in oil shales and to recover the unaltered kerogen for characterization studies.[8–10] Although considerable progress has been achieved from these studies, the complete isolation of kerogen from oil shales remain difficult.

In the case of these petroleum precursors, i.e., both the source rocks and the kerogens, little information is presently available to describe their physical behavior.[11] Only a few relevant studies have been published which utilize both chemical and instrumental analysis to reconstruct a stochastic two-dimensional model of kerogens.[12-16] The work of Durand and co-workers dealt with type I and type II kerogens.[12] More recently, two-dimensional (2D) models of kerogen have been proposed by Siskin[13] for type I Green River Oil Shale (GROS) and Lille[14] for kukersite (a type II/I kerogen). A much larger (more than 10^4 core structures with approximately 10^6 atoms), more general 2D kerogen model[16] has also been developed using the data from various solid state analyses to construct the cores; this model has been used to predict oil and gas compositional yields.

A potential solution to aid in the isolation of kerogen is the analysis of its three dimensional (3D) molecular structure using molecular modeling and simulation. Atomistic modeling is routinely used in many industries (pharmaceutical, polymers, coatings, explosives, membrane proteins, etc.) to gain insight to material properties and behavior. Faulon[15] reported some preliminary data on 3D structures of kerogen but there has been a lack of modeling work that utilizes the molecular modeling tools that are

available today. Hence, little is known about the 3D characteristics of any of the kerogen models. The 3D characteristics of kerogen will not only define the manner in which the kerogen folds and interacts with both the extractable bitumen and the mineral matter, but the structural information will provide a new view of the structure and which portions of the structure are exposed on the surface, which portions are accessible through channels, and/or which portions may be isolated in the interior of the structure.   An understanding of where the various functional groups are located may serve as useful guides for developing novel processing schemes for resource recovery.   In addition, the surface exposure of polar functional groups will provide new information on the interaction of the kerogen structure with the inorganic matrix that appears to bind tightly to the mineral matter.[17-20]

In this work, the 3D structure of the Green River Siskin model[13] was obtained using a combination of *ab initio* and molecular mechanics calculations. The 3D structure was then used to calculate the ^{13}C chemical shifts, from which a simulated ^{13}C spectrum can be generated, as well as to simulate the expected atomic pairwise distribution function (PDF) plot. A PDF plot is gives the probability of finding an atom at a given radial distance from another atom; the peaks observed correspond directly to interatomic distances within the sample and is suitable for this study as it provides local structural information independent of long-range order.[21,22] ^{13}C solid state NMR (SSNMR) is also a powerful tool to obtain structural information on insoluble samples such as kerogens. Using the methodology developed by Grant and Pugmire[23] and used extensively on fossil fuel samples, SSNMR ^{13}C spectra can be analyzed to provide detailed structural data such as the average aromatic cluster size and the average number of substituents on the clusters.[23]

The ^{13}C SSNMR spectrum and PDF plot simulated using our model are compared with their experimental counterparts on the kerogen extracted from a segment of a Green River basin shale core.[24]   The comparison of the simulated and experimental properties allows for an evaluation of the quality of the 3D model as well as the underlying 2D one. The existence of a 3D model that has been validated against experimental data will allow for further study on the interaction between the kerogen and the mineral matrix as well as the further processing of the kerogen in oil production process.

Computational and Experimental Details

Generation of 3D Model: A 3D structure corresponding to the 2D Siskin's kerogen model[13] (chemical formula of $C_{645}H_{1017}N_{19}O_{17}S_4$; molecular weight of 9438.35 dalton) was built using HyperChem.[25] A preliminary chemical structure was obtained via the molecular mechanics energy minimization routine in HyperChem using the MM+[26] force field. This minimized structure was further optimized using the *ab initio* software package GAMESS[27] at the restricted Hartree-Fock (RHF) level of theory using the minimal STO-3G[28] basis set.

After a minimum energy structure was identified by the above procedure, this structure was used to initiate a series of molecular mechanics calculations, which using simulated annealing[29] generate several monomer conformations. This procedure involves three steps: heat, run, and cool. The first step was completed using simulation period of heat time (0.1 ps) and a starting temperature of 10 K to set initial velocities with rescaling of velocities at temperature increments of 119 K per 0.01 ps to reach the simulation

temperature of 1200 K. In the second step, the velocities are rescaled at a constant temperature of 1200 K for a run time of 0.5 ps. The final step was the simulation period of cool time (1 ps), with rescaling of velocities at temperature increments of 9 K per 0.01 ps to reach the final temperature of 300 K. The process was repeated until four monomer conformations were obtained from the parent.

Each of these generated conformers was then locally optimized using GAMESS at the RHF/STO-3G level of theory in the same manner as the original 3D structure. The energies of these structures were compared and the structure with the overall minimum energy was then chosen as the "parent" for the next simulated annealing cycle. The lowest energy conformation obtained in the second annealing cycle was used in the simulation of the PDF and NMR spectra. Molecular images were generated using Mercury.[30]

Calculation of ^{13}C Chemical Shielding: The NMR calculations were done using the density functional theory approach with the PBE1PBE[31] exchange correlation functional and using the 4-31G basis set[32] as implemented in Gaussian09 suite of programs[33]. The calculated chemical shielding values were converted to chemical shifts on the tetramethylsilane (TMS) scale using the shielding calculation of methane at the same level of theory, 200.5 ppm, adjusted by -7 ppm which is the chemical shift of dilute methane on TMS scale.[34] Gaussian broadening of 2 ppm along with Lorentzian broadening of 1 ppm was applied on the aliphatic region, with 5 ppm Gaussian broadening used in the aromatic region to obtain the simulated SSNMR spectrum.

Calculation of Atomic PDF: The PDF plots were calculated using DISCUS and plotted using KUPLOT, both part of the DIFFUSE[35] suite of packages. Atomic coordinates of the model were used to calculate a PDF using the following equation

$$G(r) = \frac{1}{r} \sum_{v} \sum_{\mu} \frac{f(0)_v f(0)_\mu}{\langle f(0) \rangle^2} \delta(r - r_{v\mu}) - 4\pi r \rho_o \qquad (1)$$

where r is the radius, δ is the Dirac delta function, ρ_o is the average number density of the kerogen , $f(0)_v$ and $f(0)_\mu$ are the x-ray atomic form factors for atoms v and μ while $<f(0)>^2$ is the square of the average x-ray atomic form factors. The sum goes over all pairs of atoms v and μ within the model separated by $r_{v\mu}$. The subtraction of $4\pi r \rho_o$ from the G(r) in the above equation leads to the function being equal to zero at large radial distances. While this equation applies for infinite materials with homogenous density confined within well-defined boundaries, kerogen models are finite with irregular shapes and cannot be bound in any way to avoid void space within the boundaries. This leads to a lower average density for the bound model which presents a problem when calculating the pair distribution function using the above equation. To correct for this effect, a modified term is used to describe the shape and size of the kerogen model. The modified equation that allows adjustments for model shape and size, can be derived from Eq. 4 in the paper of Neder and Korsunskiy,[36] is as follows:

$$G(r) = \frac{1}{r} \sum_{v} \sum_{\mu} \frac{f(0)_v f(0)_\mu}{\langle f(0) \rangle^2} \delta(r - r_{v\mu}) - 4\pi r \rho_o \tanh(S(R - r)) \qquad (2)$$

where S is related to the model shape and R the model diameter.

Sample Details: As mentioned in the introduction, experimental data was obtained on a kerogen extracted from a segment of a Green River basin shale core.[24] An elemental

analysis of the kerogen sample used gave an approximately 5% mineral matter content and a dry ash free atomic composition of $C_{100}H_{150}N_3O_8S_1$ for the organic content. This can be compared to the atomic composition of the Siskin model ($C_{645}H_{1017}N_{19}O_{17}S_4$); the only large difference is that the kerogen sample used has a higher oxygen content.

Measurement of Atomic PDF: Measurement of the atomic pair distribution function for a powdered (100 mesh) demineralized Green River kerogen sample[24] was made on instrument 11-ID-B at the Advanced Photon Source (APS), Argonne National Laboratory. High-energy X-rays (60 KeV, λ=0.2128Å) were used with a Perkin Elmer amorphous silicon based detector[38] to collect diffraction data to high values of momentum transfer, Q (Qmax~18Å^{-1}; Q=4πSinθ/λ). The 2D diffraction images were processed in Fit2D[37] software to perform x-ray polarization correction and radial integration for peak intensity. Extraction of the experimental pair distribution function from these data was made with PDFgetX2.[39] This software applies corrections to the scattering data for oblique incidence of the x-rays on the image plate, background subtraction, and Compton scattering to produce a structure function, S(Q). The reduced pair distribution function, F(Q) [F(Q)=Q(S(Q)-1)] is Sine-Fourier transformed to yield the atomic pair distribution function, G(r):

$$G(r) = \frac{1}{2\pi} \int_0^\infty Q[S(Q)-1]Sin(Qr)dr \qquad (3)$$

where the transform is truncated at Qmax=18 Å^{-1} due to experimental limitations. The resulting experimental G(r) function yields information on the average bond distances in the kerogen material and can be compared to calculated PDF of kerogen models. Previously, this approach was shown to provide a reasonable comparison and validation of a coal model.[40]

Measurement of ^{13}C solid state NMR: The ^{13}C spectrum of the same Green River kerogen sample used in the PDF measurement was obtained on a Varian Direct Drive (Oversampled) NMR spectrometer operating at a carbon frequency of 25.152 MHz and a proton frequency of 100.02 MHz. The probe was a Chemagnetics 7.5 mm with a ceramic housing for reduced carbon background. The spinning speed was set at 4100 Hz. The pulse delay was 1 s, which is significantly longer than five times the T_1 for the protons. The data was collected using the cross-polarization (CP) method and TPPM[41] decoupling. The contact time was 3 ms which was also more than five times the longest T_{CH} of the aromatic region, as determined from a variable contact time fit[42] of the data. Within the signal to noise ratio differences, the CP spectrum was essentially identical to a single pulse (SP) spectrum. No line broadening was used in this CP spectrum and a total of 146,200 scans were taken.

Results and Discussion

3D Modeling: Our work began with the assumption that the Siskin 2D model of the Green River oil shale kerogen was the most complete and reliable structural model that is presently available (Figure 1). This structure was incorporated into the molecular modeling scheme using the general procedure described above. The initial starting point was the 3D structure designated as S1 in Figure 2; this represents the starting point for the folded structure which was used to begin the search for lower local energy minima structures. The RHF single point energy of this local structure is −28569.2846 Hartree (1 Hartree = 627.509 kcal/mol).

Following the annealing/optimization process described above using the S1 structure, four additional low energy structures, shown in Figure 3, were identified: S2 (E_{RHF} = −28569.7319 Hartree), S3 (E_{RHF} = −28569.6691 Hartree), S4 (E_{RHF} = −28570.3721 Hartree), and S5 (E_{RHF} = −28569.9504 Hartree). The lowest energy of these initial five structures, S4, was then used as the parent for another annealing/optimization cycle, generating structures S4-1 through S4-5. These structures are shown in Figure 4. These ten structures were all optimized at the RHF level to relax the geometries obtained from the MM+ calculations. It should be noted that due to the size of these systems, it is not feasible to obtain a completely optimized structure. The initial and final RHF energies are listed in Table 1. This shows that the structures obtained from MM+ are, on the average, 1 Hartree higher than those calculated from RHF. The lowest energy structure after the optimization is S4-5 (E_{RHF} = -28571.4952 Hartree). This S4-5 structure was the one used to obtain the simulations of ^{13}C NMR and PDF measurements, used to validate the model.

NMR: In order to explore the sensitivity of the simulated ^{13}C NMR spectrum to the structure of the model, calculations of the chemical shielding were completed on structures S4-1 through S4-5 and these calculations were used to simulate the spectra shown in Figure 5. As can be seen in this figure, the spectra obtained by from any of these models are very similar, with only slight differences in the aliphatic chemical shift region. This is not unexpected, as nearly all the structural changes in the models are occurring in the flexible aliphatic chains while the aromatic structures are very rigid and fixed.

A comparison between the spectrum simulated for model S4-5 and an experimental ^{13}C SSNMR spectrum of a Green River kerogen is shown in Figure 6. The agreement between the simulation and the experimental spectrum is quite good in terms of the agreement of the line shape for both the aliphatic and aromatic regions as well as in the relative intensities of the two regions. The agreement of the relative intensities is a reflection that the model accurately reflects the experimentally observed ratio between aromatic and aliphatic carbons (28% aromatic/olefinic/carbonyl for the model and 24% from the experimental NMR). The similarity in the lineshapes, is an indication that the distribution of carbon types in also being accurately reproduced in the model. For instance, both the experimental and the simulated spectra show the same tail to higher chemical shifts, due to the presence of the carbonyl carbons.

PDF: A similar analysis was completed with the atomic pairwise distribution functions in order to obtain a second independent validation of the model. The PDF simulated based on the S4-5 monomer model is shown in Figure 7, along with the decomposition to the pairings between different atom types. The plot shows that the atom-atom correlations are consistent with the separations expected based on typical carbon bond lengths and angles: C−H (1.12 Å), C−C (1.52 Å), ∠ C−C−H (2.18 Å), ∠ C−C−C (2.56 Å), and dihedral C−C−C−C (3.90 Å). The features above 3 Å are a function of the 3D structure and should show sensitivity to changes in the model. A comparison of the PDFs of the structures S4-1 to S4-5 is shown in Figure 8. The plots do not show any significant deviation from each other which indicates that in general the average of various geometrical parameters such as bond lengths, bond angles, and torsional angles are the same for all structures.

To gauge the sensitivity of the PDF analysis to the structural model a stoichiometric equivalent 2D model of the kerogen Siskin model but using only aliphatic groups was built and its PDF was generated. As shown in Figure 8, the PDF of the aliphatic model is clearly different from the PDF obtained from the other models in the region above 3 Å. Hence, the PDF approach provides unique plots for different chemical structures and can be used for our analysis.

The ultimate test, of course, is how well the PDF of the models correlate with the experimental PDF. A preliminary comparison of the model and experimental PDFs suggested that both have the same features in the short range region ($r < 3$ Å) but deviates heavily at longer distances. There are two possible reasons for this discrepancy: (1) the model is considerably smaller than the experimental structure and (2) a correction term as discussed in the experimental section which accounts for the shape and size of the model is necessary for comparison with experiment.

To explore the effect of the size of the model, a much larger model was built by confining twelve of the unoptimized Siskin model structures (S1) in a bounding box just large enough to accommodate the model. This last point is crucial as the correction term mentioned in point two above, assume a totally filled rectangular box with no void spaces.

The PDF of the 12-unit kerogen model and the experimental PDF for the Green River kerogen are shown in Figure 10. The PDF of the model is corrected accordingly for size and shape. The first peak in the PDFs corresponds to C-H distances whereas the second corresponds to the C-C distance between directly bonded carbons. This distance is approximately 1.5 Å for aliphatic carbons and 1.4 Å for aromatic ones. The second peak at approximately at 2.5 Å corresponds to the geminal distance between carbons two bonds apart. This distance is approximately 2.4 Å and 2.6 Å for aromatic and aliphatic carbons, respectively. The peak at approximately 3 Å corresponds to the distance between carbons separated by four bonds in a *cis* configuration and the one at approximately 3.8 Å to carbons in a *trans* configuration. For these peaks good agreement in terms of peak position and intensity is observed. ANYTHING ELSE HERE?

Conclusion

Several 3D models based on Siskin's 2D model for a Green River kerogen were constructed by the geometry optimization of different conformations provided by simulated annealing techniques. These models were used to obtain simulated PDF plots and ^{13}C NMR spectra which were compared with experimental data obtained on a Green River kerogen sample. This process allowed for the exploration of both the sensitivity of these experimental methods to the 3D structure as well as for the validation of the use of the models for subsequent modeling work.

Using different single unit models, simulations of the expected ^{13}C NMR spectrum were completed. These simulated spectra are all similar, but do show differences in the line shape in the aliphatic region. The comparison between the experimental and simulated spectra is quite good, in terms of the lineshapes of both the aromatic and aliphatic region as well as in the relative signal intensity between the two peaks.

The initial models consisting of a single kerogen unit were not sufficient to mimic the bulk kerogen as can be seen in their respective PDF plots. A larger 12-unit model

was therefore constructed in a manner which minimized the amount of "dead" spaces around the corners of our confining box, as the calculation of the PDF is based on a rectangular box with no void spaces around the molecule. Overall there is good agreement between the model and experimental PDF plots especially at shorter distances, however less accurate for distances between 4 Å and 6 Å. For distances above 6 Å the PDF provides very poor resolution and while there is overall agreement between the model and experimental one, this does not provide any apparent structural information.

References
(1) Behar, F.; Vandenbroucke M. *Revue De L'Institut Francais Du Petrole* **1986**, *41*, 173.
(2) Rullkötter, J.; Michaelis, W. *Org Geochem* **1990**, *16*, 829.
(3) Siskin, M.; Katritksy, A. In *Composition, Geochemistry and Conversion of Oil Shales*, NATO ASO Series, Series C: Mathematical and Physical Sciences-Vol. 455, C. Snape, ed., Kluwer Academic Publishers, Dordrecht/Boston/London, **1995**, p. 313.

(4) Nomura, M.; Artok, L.; Murata, S.; Yamamoto, A.; Hama, A.; Gao, H.; Kidena, K. *Energy Fuels* **1998**, *12*, 512.
(5) van Krevelen, D.W. *Coal: Typology – Chemistry – Physics – Constitution*. Netherlands: Elsevier; **1961**.
(6) Brons, G.; Siskin, M.; Botto, R.I.; Guven, N. *Energy Fuels* **1989**, *3*, 85.
(7) Siskin, M.; Katritzky, A.R. *Science*. Washington, DC; **1991**, *254*, 231.
(8) Smith, J.W.; Higby, L.W. *Anal. Chem.* **1960**, *32*, 17.
(9) Reisberg, J. *Prepr. Pap. – Am. Chem. Soc., Div. Fuel Chem.* **1980**, *25*, 116.
(10) Reisberg, J. In: Stauffer, H.C., editor. *Oil Shale, Tar Sands, and Related Materials*. ACS Symposium Series 163; American Chemical Society, Washington, DC; **1981**, p. 155.
(11) Vanderbroucke, M. Oil & Gas Science and Technology-Rev. IFP, **2003**, *58* (2), 243.
(12) Durand, B; Vanderbroucke, M. As cited in *Kerogen, Insoluble Organic Matter From Rocks*, B. Durand, ed., Technip, **1980**, p. 218 and 319.

(13) Siskin, M.; Scouten, C.G.; Rose, K.D.; Aczel, D.; Colgrove, S.G.; Pabst, R.E. In: Snape, C., editor. *Composition, geochemistry and conversion of oil shales*. Netherlands: Kluwer Academic; **1995**, p. 143.
(14) Lille, U.; Heinmaa, I.; Pehk, T. *Fuel* **2003**, *82*, 799.
(15) Faulon, J.L.; Vandernbroucke, M.; Drappier, J.M.; Behar, F.; Romero, M. *Organic Geochemistry*, **1990**, *6*, 981; Faulon, J.L. *Prediction, elucidation et modelisation moleculaire: algorithms et applications*. **1991,** Ph. D. Thesis.

(16) Freund, H.; Walters, C.C.; Kelemen, S.R.; Siskin, M.; Gorbaty, M.L.; Curry, D.J.; Bence, A.E. *Org. Geochem.* **2007**, *38*, 288.

(17) Vandergrift, G.F.; Winans, R.E.; Horwitz, E.P. *Fuel* **1980**, *59*, 634.

(18) Jeong, K.M.; Patzer II, J.F. *Indigenous Mineral Matter Effects in Pyrolysis of Green River Oil Shale*, In Geochemistry and Chemistry of Oil Shales, American Chemical Society, **1983**, p. 529.

(19) Jeong K.M.; Kobylinski, T.P. *Organic-Mineral Matter Interactions in Green River Oil Shale*, American Chemical Society, **1983**, p. 493.

(20) Sheu, E.Y. *Self-Association of Asphaltenes; Structure and Molecular Packing*, In: Mullins, O.C.; Sheu, E.Y., editors. Structure and Dynamics of Asphaltenes, Plenum Press, New York, **1998**, p.115.

(21) Egami, T.; Billinge, S.J.L. *Underneath the Bragg Peaks: Structure Analysis of Complex Materials*; Oxford/Pergamon Press, New York, **2004**.

(22) Nield, V.; Keen, D.A.; *Diffuse Neutron Scattering from Crystalline Materials*; Oxford/Clarendon Press, Oxford, **2001**.

(23) Solum, M.S.; Pugmire, R.J.; Grant, D.M. *Energy & Fuels*, **1989**, *3*, 187-193.

(24) Solid state ^{13}C NMR and PDF measurements were completed on a sample of kerogen isolated following the process outlined by Vandergrift, G. F.; Winans, R. E.; Scott, R. G.; Horwitz, E. P., in Fuel 1980, 59(9), 627, on a one foot section from the peak organic content of the Mahogany zone of a core drilled in the Green River Formation of the Uinta Basin in Utah in spring 2010. The experimental results will be discussed further in a separate publication.

(25) HyperChem(TM) Professional 7, Hypercube, Inc., 1115 NW 4th Street, Gainesville, Florida 32601, USA.

(26) Allinger, N.L. *J. Am. Chem. Soc.*, **1977**, *99*, 8127.

(27) Schmidt, M.W.; Baldridge, K.K.; Boatz,J.A.; Elbert, S.T.; Gordon, M.S.; Jensen, J.J.; Koseki, S.; Matsunaga, N.; Nguyen, K.A.; Su, S.; Windus, T.L.; Dupuis, M.; Montgomery, J.A. *J.Comput.Chem.*, **1993**, *14*, 1347.

(28) Hehre, W.J.; Stewart, R.F.; Pople, J.A. *J. Chem. Phys.* **1969**, *51*, 2657.

(29) Kirkpatrick, S.; Gelatt, C.D.; Vecchi, M.P. *Science* **1983**, *220*, 671.

(30) Macrae, C.F.; Bruno, I.J.; Chisholm, J.A.; Edgington, P.R.; McCabe, P.; Pidcock, E.; Rodriguez-Monge, L.; Taylor, R.; van de Streek, J.; Wood, P.A. *J. Appl. Cryst.* **2008**, *41*, 466.

(31) Adamo, C; Barone, V., *J. Chem. Phys.*, **1999**, *110*, 6158-69.

(32) Ditchfield, R.; Hehre, W.J.; Pople, J.A. *J. Chem. Phys.*, **1971**, *54*, 724; Hehre, W.J.; Ditchfield, R.; Pople, J.A. *J. Chem. Phys.*, **1972**, *56*, 724.

(33) Gaussian 09, Revision B.01, Frisch, M. J.; Trucks, G. W.; Schlegel, H. B.; Scuseria, G. E.; Robb, M. A.; Cheeseman, J. R.; Scalmani, G.; Barone, V.; Mennucci, B.; Petersson, G. A.; Nakatsuji, H.; Caricato, M.; Li, X.; Hratchian, H. P.; Izmaylov, A. F.; Bloino, J.; Zheng, G.; Sonnenberg, J. L.; Hada, M.; Ehara, M.; Toyota, K.; Fukuda, R.; Hasegawa, J.; Ishida, M.; Nakajima, T.; Honda, Y.; Kitao, O.; Nakai, H.; Vreven, T.; Montgomery, Jr., J. A.; Peralta, J. E.; Ogliaro, F.; Bearpark, M.; Heyd, J. J.; Brothers, E.; Kudin, K. N.; Staroverov, V. N.; Kobayashi, R.; Normand, J.; Raghavachari, K.; Rendell, A.; Burant, J. C.; Iyengar, S. S.; Tomasi, J.; Cossi, M.; Rega, N.; Millam, N. J.; Klene, M.; Knox, J. E.; Cross, J. B.; Bakken, V.; Adamo, C.; Jaramillo, J.; Gomperts, R.; Stratmann, R. E.; Yazyev, O.; Austin, A. J.; Cammi, R.; Pomelli, C.; Ochterski, J. W.;

Martin, R. L.; Morokuma, K.; Zakrzewski, V. G.; Voth, G. A.; Salvador, P.; Dannenberg, J. J.; Dapprich, S.; Daniels, A. D.; Farkas, Ö.; Foresman, J. B.; Ortiz, J. V.; Cioslowski, J.; Fox, D. J. Gaussian, Inc., Wallingford CT, 2009.

(34) Jameson, A.K.; Jameson, C.J. *Chem. Phys. Lett.* 1987, *134*, 461.

(35) Proffen, T.; Neder, R.B. *J. Appl. Crystallogr.* **1997**, *30*, 171.

(36) Neder, R.B.; Korsunskiy, V.I. *J. Phys.: Condens. Matter*, **2005**, *17*, S125.

(37) Hammersley, A.P.; Svensson, S. O.; Hanfland, M.; Fitch, A.N.; Hausermann, D. *High Pressure Research*, **1996**, *14*, 235.

(38) Chupas, P. J.; Chapman, K. W.; Lee, P. L. *J. Appl. Cryst.*, **2007**, *40*, 463.

(39) Qiu, X.; Thompson, J.W.; Billinge, S.J.L. *J. Appl. Cryst.*, **2004**, *37*, 678.

(40) Winans, R.E.; Chapman, K.W.; Chupas, P.J.; Seifert, S.; Clemens, A.H.; Calo, J.; Bain, E.; Mathews, J.P.; Narkiewicz, M.R. *Prep. Pap. - Am. Chem. Soc., Div Fuel Chem.*, **2008**, *53(1)*, 283.

(41) Bennett, A. E., Rienstra, C. M., Auger, M., Lakshmi, K. V., Griffin, R. G.; *J. Chem. Phys.,* 103, **1995**, 6951.

(42) Kolodziejski, W., Klinowski, J., *Chem. Rev.*, 102, **2002**, 613.

Table 1: RHF/STO-3G initial and final energies (in Hartree) of the different monomer kerogen models. The S2 to S5 structures were obtained from the simulated annealing procedure on S1. Structures S4-1 through S4-5 were derived from the lowest energy conformer (S4) from the first annealing step.

	Energy (Hartree)	
	Initial Structure	Final Structure
S1	−28569.2846	-28570.5355
S2	−28569.7319	-28570.5929
S3	−28569.6691	-28570.4581
S4	−28570.3721	-28571.1721
S5	−28569.9504	-28570.4481
S4-1	−28569.8771	-28571.4328
S4-2	−28569.8316	-28571.3913
S4-3	−28569.9410	-28571.4887
S4-4	−28569.8622	-28571.4575
S4-5	−28569.9061	-28571.4952

Chemical Formula: $C_{20}H_{42}$
Exact Mass: 282.33
20 Aliphatic C

Chemical Formula: $C_{18}H_{38}$
Exact Mass: 254.30
18 Aliphatic C

Chemical Formula: $C_{75}H_{117}N_4O_5$
Molecular Weight: 1154.76
Elemental Analysis: C, 78.01; H, 10.21; N, 4.85; O, 6.93
16 Aromatic C; 2 Aromatic N; 2 Olefinic C; 2 Aliphatic N; 1 Ammoniacal N

Chemical Formula: $C_{18}H_{30}$
Exact Mass: 246.23
6 Aromatic; 12 Aliphatic C

Chemical Formula: $C_{45}H_{60}O$
Molecular Weight: 616.96
Elemental Analysis: C, 87.60; H, 9.80; O, 2.59
18 Aromatic C; 2 Olefinic C

Chemical Formula: $C_{367}H_{547}N_{10}O_{10}S_2^{3-}$
Molecular Weight: 5323.46
Elemental Analysis: C, 82.80; H, 10.36; N, 2.63; O, 3.01; S, 1.20
7 Aromatic N; 3 Aliphatic N; 3 Ammoniacal N; 94 Aromatic C; 24 Olefinic C

Chemical Formula: $C_{102}H_{167}NOS_2$
Molecular Weight: 1487.55
Elemental Analysis: C, 82.36; H, 11.32; N, 0.94; O, 1.08; S, 4.31
20 Aromatic C; 2 Olefinic C; 1 Aliphatic N

Type I Kerogen (Green River)
Chemical Formula: $C_{645}H_{1017}N_{19}O_{17}S_4$
Molecular Weight: 9438.35
Elemental Analysis: C, 82.08; H, 10.86; N, 2.82; O, 2.88; S, 1.36

Fig. 1: The 2D Siskin model of Green River kerogen, taken from ref 13.
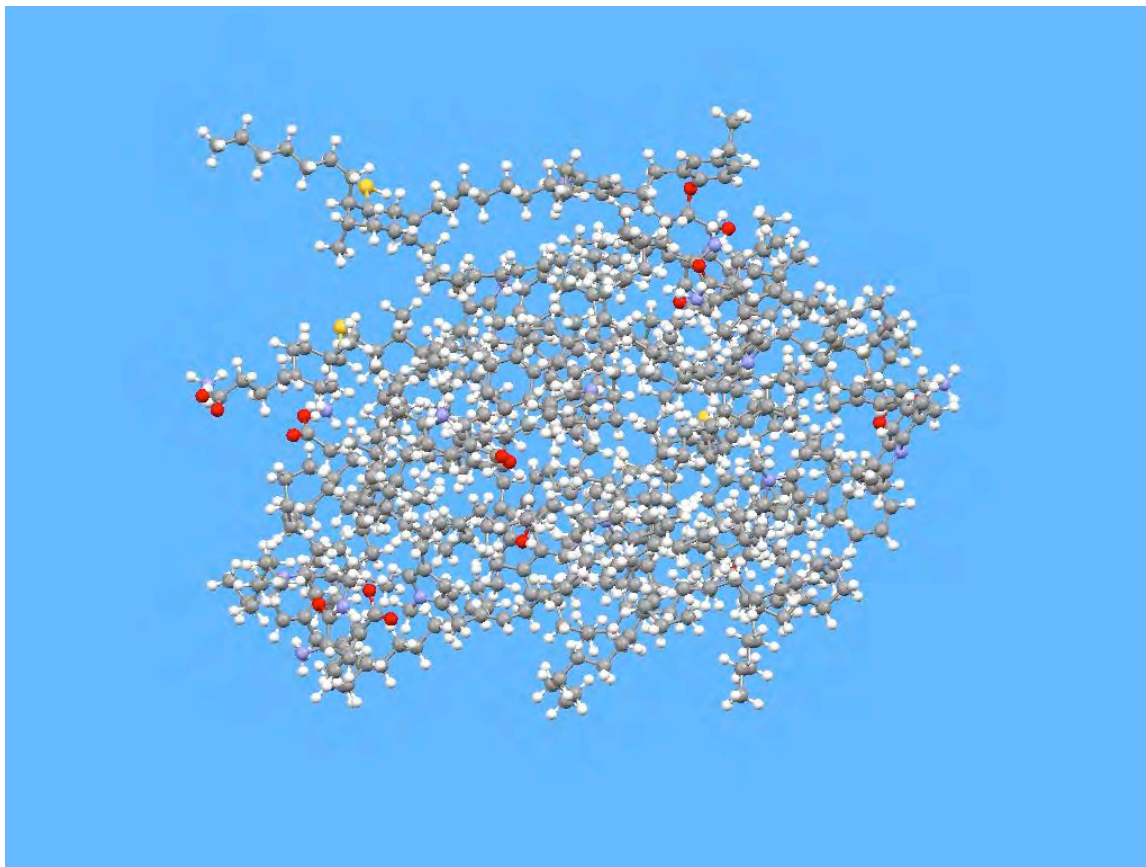
Fig. 2: Initial 3D model (S1) of the Green River kerogen Siskin model (1702 atoms). The atom colors are as follows: C - gray, O - red, N - blue, S - yellow, H - white. The tubes represent the molecule's backbone and the spheres represent the atoms.
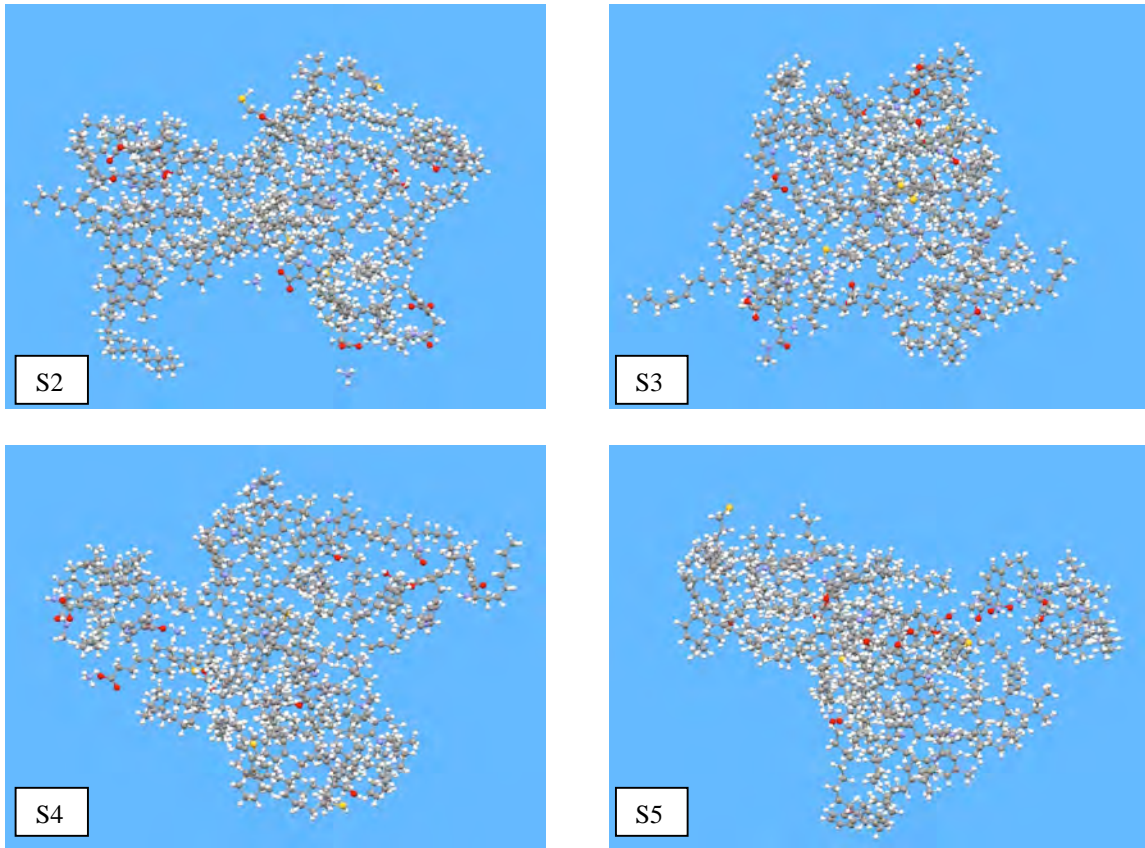
Fig. 3: Local structures generated by applying the simulated annealing procedure described on the initial 3D kerogen model S1. The atom colors and molecule description are the same as in Fig. 2.
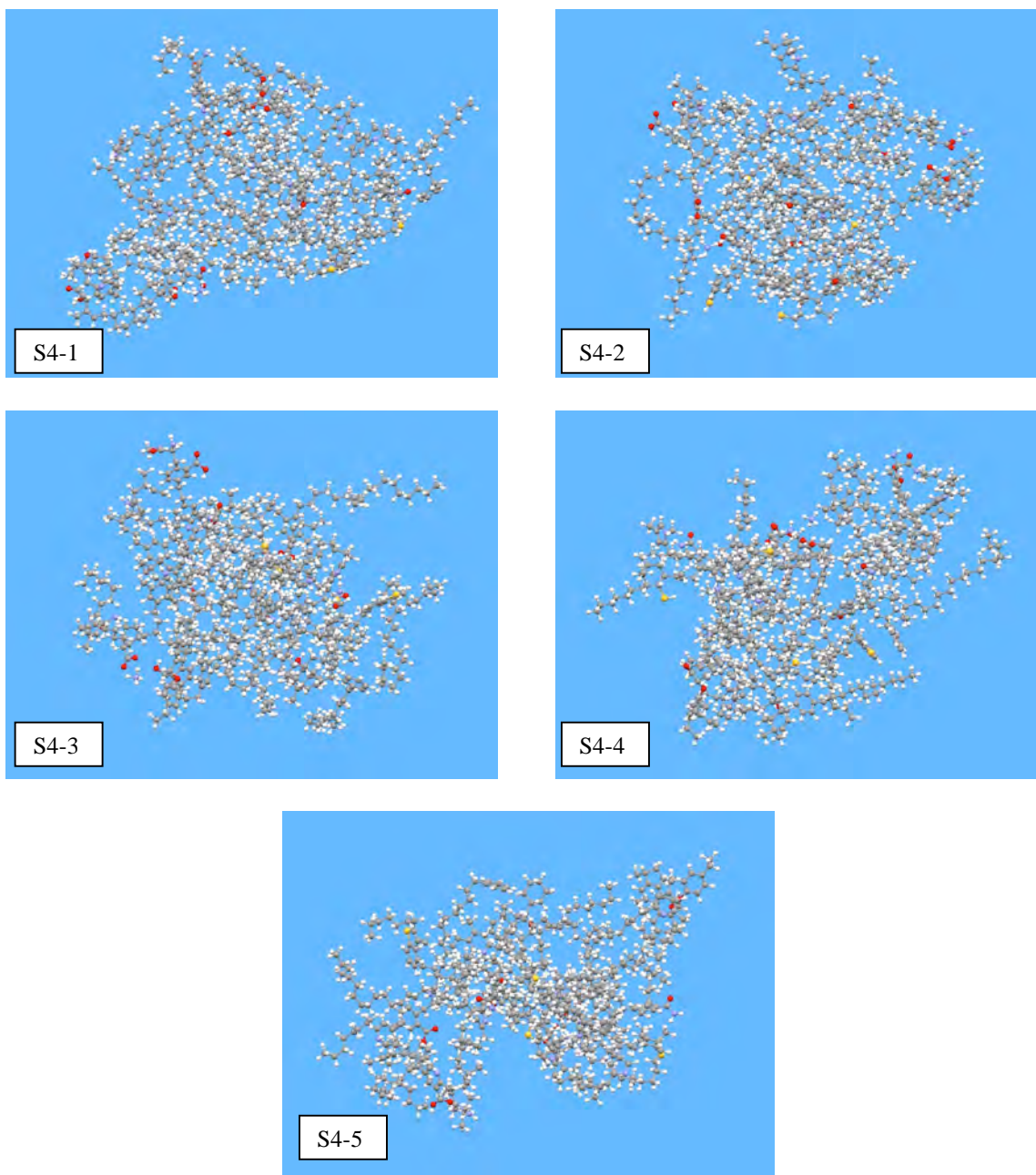
Fig. 4: Local structures generated by subjection kerogen structure S4 to the simulated annealing procedure. The atom colors and molecule description are the same as in Fig. 2.
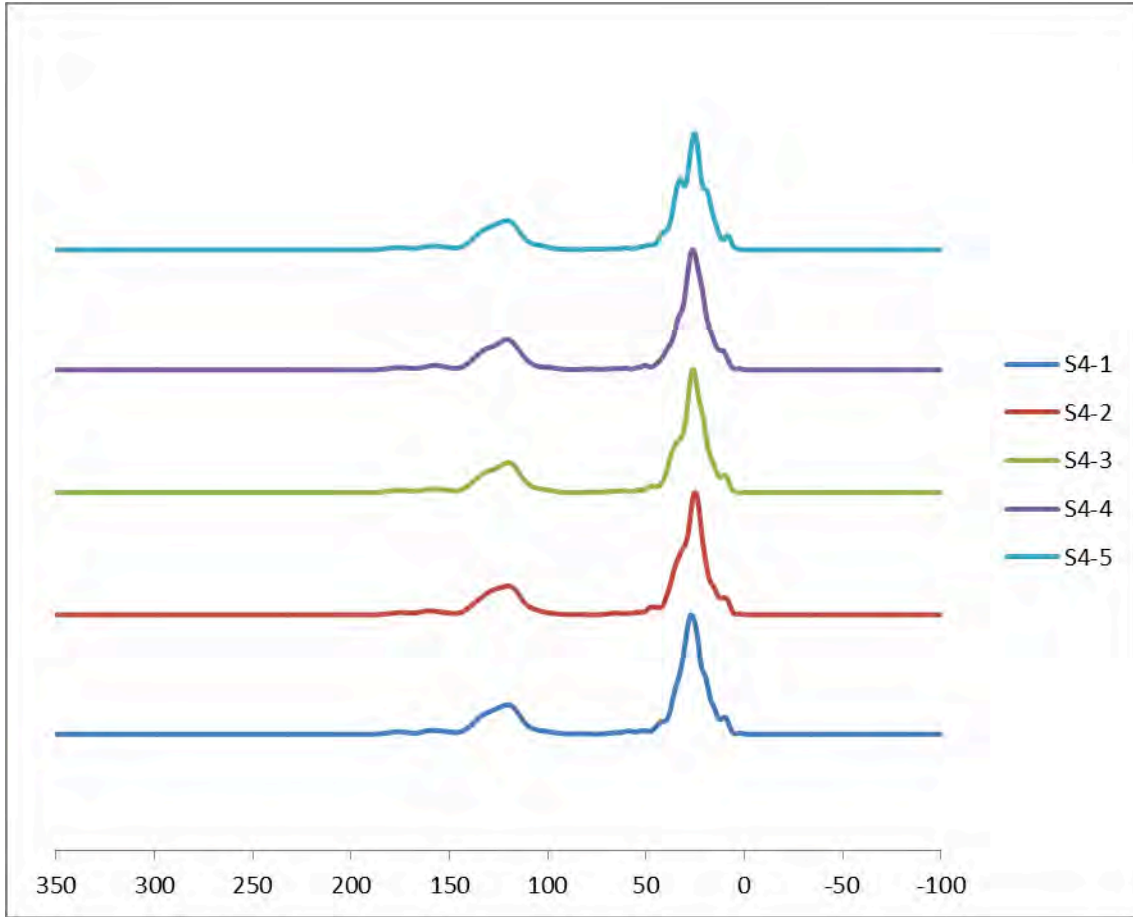
Fig 5: Simulated ^{13}C NMR spectra for models S4-1 thorough S4-5
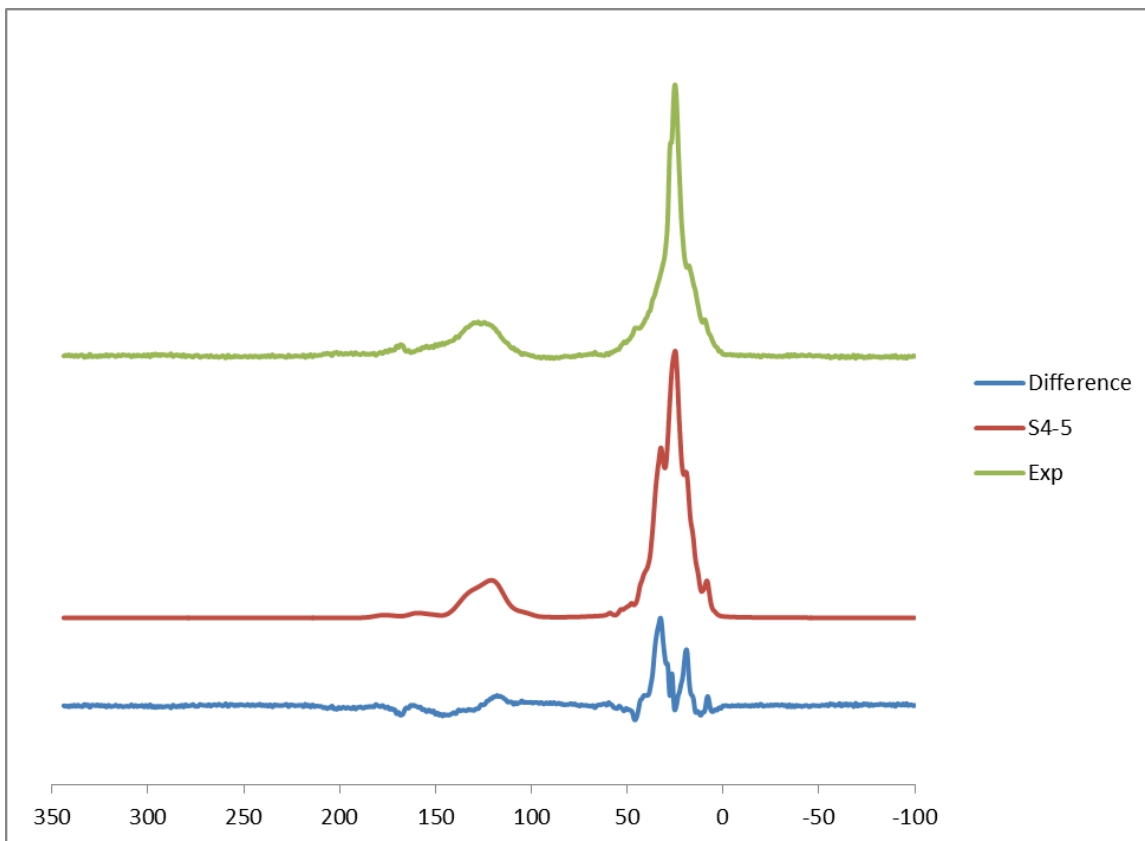
Fig 6: Comparison between simulated ^{13}C NMR spectrum from model S4-5 and the experimental solid state ^{13}C NMR spectrum obtained on a Green River oil shale kerogen. The RMS difference between S4-5 and experimental spectrum is 8 ppm.
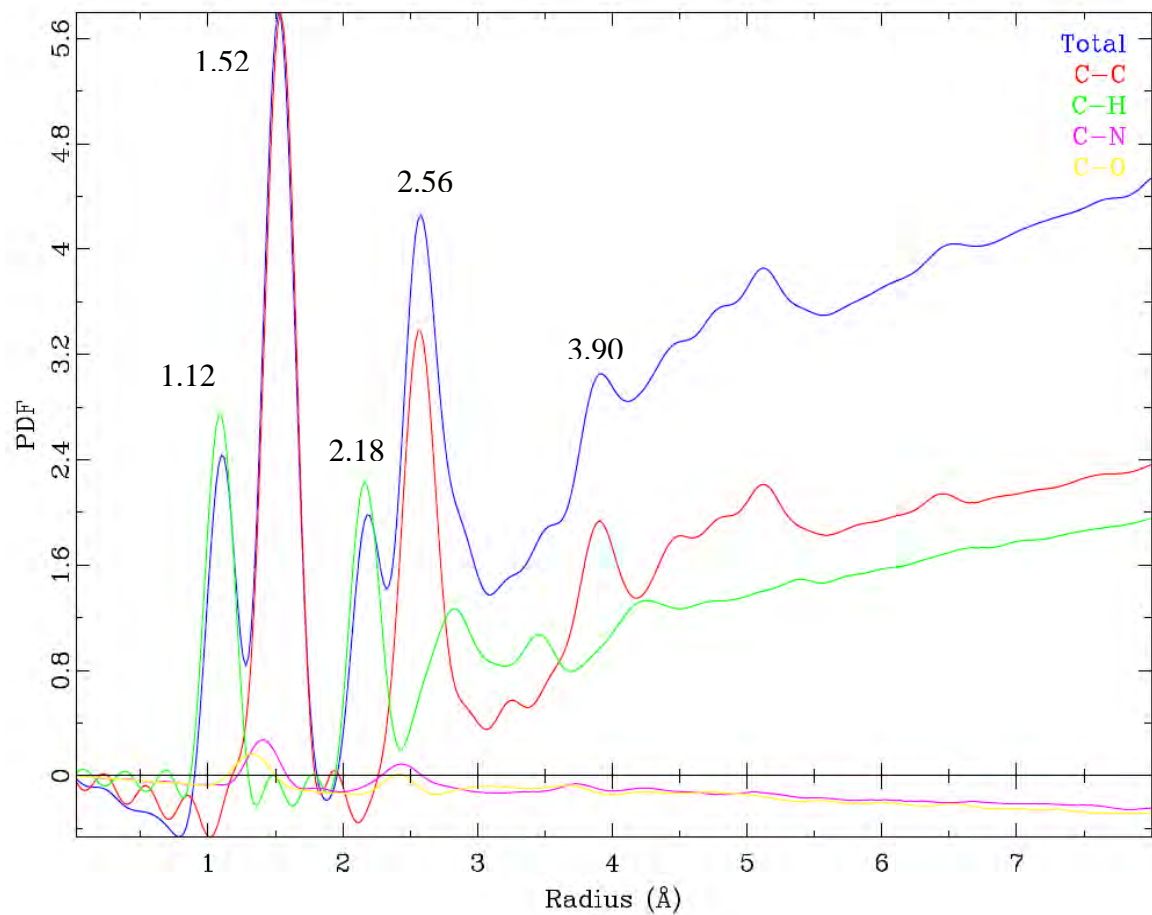
Fig. 7: Pair distribution functions (PDFs) of atom-atom correlations in the kerogen monomer model S4-5. The correlation is decomposed to the contributions from different atomic pairings.
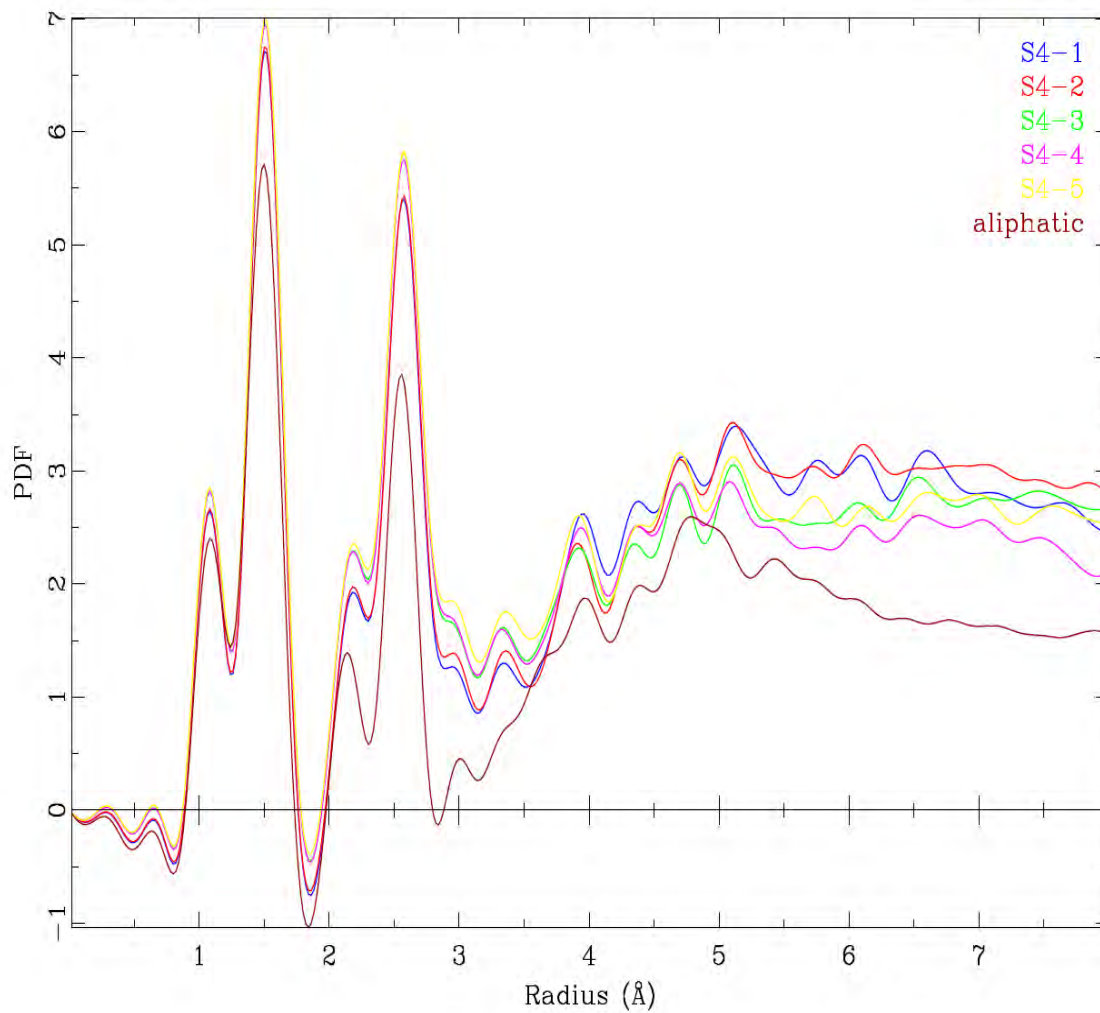
Fig. 8: PDFs of the five monomer conformations of kerogen obtained from the lowest energy structure S4. A stoichiometric equivalent aliphatic structure is included to show that the PDF method is sensitive to varying structures.
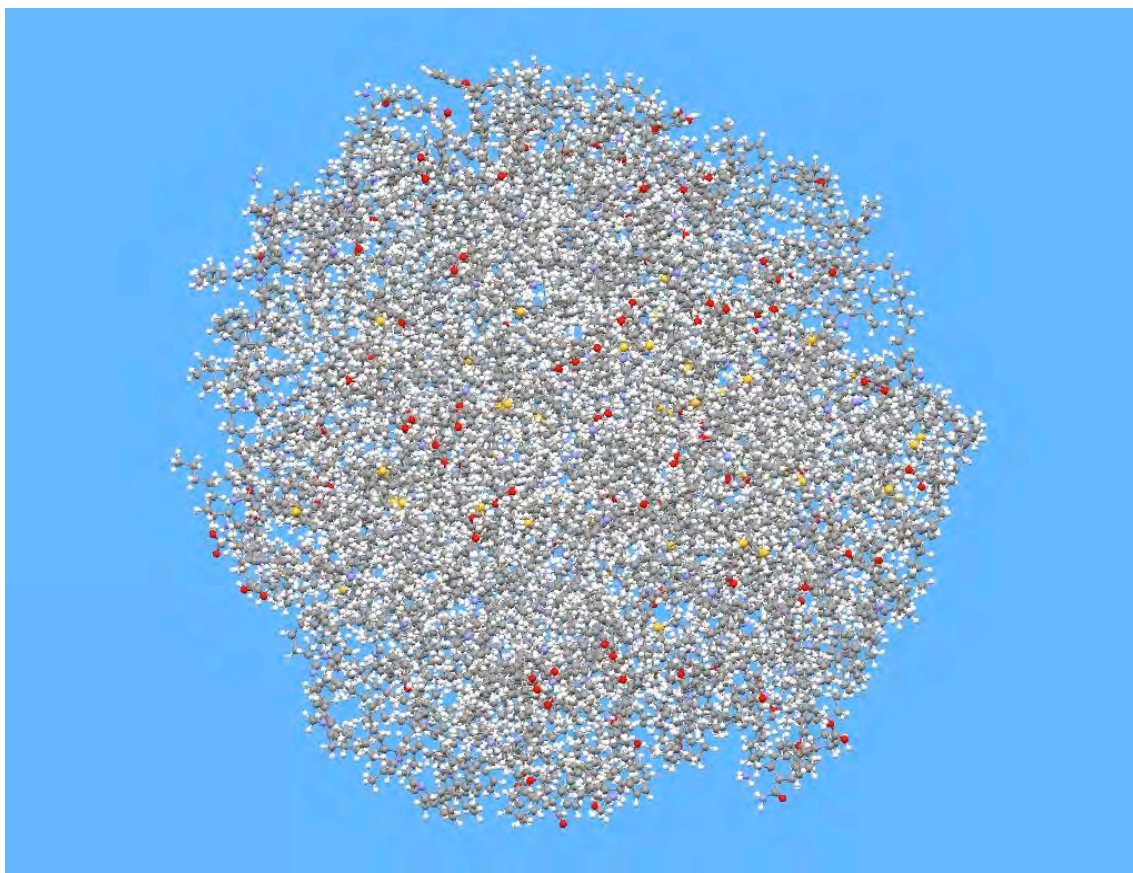
Fig. 9: Three-dimensional structures of the 12-unit kerogen models. The atom colors and molecule description are the same as in Fig. 2.
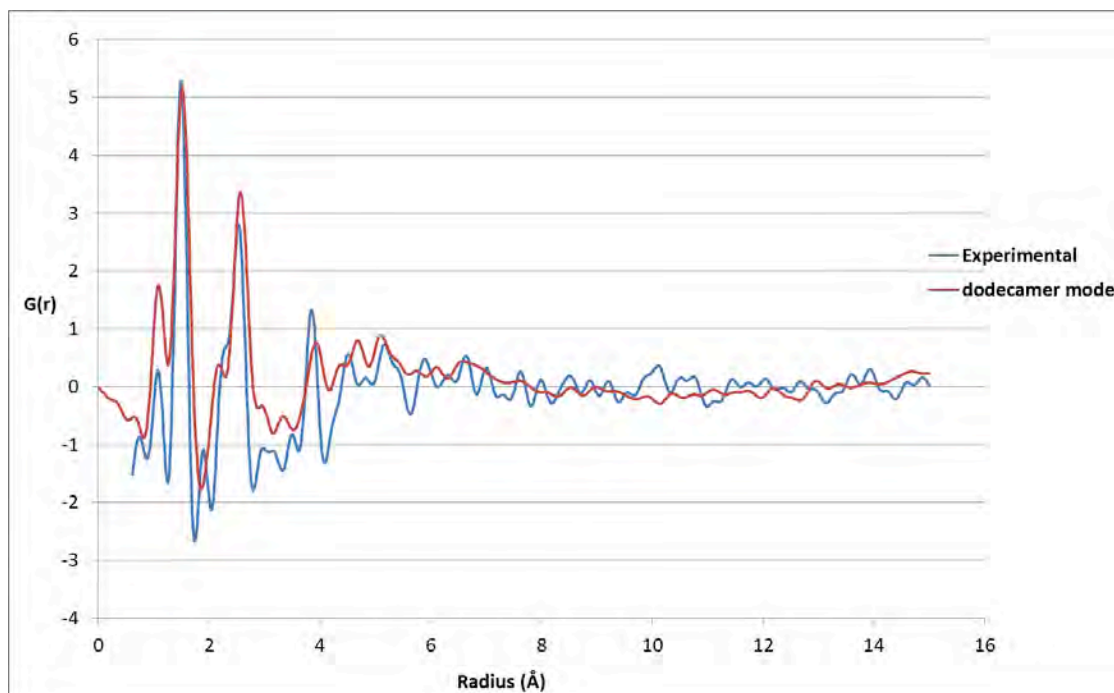
Fig. 10: Comparison of experimentally determined PDF for Green River kerogen and the 12-unit model. The dodecamer model was shape and size corrected using the modified function $-4\pi r\rho_o\tanh(S(R-r))$ with S=0.05 and R=19.3 Å.

First Results and Simulation of AMSO's RD&D Process Tests

Alan K. Burnham et al.

Chief Technology Officer

American Shale Oil, LLC

Presented at:

Unconventional Fuels Conference

Salt Lake City, UT, May 15, 2012

AMSO is one of three RD&D Leaseholders in Colorado's Piceance Basin

- ❑ **AMSO LLC is a 50/50 joint venture of Genie Energy Ltd and TOTAL S.A.**

  - ▪ Genie is the operating partner during R&D; Total is during commercial operations

  - ▪ Genie also has an oil shale venture in Israel (IEI)

  - ▪ TOTAL also has other oil shale ventures (e.g., with Red Leaf in Utah)

- ❑ **The lease was originally issued to EGL Resources in 2007**

- ❑ **Using the USGS 2-million barrels-per-acre estimate, this area contains ~10 billion barrels of potential resource**
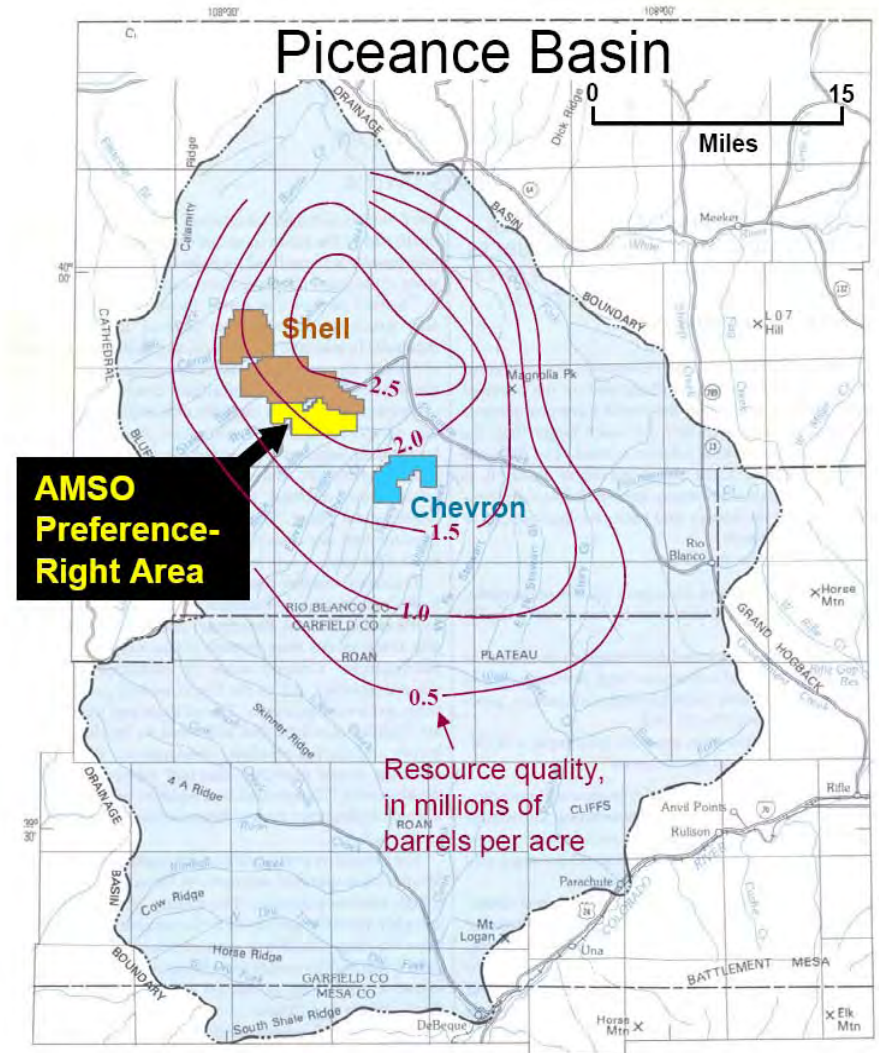
Piceance Basin
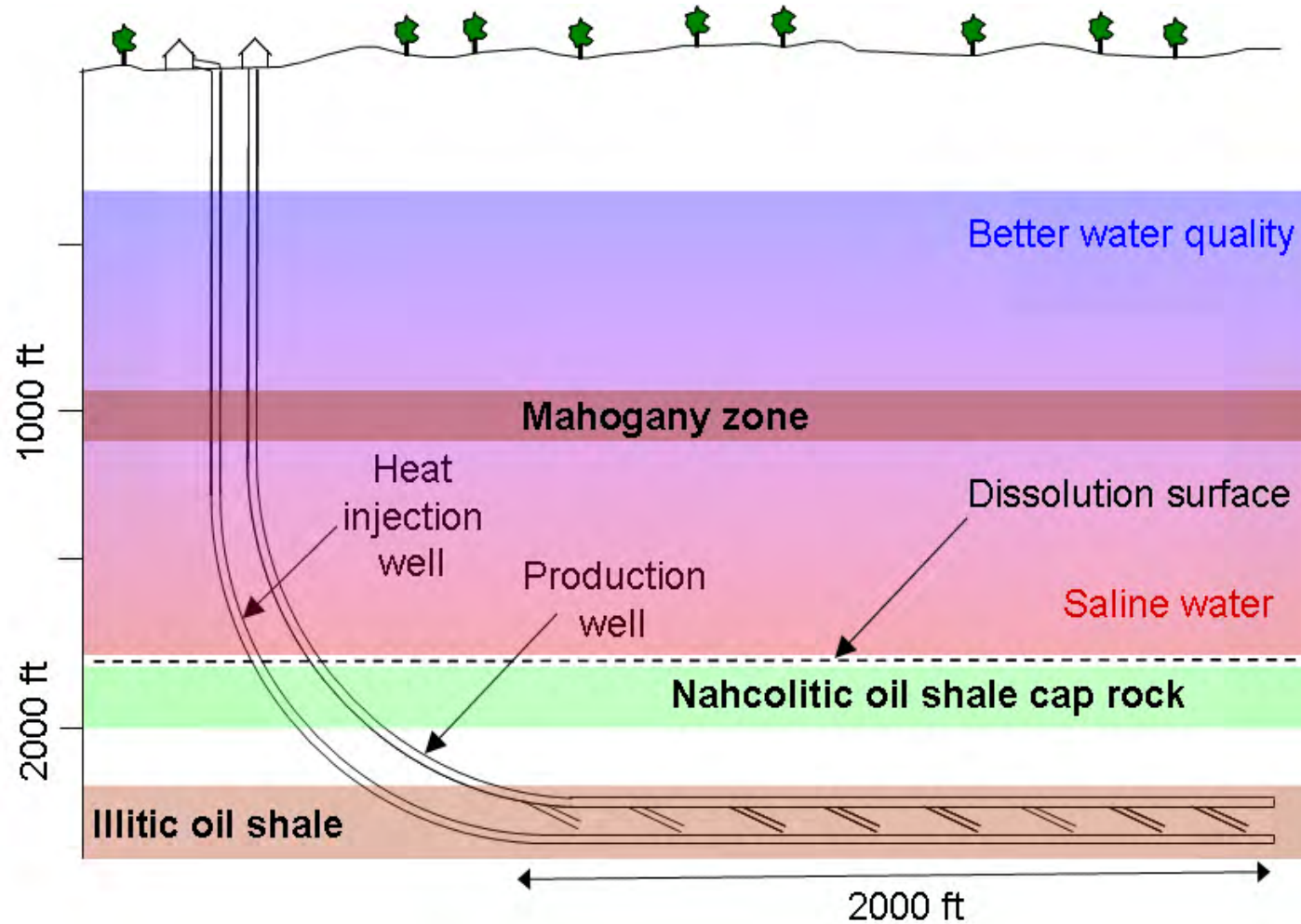
- ❑ Minimal surface footprint
- ❑ Protection of aquifers
- ❑ Low water usage

- ❑ High energy efficiency
- ❑ Low gas emissions
- ❑ High-value jobs

Our RD&D Plan aims to demonstrate important aspects of our process

- ❑ **Geochemical and geomechanical properties of the illitic oil shale**

- ❑ **Hydrologic isolation of the illitic oil shale from protected waters**

- ❑ **Adequate heat transfer using a boiling oil pool**
  - ▪ Central to the Conduction, Convection, Reflux (CCR^{TM}) concept
  - ▪ Enhancement by thermo-mechanical fragmentation

- ❑ **Premium oil quality**
  - ▪ High API gravity, low metals content, low nitrogen content

- ❑ **Minimal water usage (<1 barrel of water per barrel of oil)**

- ❑ **Ability to meet all applicable air emission regulations**

- ❑ **Technology for carbon sequestration**

- ❑ **Economic viability**

The AMSO process uses convective heat transfer via permeability from thermo-mechanical fragmentation

Vapor Product Out

Rubble-Filled Retort

Condensate — Vapor — Condensate

Boiling Oil

Heating well
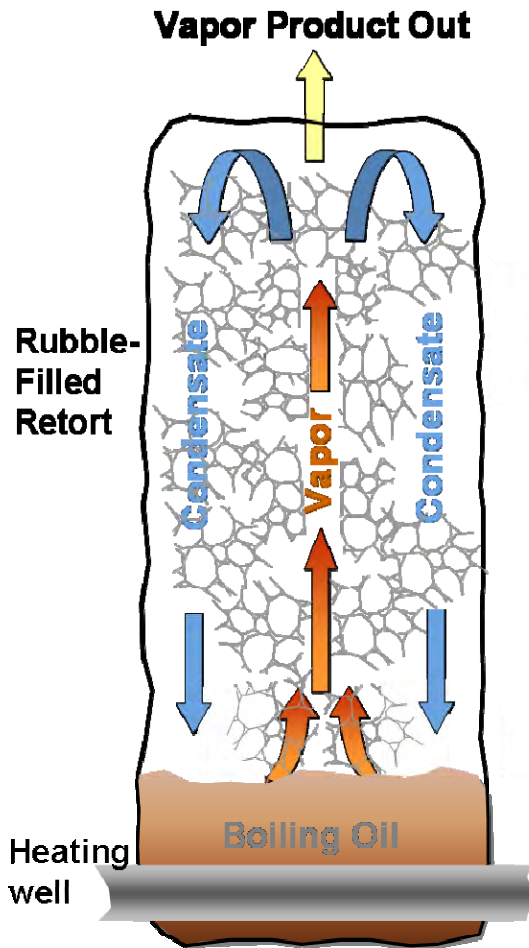
From Prats et al., JPT, 1977
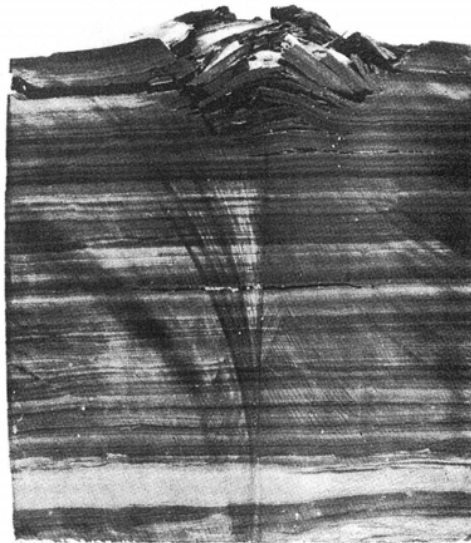
Confined on all but one side
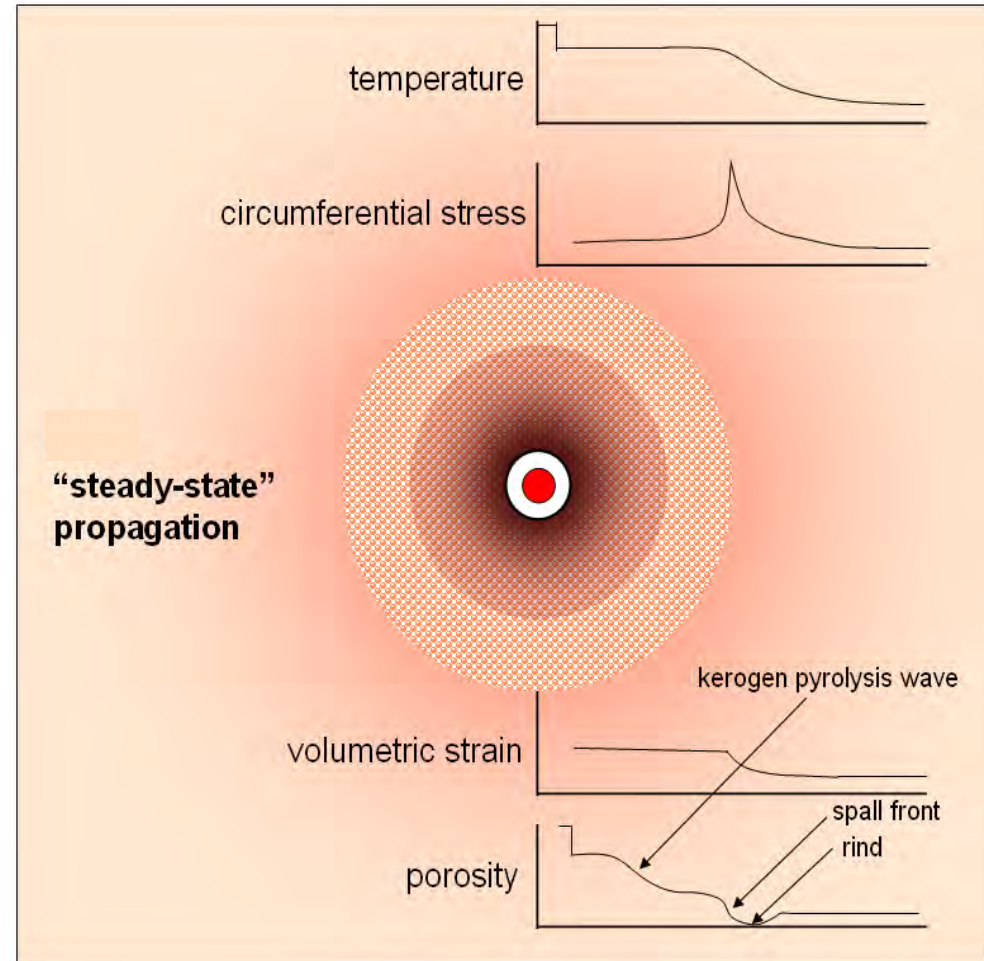
temperature

circumferential stress

"steady-state" propagation

kerogen pyrolysis wave

volumetric strain

spall front
rind

porosity

- ❑ Developing rock mechanics models to estimate load-bearing capability, thermal fracture (crack) characteristics, and porosity and permeability

- ❑ Modeling the relative importance of conductive and convective heat transfer rates as a function of rubble characteristics

- ❑ Simulating heat transfer rates in our pilot test geometry at various levels of approximation

- ❑ Developing reservoir simulators capable of modeling the entire range of important chemical and physical processes

*ICSE = Institute for Clean and Secure Energy

❑ Oil shale changes from elastic to viscoelastic to plastic as temperature increases, so modeling is difficult
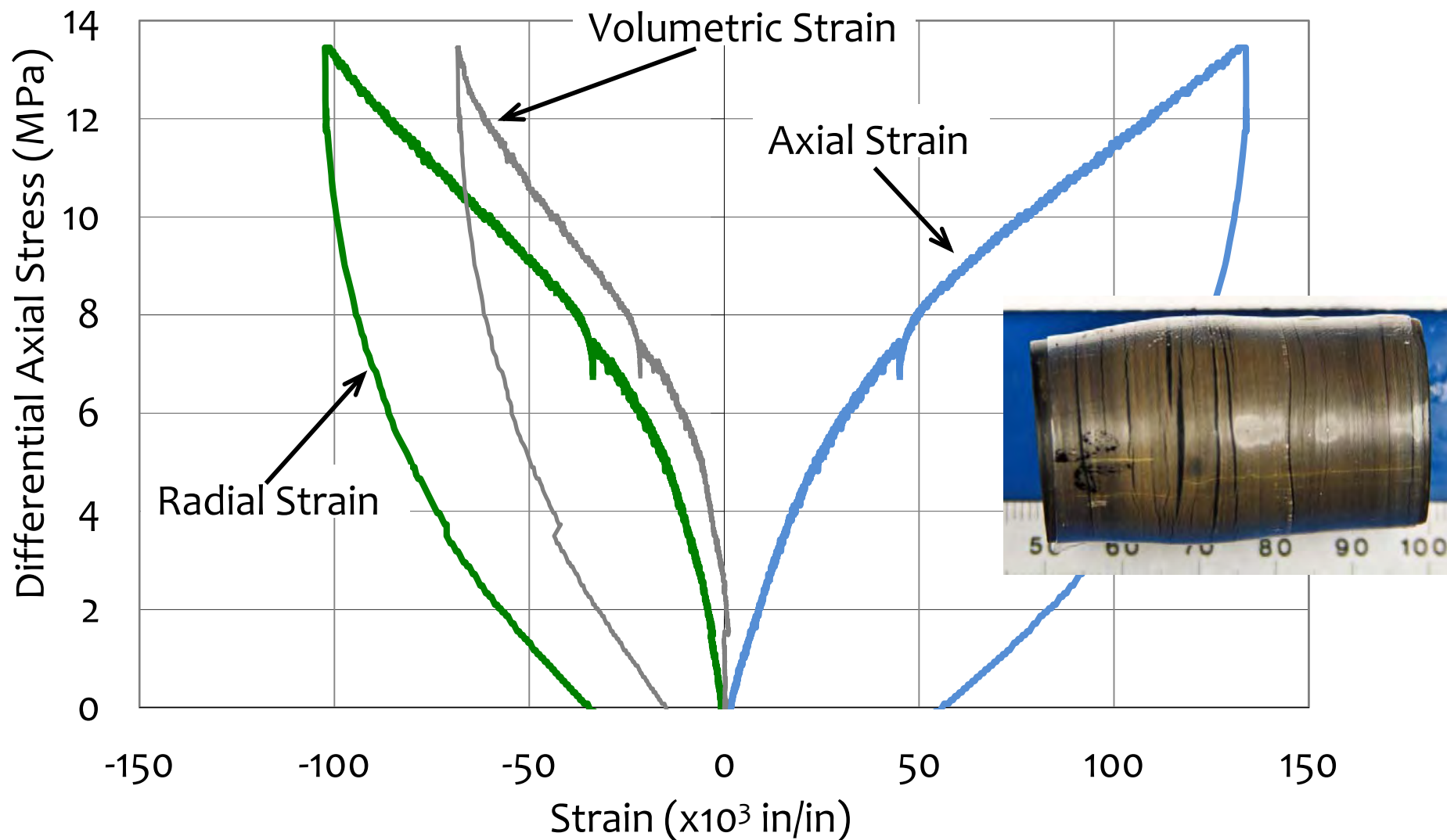
ICSE is exploring the most efficient way of incorporating these properties into models

- Hyperbolic relationships (Duncan-Chang) between stress and deformation
- Neural networking protocols to interrelate behavior to the governing independent variables (e.g., temperature, grade)

Initial Computational Geometries

P. Smith, M. Hradisky, D. Coates, U Utah
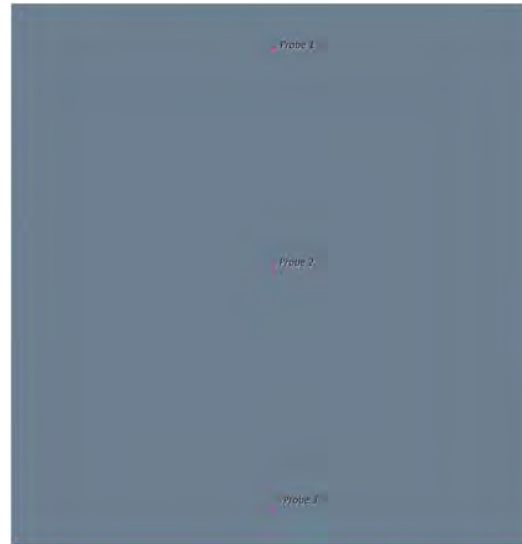
Solid shale

Empty volume

Crack size 0.005 m

Crack size 0.010 m

Crack size 0.015 m
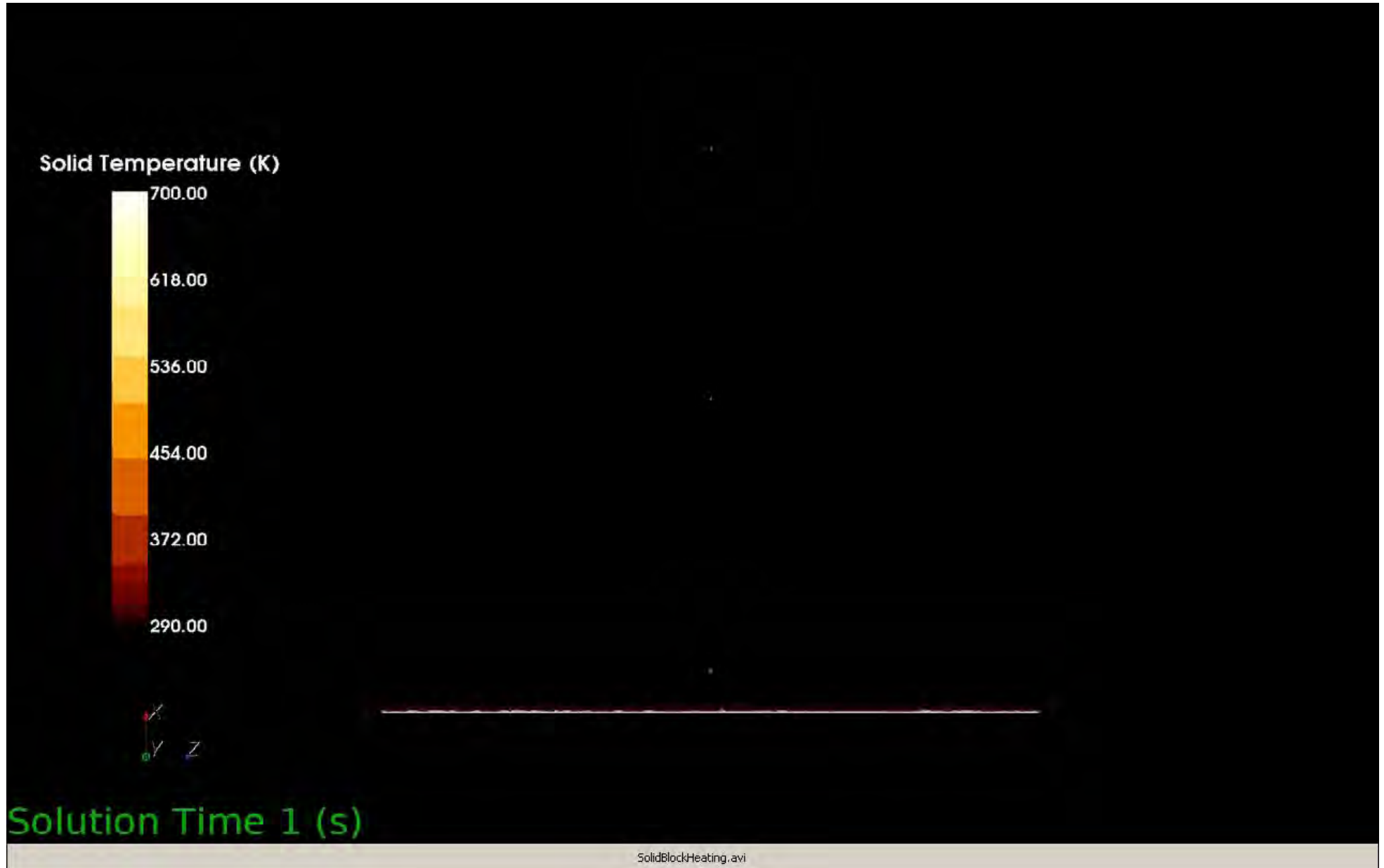
Solid Temperature (K)

700.00

618.00

536.00

454.00

372.00

290.00

Fluid Temperature (K)

700.00

618.00

536.00

454.00

372.00

290.00
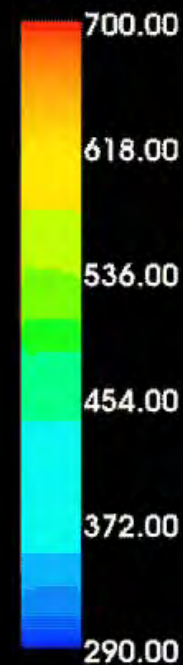
Solution Time 1 (s)

Crack0p015-old.avi

Our production well is insulated with silca aerogel, the best insulation known

Aerogel granules <1/8"

Carbon black added for blocking radiative heat transfer

Filling the production well

- ❏ **Heater power up to about half its design value**
  - ▪ Limited by a leaky weld that prevented drawing a vacuum on the reflux heater
- ❏ **Discovered flaws in some other downhole equipment that required fixing**
- ❏ **The test propagated a steam front at about 250 °C up the lower lateral of the triangular convection loop.**
- ❏ **The heater test provided valuable information for benchmarking process models**
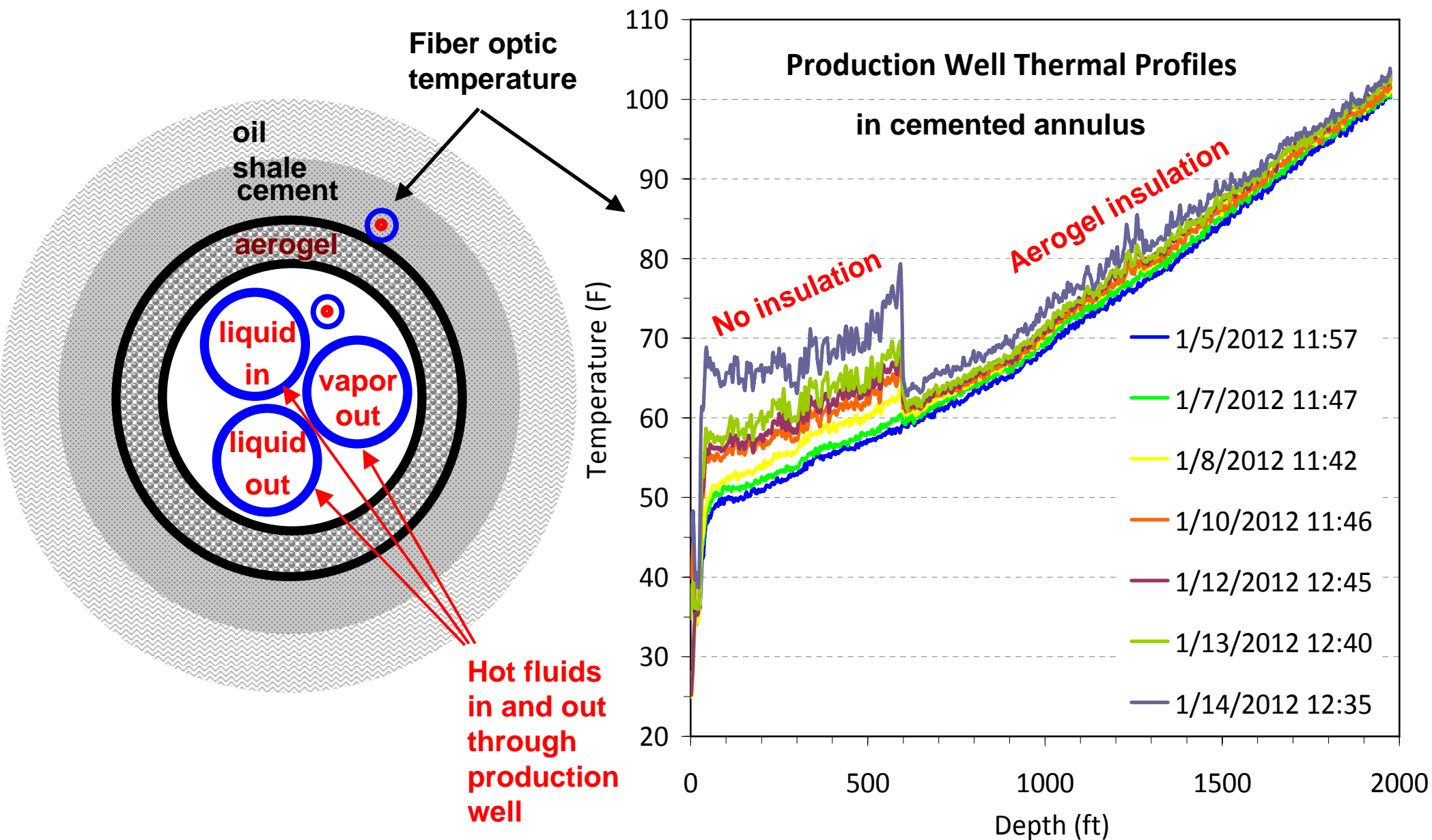
The Pilot Test has six geophysical monitoring wells, including fiber optic temperatures
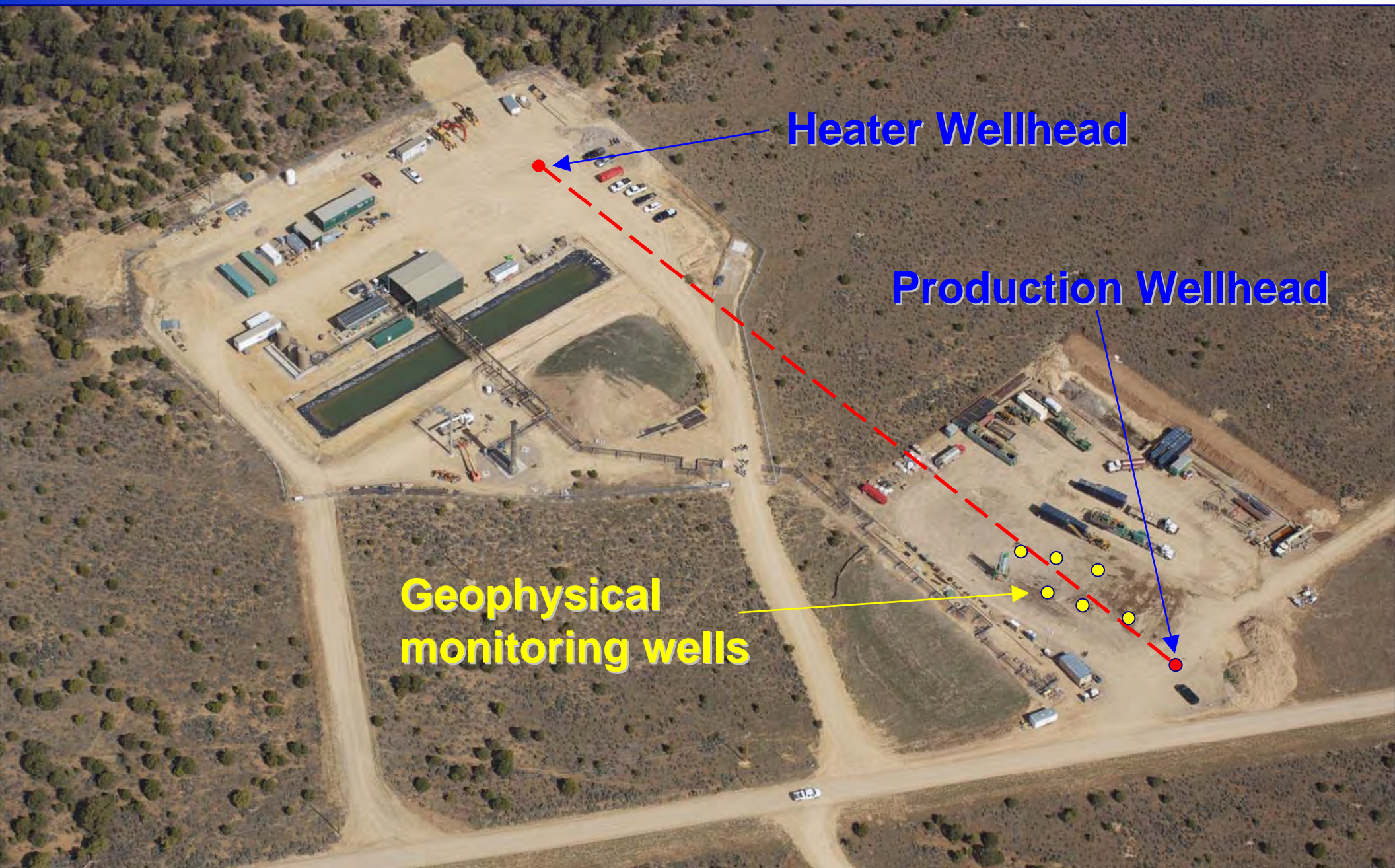
Heater Wellhead

Production Wellhead

Geophysical monitoring wells
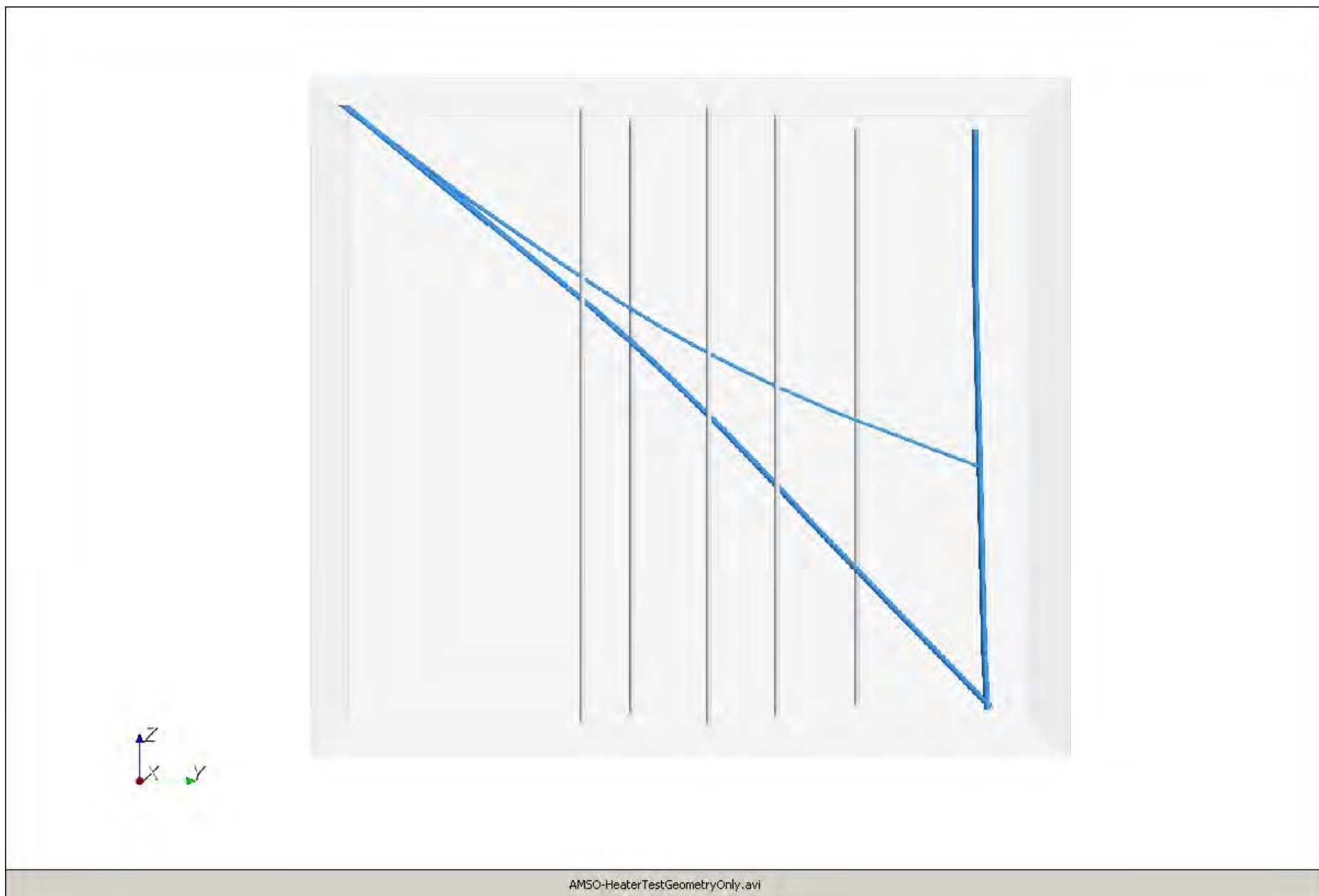
AMSO-HeaterTestGeometryOnly.avi
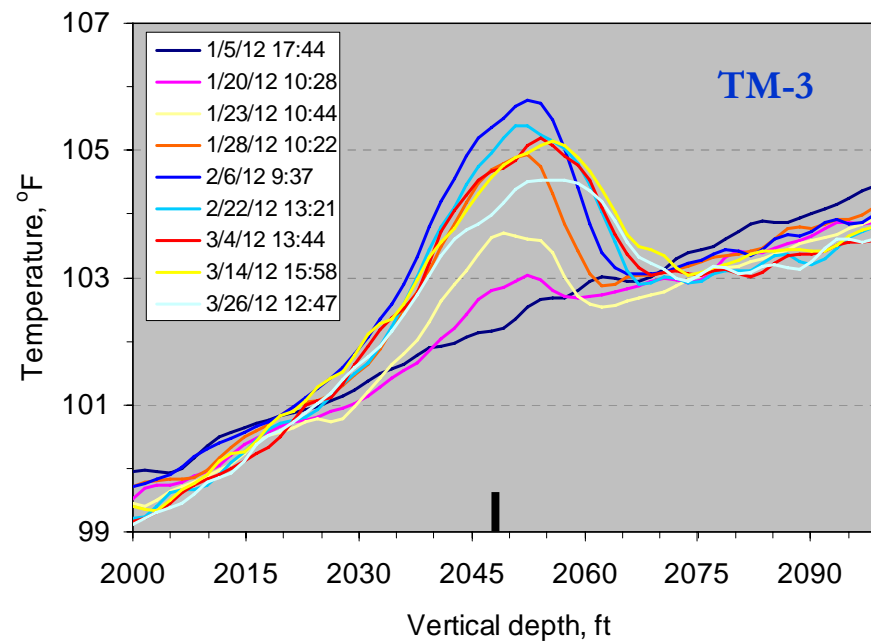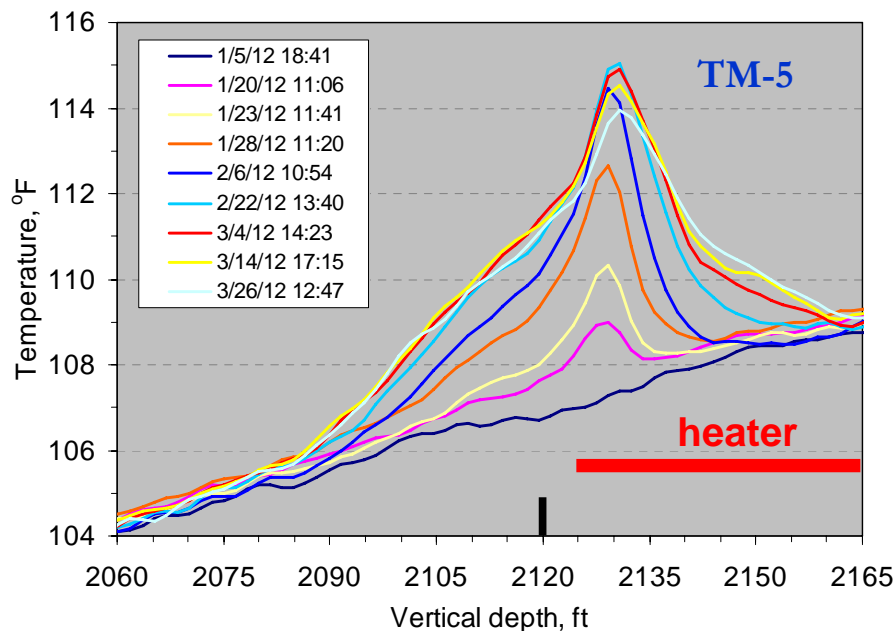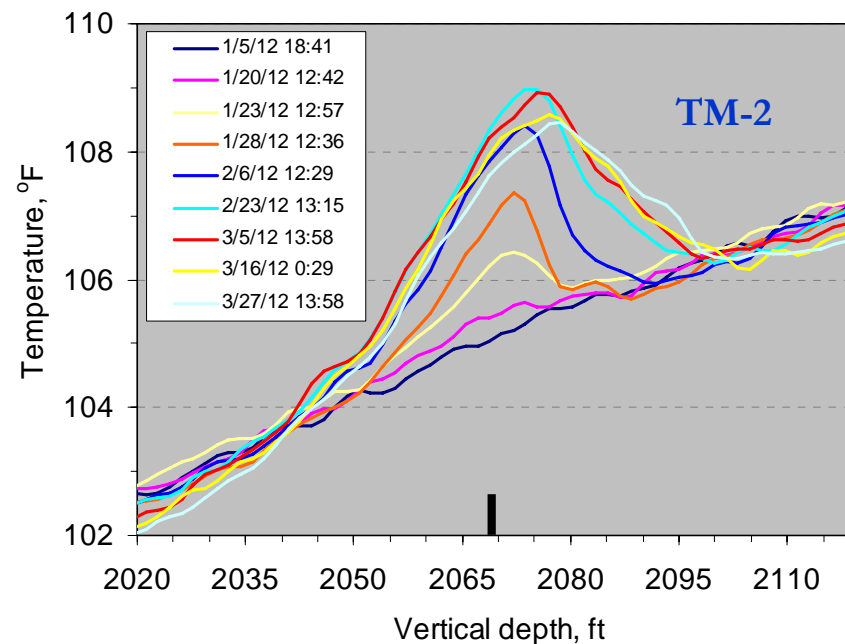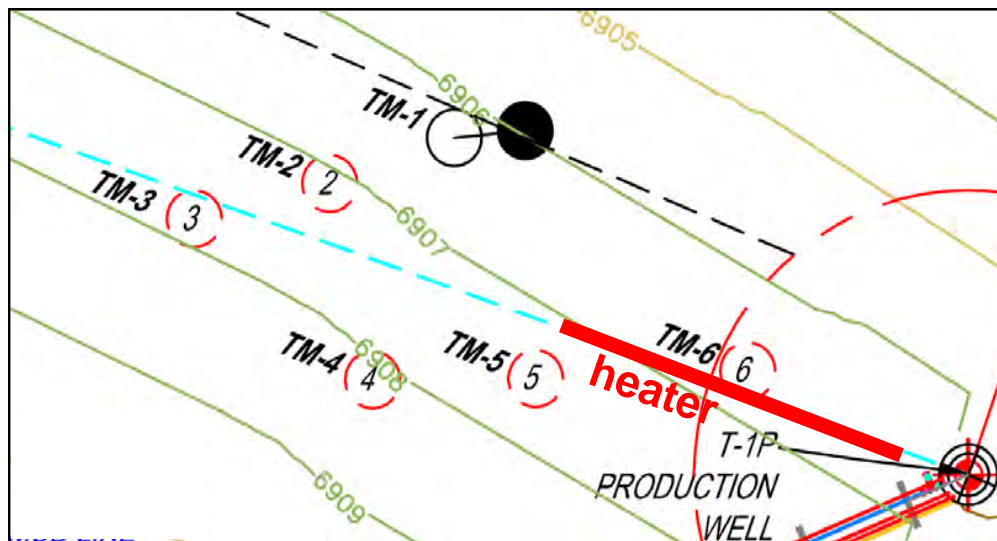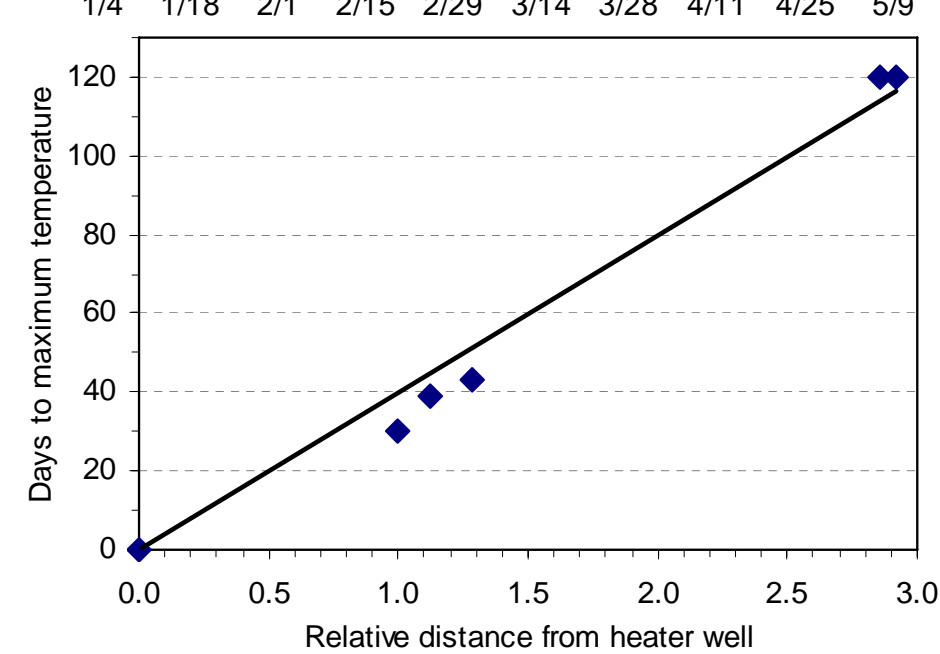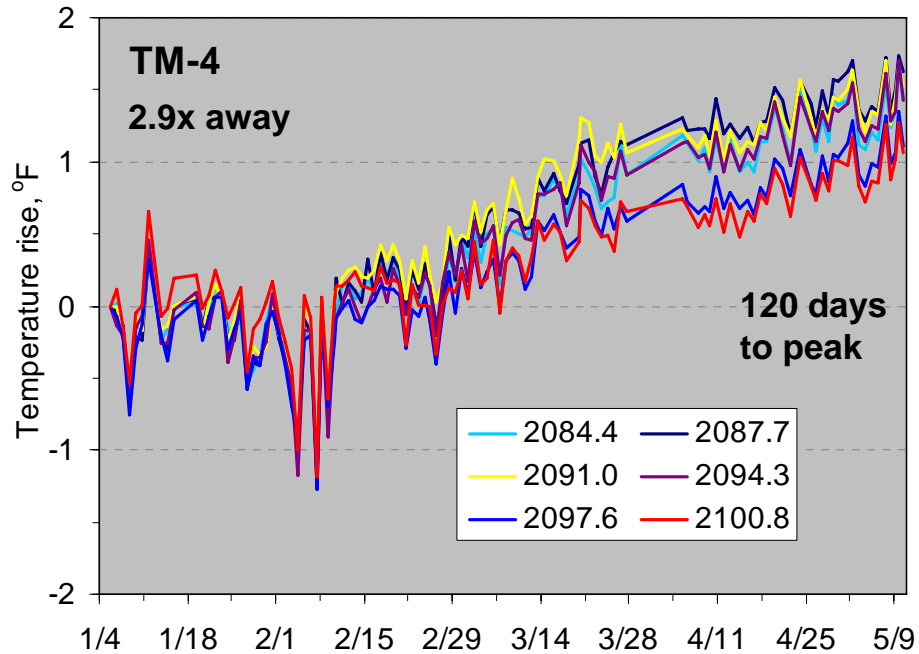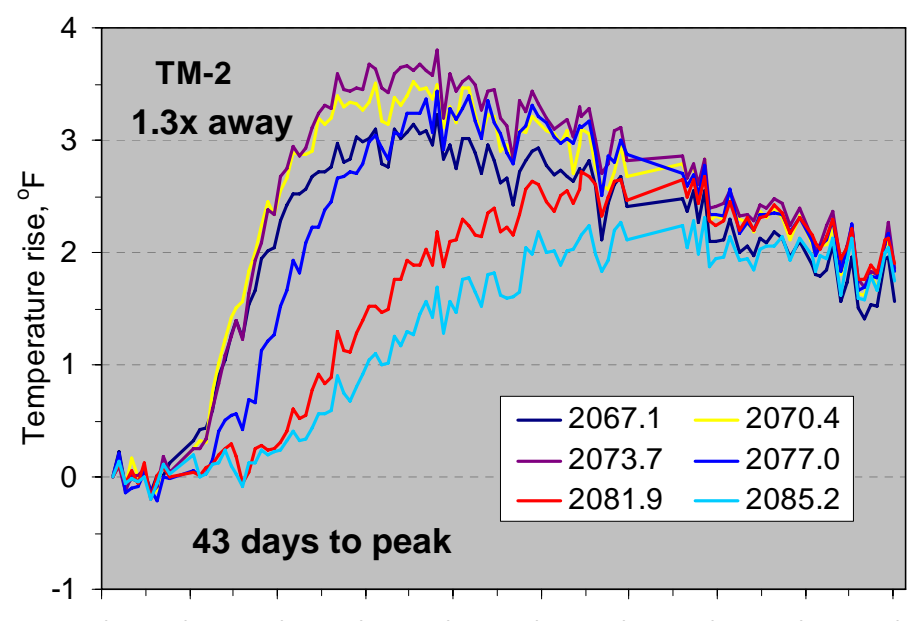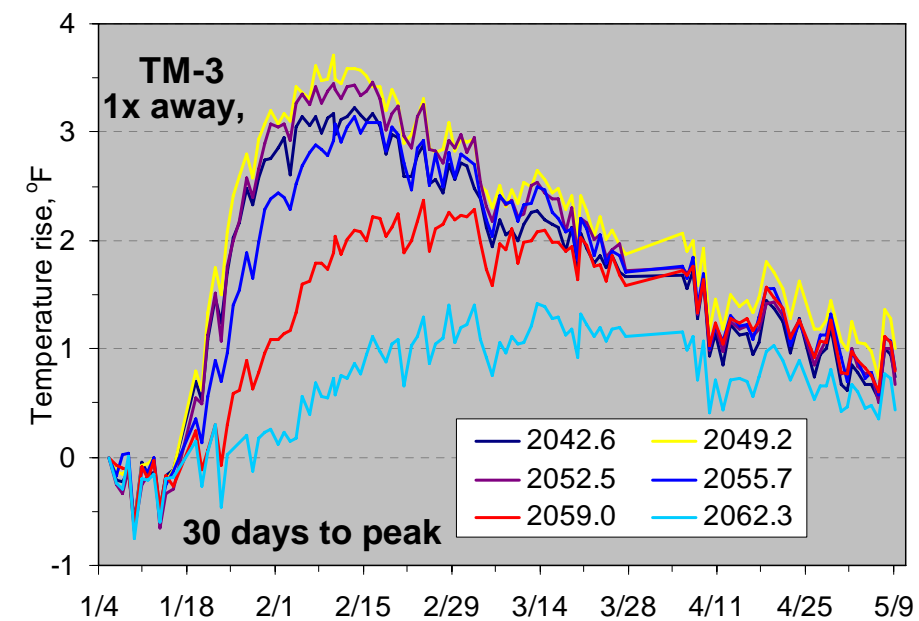
Pilot Status Summary

❑ **Replacement parts were fabricated, and the heater casing and defective instrumentation have been reinstalled**

❑ **The heater is scheduled to arrive and be installed in late May**

❑ **Start of heating is estimated for late spring**

❑ **Completion of the pilot is estimated to be approximately the end of 2012**

National Energy Technology Laboratory

626 Cochrans Mill Road
P.O. Box 10940
Pittsburgh, PA 15236-0940

3610 Collins Ferry Road
P.O. Box 880
Morgantown, WV 26507-0880

13131 Dairy Ashford, Suite 225
Sugarland, TX 77478

1450 Queen Avenue SW
Albany, OR 97321-2198

2175 University Ave. South
Suite 201
Fairbanks, AK 99709

Visit the NETL website at:
www.netl.doe.gov

Customer Service:
1-800-553-7681